

DESIGN AND IMPLEMENTATION OF A FEEDBACK LINEARIZING
CONTROLLER AND KALMAN FILTER FOR A
MAGNETIC LEVITATION SYSTEM

by

JOHN A. HENLEY

Presented to the Faculty of the Graduate School of
The University of Texas at Arlington in Partial Fulfillment
of the Requirements
for the Degree of

MASTER OF SCIENCE IN MECHANICAL ENGINEERING

THE UNIVERSITY OF TEXAS AT ARLINGTON

May 2007

Copyright©by John A. Henley 2007

All Rights Reserved

ACKNOWLEDGEMENTS

I would like to express my thanks to my fiancée, Megan Hamilton, whose love and support made this thesis a reality. In the toughest of times, when I had lost all hope of completing this research and doubted everything about myself, she carried me through to the end, with the kindest of words and steadfast confidence. She believed in me even when I did not and I can not say enough to quantify how amazing she is to me.

I would also like to express my thanks to my advising professor, Dr. Panayiotis Shiakolas, for his encouragement, advice, counsel and confidence during these many months. I am also thankful for the participation and input from the other members of my committee.

My education would not have been possible without the support and sacrifices made by my mother, Maureen Henley. She single-handedly made it possible for her three children to attend college. In this, she gave each of us the gift of self-reliance and determination, whose fruits will nourish each of us and our families all of our days. I can not say it enough, thank you for everything that you have done for me.

Here at the end, I think of the beginning and can not leave out my grandparents, John and Margaret Bradshaw. You made sure that I got off on the right foot when leaving home. I stand in awe of you both for the things I know and those I do not.

March 14, 2007

ABSTRACT

DESIGN AND IMPLEMENTATION OF A FEEDBACK LINEARIZING CONTROLLER AND KALMAN FILTER FOR A MAGNETIC LEVITATION SYSTEM

Publication No. _____

John A. Henley, M.S.

The University of Texas at Arlington, 2007

Supervising Professor: Panayiotis S. Shiakolas

The principal investigation undertaken in this research is the development and subsequent implementation of a feedback linearizing nonlinear controller and extended Kalman filter for a laboratory-based Magnetic Levitation (Maglev) device. The Maglev hardware is both highly nonlinear and open-loop unstable in its dynamic response. The control and estimation scheme proposed in this work is first validated using an increasingly sophisticated level of simulations. The control and estimation algorithm had the sensor noise identified using hardware data. Then, the plant noise covariance is

tuned using both on-line and off-line hardware data. Additionally, the output of the nonlinear controller is then mapped to hardware-suitable levels using a digital lead-lag controller. Experimental results are included where the system is given a set of reference trajectories to track.

TABLE OF CONTENTS

ACKNOWLEDGEMENTS.....	iii
ABSTRACT	iv
LIST OF FIGURES.....	x
LIST OF TABLES	xiii
Chapter	
1. INTRODUCTION.....	1
1.1 Background.....	2
1.2 Prior Related Research.....	3
1.3 Thesis Organization	4
2. SYSTEM DESCRIPTION AND DESIGN	5
2.1 Hardware Description	5
2.2 Real-Time Development Environment	7
2.3 Magnetic Levitation Dynamics	8
2.3.1 Magnetic Levitation System Operation.....	8
2.3.2 Electromagnet Dynamics.....	9
2.3.3 Levitated Object Dynamics.....	9
2.3.4 Vector Format and Equilibrium Points.....	11
2.4 Exact Feedback Linearizing Controller	12
2.4.1 Determination of Relative Degree.....	12

2.4.2 Necessary and Sufficient Conditions for Feedback Linearization.....	14
2.4.3 Coordinate Transformation and Nonlinear Feedback	16
2.4.4 Linear Control Law and Asymptotic Reference Tracking.....	18
2.5 Continuous-Discrete Time Extended Kalman Filter	21
2.5.1 Dynamic Model.....	22
2.5.2 Initialization of the Filter	23
2.5.3 Measurement Equation	24
2.5.4 Kalman Gain Equation	25
2.5.5 Update Equations	26
2.5.6 Propagation Equations.....	26
2.5.7 Filter Tuning	27
2.6 Conclusions.....	27
3. SIMULATION VERIFICATION AND HARDWARE IMPLEMENTATION	29
3.1 Controller / Estimator Simulations	29
3.1.1 Fixed Step Numerical Integration	33
3.1.2 Step Input Response	33
3.1.3 Sine Wave Response	40
3.2 Enhanced Controller / Estimator Simulations	44
3.2.1 Simulink Controller / Estimator Algorithm Structure.....	44
3.2.2 Step Input Response	47

3.2.3 Sine Wave Response	51
3.3 Position Sensor Modeling	55
3.4 Measurement Noise Characterization	59
3.5 Kalman Filter Plant Noise Characterization.....	61
3.5.1 Continuous-Time Extended Kalman Filter.....	62
3.5.2 Continuous-Discrete Time Extended Kalman Filter	66
3.6 Nonlinear Controller Output Mapping.....	76
3.6.1 Software and Hardware Interconnects.....	77
3.6.2 Output Mapping	79
3.7 Experimental Hardware Results	80
3.7.1 Steady State Tacking	81
3.7.2 Square Wave Tracking	83
3.7.3 Sine Wave Tracking	86
4. CONCLUSIONS AND FUTURE WORK	88
4.1 Conclusions	88
4.2 Future Work	92
4.2.1 Feedback Linearized Nonlinear Controller.....	92
4.2.2 State Estimation	92
4.2.3 Hardware.....	92
Appendix	
A. POWER ELECTRONICS SCHEMATIC	94
B. LIE DERIVATIVES AND LIE BRACKETS	96

C. RELATIVE DEGREE CALCULATIONS	99
D. NECESSARY AND SUFFICIENT CONDITION CALCULATIONS	102
E. CONSTRUCTION OF THE COORDINATE CHANGE AND NONLINEAR FEEDBACK	107
F. CONTROLLER/ESTIMATOR SIMULATION CODE.....	112
G. EMBEDDED M-FUNCTION CODE	120
H. NONLINEAR CONTROL OUTPUT MAPPING	124
REFERENCES	126
BIOGRAPHICAL INFORMATION	129

LIST OF FIGURES

Figure	Page
2.1 Maglev hardware- electromagnetic coil, position sensor and levitated object	6
2.2 Maglev hardware- power electronics and terminal block	7
2.3 Maglev circuit and free body diagram	8
2.4 Update and Propagation of the extended Kalman filter	22
3.1 Feedback linearized nonlinear controller / extended Kalman filter simulation structure and interoperation	30
3.2 Maglev simulated system measured position response, estimated position response to a 2.0 mm step input	35
3.3 Maglev simulated position estimate error response and +/- 3 σ error bounds to a 2.0 mm step input	37
3.4 Maglev system estimated velocity response to a 2.0 mm step input	38
3.5 Maglev simulated velocity estimate error response and +/- 3 σ error bounds to a 2.0 mm step input	39
3.6 Maglev estimated current response to a 2.0 mm step input	40
3.7 (a) Maglev simulated system measured position response, estimated position response to a 1.0 mm, 10 rad/sec sine wave and (b) position error estimate with error bounds	41
3.8 (a) Maglev simulated system velocity response, and estimated position response to a 1.0mm, 10 rad/sec sine wave and (b) velocity error estimate with error bounds	43
3.9 Maglev estimated current response to a 1.0 mm, 10 rad/sec sine wave.....	44

3.10 Simulink model for enhanced feedback linearized nonlinear controller and extended Kalman filter.....	46
3.11 (a) Maglev simulated system measured position response, estimated position response to a 2.0 mm step input and (b) position error estimate with error bounds	48
3.12 (a) Maglev simulated system velocity response, and estimated position response to a 2.0 mm, step input and (b) velocity error estimate with error bounds	50
3.13 Maglev estimated current response to a 2.0 mm step input.....	51
3.14 (a) Maglev simulated system measured position response, estimated position response to a 1.0 mm, 10 rad/sec sine wave and (b) position error estimate with error bounds	52
3.15 (a) Maglev simulated system velocity response, and estimated position response to a 1.0 mm, 10 rad/sec sine wave and (b) velocity error estimate with error bounds	54
3.16 Maglev simulated system current response to a 1.0 mm, 10 rad/sec sine wave.....	55
3.17 Levitated object, steel ball bearing.....	56
3.18 Object position tool attached to Maglev device.....	57
3.19 Input-output sensor response graph	58
3.20 Simulink position sensor implementation (a) Position to voltage conversion and (b) voltage to position conversion	59
3.21 Simulink model used to determine the sensor noise covariance	60
3.22 Simulink model for digital lead-lag controller	63
3.23 Simulink model used for off-line plant noise covariance tuning using hardware data.....	64
3.24 Digital lead-lag controller and continuous time extended Kalman filter for Maglev system plant noise covariance tuning	65

3.25	Digital lead-lag controller tracking 14.8 mm reference input	67
3.26	(a) Offline position estimate, hardware –measured position and reference trajectory using experimentally tuned plant noise covariance, (b) Position error between hardware-measured position and estimated position with mean estimate error baseline	68
3.27	(a) Offline velocity estimate, and reference velocity trajectory using experimentally tuned plant noise covariance, (b) Velocity error between estimated velocity and reference velocity trajectory with mean estimate error baseline.....	70
3.28	Offline current estimate using experimentally tuned plant noise covariance and mean estimate current	71
3.29	Offline covariance responses using experimentally tuned plant noise covariance	73
3.30	On-line position estimate produced by the extended Kalman filter with experimentally tuned plant noise covariance.....	74
3.31	On-line velocity estimate produced by the extended Kalman filter with experimentally tuned plant noise covariance.....	75
3.32	On-line velocity estimate produced by the extended Kalman filter with experimentally tuned plant noise covariance.....	76
3.33	Simulink model allowing scaled nonlinear control output or digital lead-lag controller output to control the Maglev system.....	78
3.34	Nonlinear controller output versus linear controller output, along with linear best fit	79
3.35	Nonlinear output to linear output scaling block	80
3.36	Steady state tracking of the Maglev with levitated object to a reference trajectory 14.8 mm and 14.5 mm.....	82
3.37	Square wave tracking for the Maglev with an amplitude of 0.05mm and frequency of (a) 1.0 rad/sec and (b) 2.0 rad/sec	85
3.38	Sine wave tracking for the Maglev with an amplitude of 0.05 mm and frequency of (a) 1.0 rad/sec and (b) 2.0 rad/sec.....	87

LIST OF TABLES

Table	Page
3.1 Maglev simulation parameters	32
3.2 Experimentally determined position sensor noise properties	60
H.1 Nonlinear control output mapping results	125

CHAPTER 1

INTRODUCTION

In the past few decades an increasing amount of research effort in the control systems field has been focused on the control of a magnetic levitation system. This problem is of particular interest to the controls community since the dynamics of the system are open-loop unstable and highly nonlinear. For a successful controller to be considered for such a system, it must simultaneously stabilize the open-loop behavior and correctly incorporate the nonlinear elements of the systems dynamics into the control output. Examples of magnetic levitation systems can be found throughout academia and industry. Some of these applications include semiconductor fabrication [1], production of steel [2], high speed commuter trains [3], bearing design [4] and machine tools [5] in which magnetic levitation, in various forms has played a key role in the development of these successful technologies.

The challenges presented to the designer when developing a control scheme for this system are quite formidable and, as many times as not, the simpler solution using well know principles is selected. These linear solutions (both frequency and state space based approaches) are quite capable of controlling this system. However, their strength is also a weakness in that the assumptions made to allow use of these techniques limit the region of state space that can be considered.

Additionally, even conventional linear state space approaches usually require faithful reproduction of the entire state vector, even when the state vector can not be directly measured. With the surfacing of nonlinear control these systems can be more accurately controlled over a wider range of the state space. Of the wide variety of nonlinear control schemes available, an exact feedback linearization controller is considered for the stabilization and tracking control of a single-axis magnetic levitation test bed. For successful implementation of this controller, a continuous-discrete extended Kalman filter is constructed to provide real-time accurate estimates of the velocity and current, which are not measurable with the hardware configuration.

1.1 Background

The classical approach involves describing the system with an input/output relationship or vector-matrix description based on a first order linear approximation of the system dynamics perturbed around an operating point. Once the system is characterized by the linear description, the design of a controller using various techniques is relatively straight forward. Many commercially available software packages could aid in the design and structure selection of the linear controller. Often the controller types available to linear systems only require information provided by directly measuring the output, while more sophisticated linear controllers require the full state for the control law formulation. In the event that the full state is not available, the remaining states can often be reconstructed using a state estimator. While these techniques many times satisfy the design needs, linear controllers are susceptible to a few notable limitations. The approximate linear model is only valid in a small region of

state space around the operating point. Tracking certain types of reference trajectories or user set operating points far away from the linearized set point can cause the state to venture into an unstable region. External disturbances, which are often difficult if not impossible to identify and address prior to implementation, can also cause the system to have undesirable or unstable behavior.

1.2 Prior Related Research

Many authors have proposed solutions to the control and state estimation of magnetic levitation systems which are selected since they are nonlinear and open-loop unstable. The feedback linearization technique (both input-state and input-output) has been applied to solve the nonlinear control problem posed by magnetic levitation devices [6-8]. Other nonlinear methods applied include Hybrid Neural Networks [9], Sliding Mode Control [10], Dual Neural Network/Sliding Mode Control [11], and Robustly Stabilized Feedback Linearization [12]. However, the control problem alone only addresses one half of the design challenge, accurate and timely information about the entire state is required. Some authors have chosen to numerically differentiate the position signal as a means to observe or estimate the velocity of the suspended object [6], while others have addressed the state estimation problem with Luenberger-type observers [12]. A more advanced estimator using a reduced order nonlinear observer has also been shown with much success in previous work [13].

1.3 Thesis Organization

This research is structured as follows: The general description of the system, synthesis of the nonlinear controller, and synthesis of the extended Kalman filter are presented in Chapter 2. Simulation and hardware implementation of the controller scheme is presented in Chapter 3. System simulations are considered in Sections 3.1 and 3.2. Position sensor characterization and position noise covariance are determined experimentally in Sections 3.3 and 3.4. The plant noise covariance is tuned in an off-line method, using hardware data, then verified on-line with the hardware, in section 3.5. Mapping of the nonlinear control output to suitable hardware values is carried out in section 3.6. Hardware results are presented in Section 3.7, where a number of reference trajectories are considered. Chapter 4 contains the conclusions of this research and suggestions for future work.

CHAPTER 2

SYSTEM DESCRIPTION AND DESIGN

In this chapter the pertinent system dynamics, nonlinear feedback linearized control law and state estimator used in this research are presented. The scope of this effort is to use estimated states to determine a sequence of control inputs that will allow the measured output of the system to recreate a reference trajectory. To accomplish this goal, this chapter is broadly organized into three main sections. The first addresses the system dynamics, equilibrium points and hardware / software development environments. The next main section is more extensive since it outlines the preliminaries for the existence of the proposed nonlinear control scheme. The third section discusses the proposed state estimator and the foundations that allow its extension to nonlinear systems.

2.1 Hardware Description

The hardware device used in this research is a Magnetic Levitation (Maglev) System and is shown in Figure 2.1. The Maglev consists of three primary components: the infrared position sensor, the power and analog control electronics, and the electromagnet. In operation, the position sensor emits an infrared light beam across the air gap between the suspended ferromagnetic object and the electromagnet. The voltage corresponding to the object position generated by the sensor is acquired by a commercially available Digital Acquisition Card (DAC), NI PCI 6024E [14] used in a

personal computer (PC). Once the signal is acquired by the DAC, the software state estimator uses the measured position and plant model to estimate the unmeasured states of the Maglev system. These estimated states are in turn used by the nonlinear controller to determine the appropriate control output. The control output from the PC is amplified using the power electronics in the black box shown in Figure 2.2.

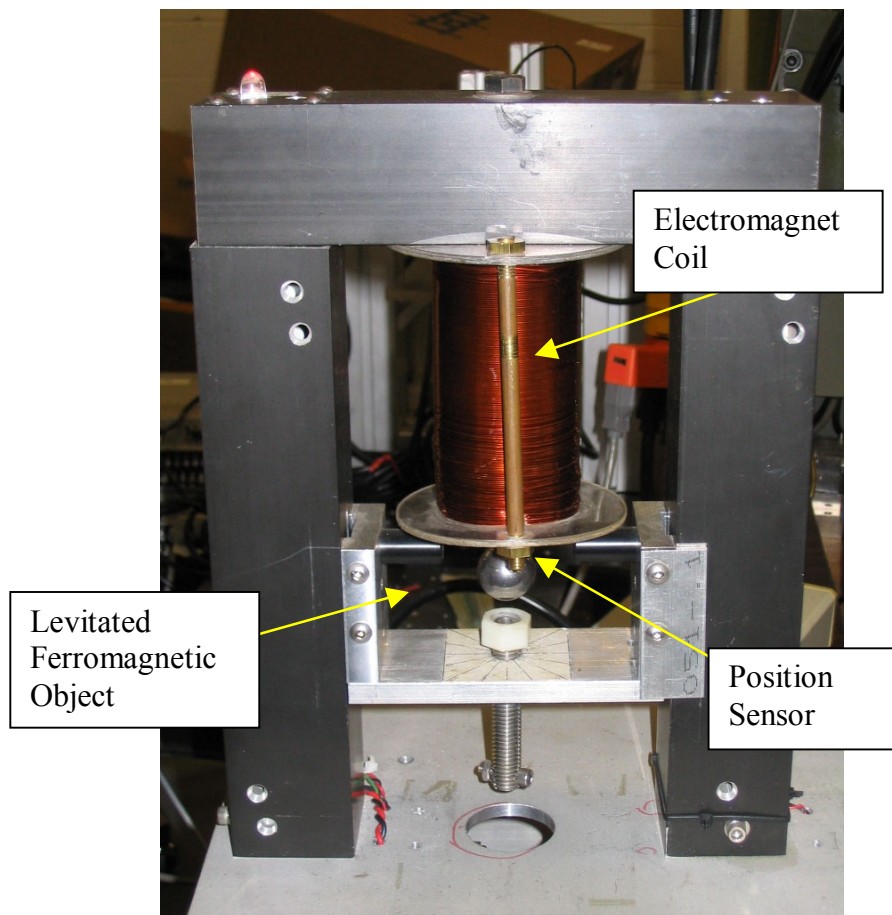


Figure 2.1 Maglev hardware – electromagnet coil, position sensor and levitated object

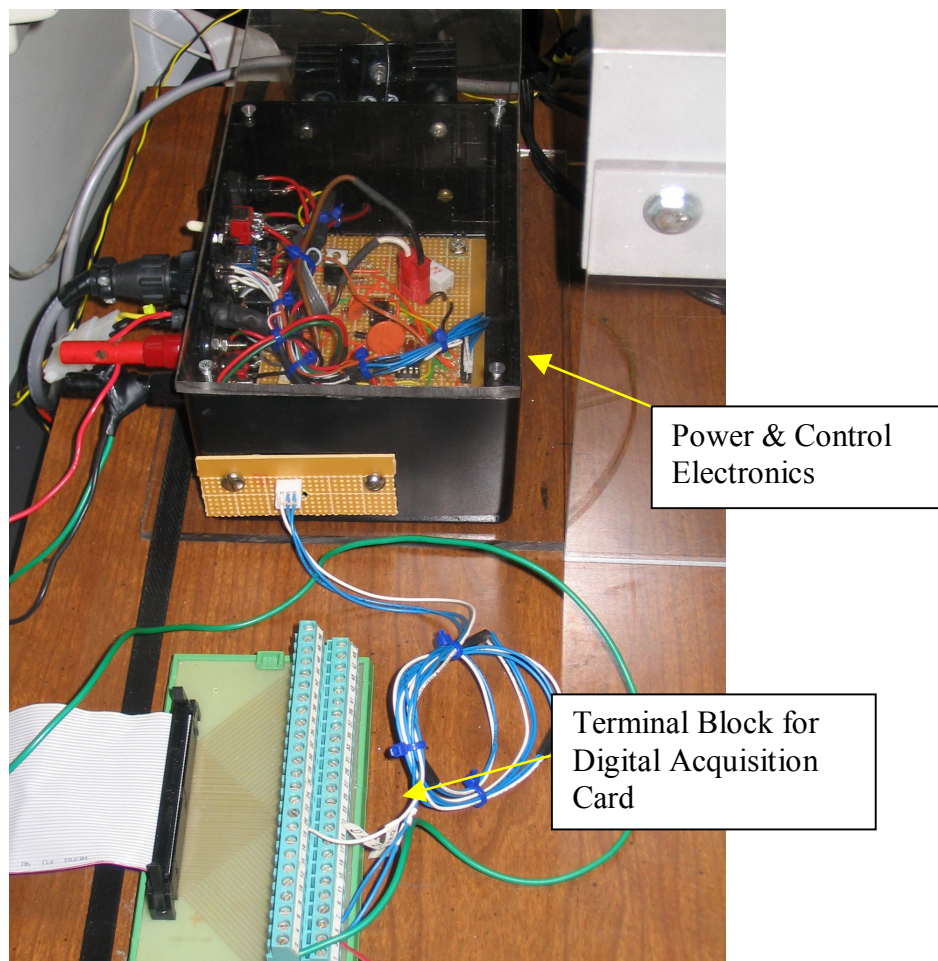


Figure 2.2 Maglev hardware – power electronics and terminal block

2.2 Real-Time Development Environment

This work was implemented and verified on a hardware in the loop (HIL) environment using xPC Target [15], a MATLAB toolbox allowing for real time embedded development. xPC allows the system designer to develop and incorporate the design and analysis tools of MATLAB into a readily deployable executable. The current xPC setup requires two PC systems; the target system executes the real time kernel,

while the host system performs supervisory control, monitoring and parameter changes. Communication between the two systems is accomplished through a serial communication interface. This xPC setup has been used with great success for the implementation of a digital / neural net controller [16] and with the implementation of a digital / fuzzy controller [17]. The details of this system, its set-up and use have been treated by afore-mentioned authors, and its use as an educational tool has been discussed by [18].

2.3 Magnetic Levitation Dynamics

2.3.1. Magnetic Levitation System Operation

The schematic of the equivalent magnet model and the free body diagram of a suspended object of mass, m , vertically is shown in Figure 2.3.

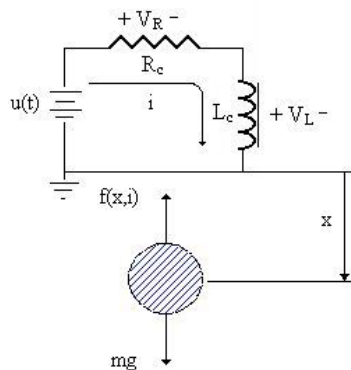


Figure 2.3 Maglev circuit and free body diagram

When a ferromagnetic object is placed beneath the electromagnet at a distance x , typically denoted as an air gap, it will be acted upon by the attractive force produced by the electromagnet. Simultaneously, the object will block a portion of the infrared light being emitted and received by the position sensor. A relationship describing the amount

of blocked light to the object distance allows the sensor voltage signal to be converted into a position below the electromagnet coil. The signal is fed back into the target where it is further used to determine the state of the system and subsequently used to generate a control signal.

2.3.2. Electromagnet Dynamics

The dynamics of the coil are usually represented as an equivalent R-L circuit in series as shown in Figure 2.3. Applying Kirchoff's voltage law around the circuit, one can describe the relevant dynamics of this 1st order system. The voltage drop across the resistor and inductor is described by Ohm's and Ampere's laws respectively [19]

$$V_R = i * R_C \quad (2.1)$$

$$V_L = L_c \frac{di}{dt} \quad (2.2)$$

Applying Kirchoff's voltage law and substituting equations 2.1 and 2.2 yields

$$u(t) = V_R + V_L = i * R_c + L_c \frac{di}{dt} \quad (2.3)$$

Recasting equation 2.3 as a first order differential equation gives

$$\frac{di}{dt} = -\frac{R_c}{L_c} i + \frac{u(t)}{L_c} \quad (2.4)$$

2.3.3. Levitated Object Dynamics

A free body diagram of the levitated object being suspended vertically by balancing the force generated by the electromagnet, $f(x,i)$, and the gravity force, $m g$, is shown in Figure 2.3. The force experienced by the levitated object $f(x,i)$, is a

function of the air gap or distance below the electromagnet, x , and the current supplied to the magnet, i , is found by direct application of both Ampere's and Faraday's laws [20].

$$f(x,i) = -\frac{i^2}{2} \frac{dL(x)}{dx} \quad (2.5)$$

The total inductance, $L(x)$, is a nonlinear function of the position in the electromagnetic field. A typical approximation is to assume that the inductance varies in an inverse relationship with respect to the position [21], as shown in equation 2.6

$$L(x) = L_c + \frac{L_0 x_0}{x} \quad (2.6)$$

where L_c is the constant inductance of the electromagnet in the absence of the levitated object, L_0 is the additional inductance contributed by the presence of the object, and x_0 is the equilibrium position. Substituting equation 2.6 into equation 2.5 and taking the derivative, one finds equation 2.7.

$$f(x,i) = \frac{L_0 x_0}{2} \left(\frac{i}{x}\right)^2 = C \left(\frac{i}{x}\right)^2 \quad (2.7)$$

Application of Newton's 3rd Law of motion for this suspended object yields

$$m\ddot{x} = mg - C \left(\frac{i}{x}\right)^2 \quad (2.8)$$

Recasting equation 2.8 into a standard form gives the equation of motion

$$\ddot{x} = g - \frac{C}{m} \left(\frac{i}{x}\right)^2 \quad (2.9)$$

2.3.4. Vector Format and Equilibrium Points

It is necessary to arrange the dynamics expressed in equations 2.4 and 2.9 in a format better suited for the analysis to be performed in later sections. The state variables are defined as: x_1 – position, x_2 – velocity and x_3 – current. The state variable format of the dynamics becomes, assuming that the position is measured,

$$\begin{bmatrix} \dot{x}_1 \\ \dot{x}_2 \\ \dot{x}_3 \end{bmatrix} = \begin{bmatrix} x_2 \\ g - \frac{C}{m} \left(\frac{x_3}{x_1} \right)^2 \\ -\frac{R_c}{L_c} x_3 \end{bmatrix} + \begin{bmatrix} 0 \\ 0 \\ \frac{1}{L_c} \end{bmatrix} u(t) \quad (2.10)$$

$$y = c^T \cdot [x_1 \quad x_2 \quad x_3]^T = [1 \quad 0 \quad 0] \cdot [x_1 \quad x_2 \quad x_3]^T \quad (2.11)$$

In a shorter format, the vector expression found in equations 2.10 and 2.11 can be expressed as

$$\dot{x} = f(x) + g \cdot u(t) \quad (2.12 \text{ a})$$

$$y = h(x) \quad (2.12 \text{ b})$$

It is important to note that at static equilibrium, the time rate derivatives must strictly be equal to zero, $\dot{x} \equiv 0$. The state that satisfies this condition may be expressed as

$$x_0 = [x_0^1 \quad 0 \quad x_0^3]^T \quad (2.13)$$

The equilibrium current, x_0^3 , is evaluated from equation 2.9, and must satisfy the following condition [20]

$$x_0^3 = x_0^1 \sqrt{\frac{gm}{C}} \quad (2.14)$$

2.4 Exact Feedback Linearizing Controller

In this section, the conditions for the linearizing transformation and nonlinear feedback allowing the Maglev to be controlled are outlined. Of particular interest will be the coordinate transformation also known as a diffeomorphism, $z = \phi(x)$, and the feedback law, $u = \alpha(x) + \beta(x) \cdot v$, which will allow it to be accomplished. Some of the more common mathematical preliminaries related to this discussions are presented in Appendix B, for reference.

2.4.1. Determination of Relative Degree

The relative degree of a linear system is defined as the difference between the number of poles and zeros [23]. This concept can be extended to nonlinear systems but requires more mathematical treatment. Further treatment of this issue is discussed elsewhere, where the following definition is given and repeated here for completeness [23]:

Definition 2.1 [23]

Given the Single Input – Single Output System, SISO, outlined in equation 2.12a, it is said to have relative degree r at a point x_0 if:

i) $L_g L_f^k h(x) = 0$ for all x in a neighborhood of x_0 and all $k < r - 1$

ii) $L_g L_f^{r-1} h(x) \neq 0$

The terms L_g and L_f^k represent the Lie derivative of $h(x)$ taken along $g(x)$ and

k – times along $f(x)$, respectively. A more expansive treatment of this subject is

presented in Appendix B.

Applying this definition to the Maglev system yields:

$$k = 0 : \quad L_g h(x) = 0 \quad (2.15)$$

$$k = 1 : \quad L_g L_f h(x) = 0 \quad (2.16)$$

$$k = 2 : \quad L_g L_f^2 h(x) = -\frac{2C}{mL_c} \left(\frac{x_3}{x_1^2} \right) \quad (2.17)$$

At the equilibrium point (x_0, i_0) , the term $L_g L_f^2 h(x_0) \neq 0$, meaning that the relative degree of the system is 3. For the relative degree of the Maglev to remain well defined, the system will be allowed to operate in a region of state space that is bounded by $x_1 > 0$ and $x_3 > 0$. This restriction is not unreasonable since $x_1 \leq 0$ would result in the levitated object either touching the coil or existing inside the coil, and $x_3 < 0$ would

result in a negative current. Careful examination of the power electronic schematic shown in Appendix A does not allow for this possibility.

In the event the relative degree is less than the order of the system, additional steps must be taken in the construction of the coordinate transformation. The remaining $n-r$ portions of the diffeomorphism will have to be linearly independent functions to complete the transformation [24]. Additionally, the internal dynamics, the remaining $n-r$ portion of the system that is unobservable in the input-output map, must be examined to guarantee that these dynamics are in fact stable [23].

As a note, the internal dynamics of a nonlinear system can be a significant design issue if the system is inverted, in the course of improving trajectory tracking. This problem has been greatly studied and will not be addressed here, but the reader can find many useful results and methods in the open literature [25 - 33].

2.4.2. Necessary and Sufficient Conditions for Feedback Linearization

The necessary and sufficient conditions for a nonlinear system to be converted to a linear system have been well documented in literature [23, 24, 26 - 36]. Again, the main results of [23] are presented here for completeness.

Definition 2.2 [23]

Given the nonlinear system in 2.12a and 2.12b, the State Space Exact Linearization problem is solvable near a point x_0 (i.e. there exists an “output” function $h(x)$ for which the system has relative degree r at x_0) if and only if the following conditions are satisfied:

- i) The matrix $[g \quad ad_f g \quad ad_f^2 g]$ has rank n
- ii) The distribution $D = span\{g \quad ad_f g \quad ad_f^2 g\}$ is involutive near x_0 .

Checking the first condition:

$$rank[g(x_0), ad_f g(x_0), ad_f^2 g(x_0)] = rank \begin{bmatrix} 0 & 0 & \frac{-2C}{mL_c} \left(\frac{x_3}{x_1^2} \right) \\ 0 & \frac{2C}{mL_c} \left(\frac{x_3}{x_1^2} \right) & \frac{-4C}{mL_c} \left(\frac{x_2 x_3}{x_1^3} \right) \\ \frac{1}{L_c} & \frac{R_c}{L_c^2} & \frac{R_c^2}{L_c^3} \end{bmatrix}_{x_0} \quad (2.18)$$

$$= 3$$

For the second condition to be shown true, the Lie Bracket of any two vectors in the $span D$ must be equal to a linear combination of those two vectors.

$$[g(x), ad_f g(x)] = \begin{bmatrix} 0 \\ \frac{2C}{mL_c} \left(\frac{1}{x_1^2} \right) \\ 0 \end{bmatrix} = \frac{-R_c}{L_c x_3} \begin{bmatrix} 0 \\ 0 \\ \frac{1}{L_c} \end{bmatrix} + \frac{1}{x_3} \begin{bmatrix} 0 \\ \frac{2C}{mL_c} \left(\frac{x_3}{x_1^2} \right) \\ \frac{R_c}{L_c^2} \end{bmatrix} \quad (2.19)$$

Equation 2.19 shows that the span is in fact involutive at x_0 . The supporting ancillary calculations can be found in Appendix D. Note that should the state vector venture in regions of state space such that $x_1 = 0$ and/or $x_3 = 0$, not only will the system lose its relative degree (see definition 2.1) but it will also lose the necessary and sufficient conditions for a feedback linearizing coordinate transformation.

2.4.3 Coordinate Transformation and Nonlinear Feedback

The previous section introduced the necessary and sufficient conditions for the existence of a feedback linearizing coordinate transformation, also known as a diffeomorphism, and the related nonlinear feedback. The coordinate transformation process is relatively straight forward once the connection is made that the output equation, 2.12b, satisfies the conditions placed upon T_1 by [26] and [35], where T_1 is the solution to the partial differential equation

$$\langle dT_1, g(x) \rangle = \frac{\partial T_1}{\partial x_1} g(x) + \dots + \frac{\partial T_n}{\partial x_n} g(x) = 0 \quad (2.20)$$

In this work, no claim is placed upon a global transformation. To generate the transformation, one could simply take the Lie Derivative of 2.12b with respect to 2.12a until the input $u(t)$ appears in the output of the derivative [24]. The details of this procedure are presented in Appendix E. The nonlinear change in coordinates is presented in equation 2.21.

$$z = \Phi(x) = \left[x_1, \quad x_2, \quad g - \frac{C}{m} \left(\frac{x_3}{x_1} \right)^2 \right]^T \quad (2.21)$$

In the transformed coordinates, the nonlinear dynamic equations take the form shown in equation 2.22.

$$\begin{bmatrix} \dot{z}_1 \\ \dot{z}_2 \\ \dot{z}_3 \end{bmatrix} = \begin{bmatrix} \dot{y} \\ \ddot{y} \end{bmatrix} = \begin{bmatrix} x_2 \\ g - \frac{C}{m} \left(\frac{x_3}{x_1} \right)^2 \\ \frac{2C}{m} \left(\frac{x_2 x_3^2}{x_1^3} \right) + \frac{2C R_c}{m L_c} \left(\frac{x_3^2}{x_1^2} \right) - \frac{2C}{m L_c} \left(\frac{x_3}{x_1^2} \right) u(t) \end{bmatrix} \quad (2.22)$$

By defining the following terms, $\alpha, \beta, u(t)$, equation 2.22 can be written in terms of a linear system of equations,

$$\alpha(x) = \frac{-L_f^3 h(x)}{L_g L_f^2 h(x)} = L_c \left(\frac{x_2 x_3^2}{x_1^3} + \frac{R_c}{L_c} x_3 \right) \quad (2.23a)$$

$$\beta(x) = \frac{1}{L_g L_f^2 h(x)} = -\frac{m L_c}{2C} \left(\frac{x_1^2}{x_3} \right) \quad (2.23b)$$

$$u(t) = \frac{\alpha(x) + v}{\beta(x)} \quad (2.23c)$$

Restrictions of $x_1 \neq 0$ and $x_3 \neq 0$ are placed on the system to prevent equation 2.23 from becoming singular. Not only will 2.23 become singular but the rank requirement outlined in necessary and sufficient conditions of section 2.4.2 will be violated. These restrictions are also the same bounds placed on the region of state space that guarantees a well defined relative degree. The linear system of equations is expressed in terms of equation 2.22 and 2.23 as

$$\dot{z} = \begin{bmatrix} 0 & 1 & 0 \\ 0 & 0 & 1 \\ 0 & 0 & 0 \end{bmatrix} \begin{bmatrix} z_1 \\ z_2 \\ z_3 \end{bmatrix} + \begin{bmatrix} 0 \\ 0 \\ 1 \end{bmatrix} v(t) \quad (2.24)$$

where $v(t)$ is the new input for the linear system.

Equations 2.23c and 2.24 allow the construction of a linear transfer function between the linear input and the measurement equation 2.23b.

2.4.4 Linear Control Law and Asymptotic Reference Tracking

A suitable controller will need to be introduced for stability and tracking since the open loop dynamics of the Maglev are unstable. The transformation implemented in the previous section produces a linear system that is represented as a chain of integrators at the origin of the complex plane, while the transformed system is in a better structure for controller design. The controllability and observability of the linear system is full rank, see equation 2.25a and 2.25b.

$$\text{rank } C = \text{rank} \begin{bmatrix} b & Ab & A^2b \end{bmatrix} = 3 \quad (2.25a)$$

$$\text{rank } O = \text{rank} \begin{bmatrix} c^T & c^T A & c^T A^2 \end{bmatrix}^T = 3 \quad (2.25b)$$

Noting that the transformed linear system is controllable and observable, the desired poles of the closed loop system are chosen to be $\eta_1 = -60$, $\eta_2 = -80$ and $\eta_3 = -100$, which will produce a closed-loop time constant of 0.1 second. The state feedback gain, k^T , is evaluated through the placement of these poles using the Bass-Gura Formula shown in equation 2.32 [37].

$$k^T = (\lambda^T - a^T) T^{-T} C^{-1} \quad (2.32)$$

where

k^T - Feedback gain due to placing closed-loop poles at η_1, η_2 and η_3

λ - Coefficients of the desired closed loop characteristic polynomial

a - Coefficients of the open loop characteristic polynomial

T - Toeplitz matrix of the open loop characteristic polynomial, based on the system representation by equation 2.24

Determining these parameters yields the following

$$\lambda = [240 \quad 18800 \quad 480000] \quad (2.27a)$$

$$a = [0 \quad 0 \quad 0] \quad (2.27b)$$

$$T = \begin{bmatrix} 1 & 0 & 0 \\ 0 & 1 & 0 \\ 0 & 0 & 1 \end{bmatrix} \quad (2.27c)$$

$$C = \begin{bmatrix} 0 & 0 & 1 \\ 0 & 1 & 0 \\ 1 & 0 & 0 \end{bmatrix} \quad (2.27d)$$

Substituting 2.27a, 2.27b, 2.27c and 2.27d into equation 2.32 produces the state feedback gain shown in equation 2.28.

$$k^T = [480000 \quad 18800 \quad 240] \quad (2.28)$$

The linear system in equation 2.24 with its poles placed at η_1 , η_2 and η_3 is expressed in equation 2.29 as

$$\dot{z} = \begin{bmatrix} 0 & 1 & 0 \\ 0 & 0 & 1 \\ -k_1 & -k_2 & -k_3 \end{bmatrix} \begin{bmatrix} z_1 \\ z_2 \\ z_3 \end{bmatrix} + \begin{bmatrix} 0 \\ 0 \\ 1 \end{bmatrix} v(t) \quad (2.29)$$

Armed with the stabilizing gain, k^T , and knowledge of how the states z_1, z_2 and z_3 evolve, the nonlinear input derived in equation E.14, found in Appendix E, is rewritten in equation 2.30.

$$u(t) = \frac{-L_f^3 h(x) - \sum_{i=1}^3 k_i L_f^{i-1} h(x) + v}{L_g L_f^2 h(x)} \quad (2.30)$$

The next step in the synthesis of the nonlinear controller is to drive the suspended object to track a reference trajectory, $y_R(t)$. The error between the actual position and the reference position is defined as

$$e(t) = y(t) - y_R(t) \quad (2.31)$$

Equation 2.31 can be differentiated and substituted into equation 2.30 producing a nonlinear feedback control law driven by the error dynamics between the levitated object states and the reference trajectory, as shown in equation 2.32.

$$u(t) = L_c \left[\begin{pmatrix} x_2 & x_3 \\ x_1 \end{pmatrix} + \frac{R_c}{L_c} x_3 \right] + \frac{2C x_3}{m L_c x_1^3} [k_1 (x_1 - y_R) + k_2 (x_2 - \dot{y}_R) + k_3 \left(g - \frac{C}{m} \left(\frac{x_1}{x_3} \right)^2 - \ddot{y}_R \right)] + \ddot{y}_R \quad (2.32)$$

This controller will asymptotically drive the levitated object position to the reference trajectory, regardless of the initial condition as long as it stays bounded, well conditioned, and at least the first three derivatives of the reference trajectory exist.

2.5 Continuous-Discrete Time Extended Kalman Filter

The use of modern high performance controllers necessitates the need for methods of determining the state of the system since typically measuring the entire state vector is impractical if not impossible. For the purposes of this research, a continuous-discrete extended Kalman filter is proposed. This embodiment of the state estimator is of particular usefulness when dealing with a system, such as this one, in which the dynamic model is continuous but the measurements are performed at discrete time intervals.

The process for computing and estimating the states by the continuous-discrete time extended Kalman filter is outlined in Figure 2.6. The current state estimate and covariance are propagated forward in time until the next measurement occurs. Then, the Kalman Gain is computed and the state estimate and covariance are updated. These updated values are then propagated forward and the process repeats itself. The formulations presented in this section are thoroughly treated along with other filtering schemes in [38].

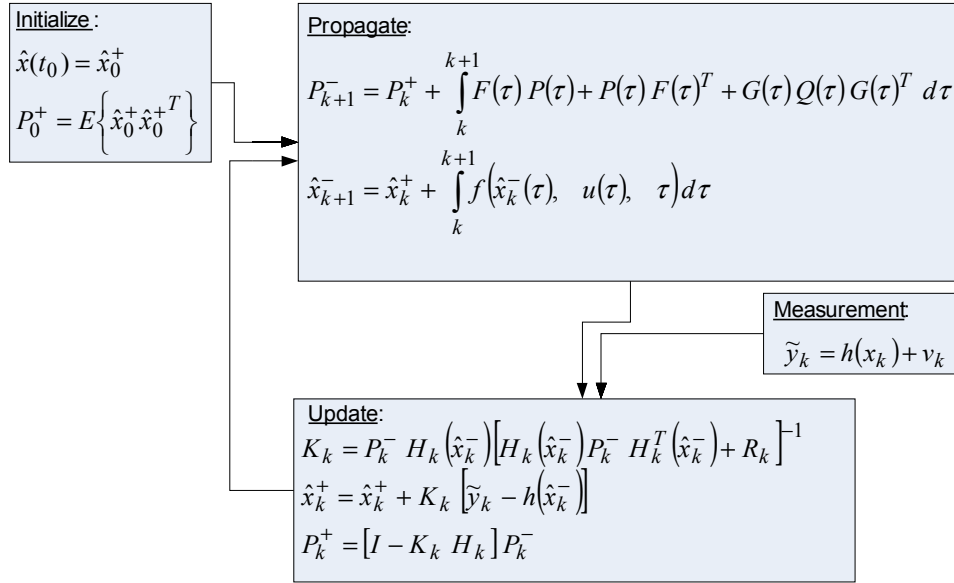


Figure 2.4 Update and Propagation of the extended Kalman filter

2.5.1 Dynamic Model

The version of the Kalman filter employed in this work assumes that the noise is Gaussian and that the system parameters are known. The dynamics of the truth model are expressed in equations 2.33 and 2.34.

$$\dot{x} = f(x) + g \cdot u(t) + \Psi(t) \cdot w(t), \quad w(t) \sim N(0, Q(t)) \quad (2.33)$$

$$\tilde{y}_k = h(x_k) + v_k, \quad v_k \sim N(0, R_k) \quad (2.34)$$

The format of these equations is very close to the dynamics of the system used in the design on the feedback linearizing controller in section 2.3. In fact, equations 2.33 and 2.34 are the augmented form of the first dynamic equations and account for un-modeled plant dynamics, and noise in the measurement. The process noise $w(t)$ is

defined as a zero mean Gaussian white-noise with covariance $Q(t)$; this term helps the filter account for un-modeled continuous plant dynamics. Accordingly, the discrete sensor noise v_k is a zero mean Gaussian white-noise term with covariance R_k . Along with the assumption of Gaussian white-noise it is assumed that the two noise sources, $w(t)$ and $v(k)$, are not correlated with each other at any point in time, and that they are also not correlated with themselves at any point in time. This notion is expressed in equations 2.35 and 2.36.

$$E\{v(t)w(t)^T\} = 0 \quad (2.35)$$

$$E = \{w(t)w(t)^T\} = Q(t)\delta(t - \tau) \quad (2.36a)$$

$$E = \{v_k v_k^T\} = \begin{cases} 0 & k \neq j \\ R_k & k = j \end{cases} \quad (2.36b)$$

Note that the term $v(t)$ in equation 2.35 is the continuous time embodiment of the discrete time measurement noise.

2.5.2 Initialization of the Filter

Of specific interest to the development of any extended Kalman filter is the initial condition of the state vector, and the initial condition of the error covariance expressed in equations 2.37 and 2.38 respectively.

$$\hat{x}(t_0) = \hat{x}_0 \quad (2.37)$$

$$P_0 = E\{\tilde{x}(t_0)\tilde{x}(t_0)^T\} \quad (2.38)$$

The continuous – discrete extended Kalman filter varies from the more traditional linear class of Kalman filters in many ways but the most pressing difference lies in the inability to prove stability of the nonlinear filtering process. Often, stability is proved or accepted when the covariance converges or the state estimator produces 'good' estimates. The implied assumption for this class of nonlinear filters is that the true state is sufficiently close to the estimated state [38]. Along these same lines, the selection of the initial state and covariance is critical for the filter to converge. The goal for the designer is to place the initial conditions close enough to the true state allowing the update process to offset the diverging tendencies of propagating process. For the purpose of this research, the initial conditions placed on the state are as follows:

- The position initial condition is the short circuit voltage of the position sensor, since there is not an object blocking the emitted light the measured portion is the maximum value in the sensor range. The characterization of the position sensor is discussed in section 3.4.
- The initial velocity of the levitated object is set equal to zero.
- The initial current is determined by substituting the appropriate values into equation 2.14 and solving for the equilibrium current.

2.5.3 Measurement Equation

Equation 2.39 allows for nonlinear terms to be used in the measurement equation. Since the Jacobian is taken of the measurement equation, attention needs to

be paid to conditions and parameters that might cause it to become unbounded or exhibit loss of rank condition.

$$H_k(\hat{x}_k^-) \equiv \left. \frac{\partial h}{\partial x} \right|_{\hat{x}_k^-} \quad (2.39)$$

The measurement equation in this research is characterized by a linear relationship between the object position and voltage output of the measuring sensor.

2.5.4 Kalman Gain Equation

For linear Kalman filters, the format of the gain expressed in equation 2.40 minimizes the error associated with the propagated state estimate [38].

$$K_k = P_k^- H_k^T(\hat{x}_k^-) [H_k(\hat{x}_k^-) P_k^- H_k^T(\hat{x}_k^-) + R_k]^{-1} \quad (2.40)$$

For nonlinear systems, certain elements of these systems scale and shift the input Gaussian functions resulting in non-Gaussian responses [39]. *"Estimators for many nonlinear systems can be based on Kalman and Kalman – Bucy filters; though not precisely "optimum" they are "optimal" in the sense that they tend toward optimum. These modified linear-optimal estimators are useful when the stochastic effects are additive and small, either as a result of the original system's structure or of reasonable assumptions regarding magnitudes of these effects. Details of the specific probability density functions may not be well portrayed, but the overall performance in state estimation can be satisfactory for two reasons. The first is that random signals are summed in estimators, and the central limit theorem assures that the probability density functions of the sums tend to become Gaussian no matter what the individual*

distributions look like. The second is that the estimators contain integration or summation, which tends to average out the Gaussian-destroying effects of the nonlinearities in producing the state estimate". [39]

2.5.5 Update Equations

When the discrete time measurement becomes available (equation 2.34) the Kalman gain computed in equation 2.40 updates the propagated estimate, according to equation 2.41. The error signal between the actual and estimated output is multiplied by the Kalman gain that in turn updates the current estimate. This structure for the state observers is very common [40-41]

$$\hat{x}_k^+ = \hat{x}_k^- + K_k [\tilde{y}_k - h(\hat{x}_k^-)] \quad (2.41)$$

$$P_k^+ = [I - K_k H_k(\hat{x}_k^-)] P_k^- \quad (2.42)$$

Along the same lines as the state update (equation 2.41), the covariance (equation 2.42) also makes use of the latest information provided by the system to refine its value.

2.5.6 Propagation Equations

At the end of the estimation process, the updated values must be propagated forward in time to the next measurement update. This is accomplished with equation 2.43 for the plant and equation 2.45 for the covariance.

$$\dot{\hat{x}}(t) = f(x) + g(x) \cdot u(t) \quad (2.43)$$

$$F(\hat{x}(t), t) \equiv \left. \frac{\partial f}{\partial x} \right|_{\hat{x}(t)} \quad (2.44)$$

$$\dot{P}(t) = F(\hat{x}(t), t)P(t) + P(t)F^T(\hat{x}(t), t) + \Psi(t)Q(t)\Psi^T(t) \quad (2.45)$$

Of particular interest is the propagation of the covariance, equation 2.45, which is accomplished using a continuous time linear Riccati equation. As mentioned previously, the Jacobian of the dynamics must be recomputed at each cycle and special attention must be paid to the behavior of this operation.

2.5.7 Filter Tuning

The most practical issue surrounding the development of the extended Kalman filter is the determination of the process noise covariance, $Q(t)$, process noise input, $\Psi(t)$, and measurement noise covariance, v_k . For the purpose of validating the structure of a control and estimation algorithm, reasonable values can be used based on the dynamic model being analyzed using published values and experimental results available in the open literature. However, when the algorithm is taken to the next stage of implementation on hardware, a systematic approach must be undertaken to better characterize these terms based on the available and collected experimental data.

2.6 Conclusions

In this chapter, the development of the feedback linearized nonlinear controller and continuous-discrete time extended Kalman filter are presented as they apply to the open loop unstable, highly nonlinear Maglev system. First, the Maglev dynamics were presented and cast into a suitable format for later manipulation. Then, the relative degree of the nonlinear system was discussed. Subsequently, the necessary and sufficient conditions for the existence of a linearizing diffeomorphism were shown,

allowing for the construction of a linearizing coordinate change and nonlinear feedback that transformed the system into an equivalent linear system. Once the dynamics were cast into a linear system, the closed loop eigenvalues were assigned using the Bass-Gura formula. Then, the nonlinear feedback was augmented such that the controller would track suitable reference trajectories. Since not all of the states are directly available to the controller, a suitable state estimator must be formulated. For this task, a continuous-discrete time extended Kalman filter was proposed. Additionally, the integration of the controller and state estimator showing the information flow are explained.

CHAPTER 3

SIMULATION VERIFICATION AND HARDWARE IMPLEMENTATION

This chapter discusses the validation of the proposed controller / estimator in phases that would allow for simulation verification and hardware implementation. First, the controller and estimator structure and operation were validated in simulation as a proof of concept to justify further development. Second, the simulations were refined using the same structure that would be implemented in hardware with particular attention placed on the propagation of the covariance. Additionally, these refined simulations validated the scheme to be used on the actual hardware. Next, plant noise parameters were tuned off-line using simulations with data taken from the actual hardware. Finally, the controller and estimator were implemented and verified on the actual hardware considering a variety of input reference trajectories.

3.1 Controller / Estimator Simulations

Validation of the feedback linearized nonlinear controller / continuous-time extended Kalman filter structure and their interaction were first examined in simulation using scripts developed in MATLAB following the structure presented in Figure 3.1.

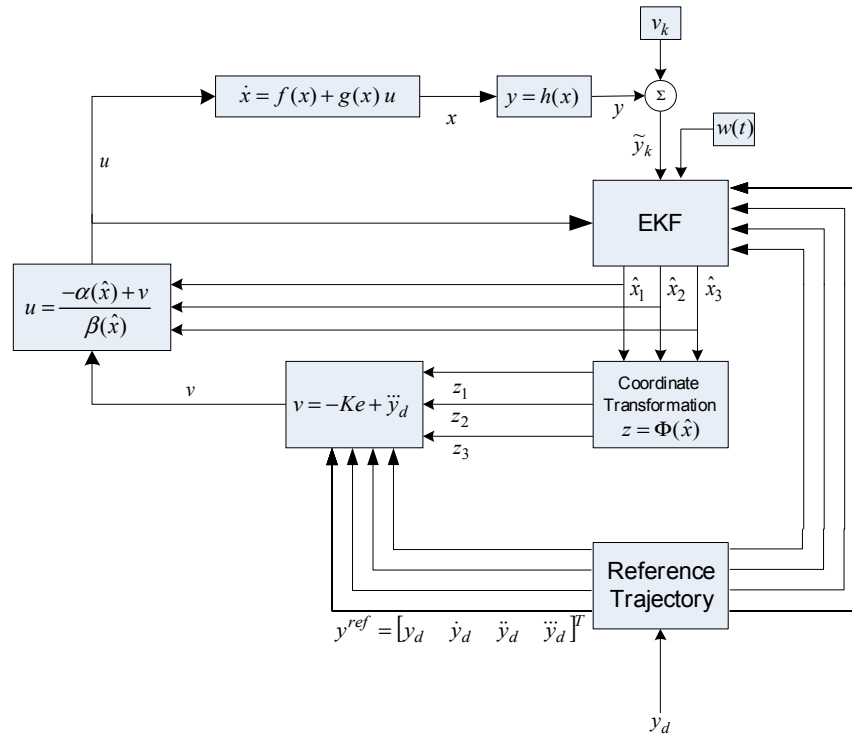


Figure 3.1 Feedback linearized nonlinear controller / extended Kalman filter simulation structure and interoperation.

These simulations represent a 'proof of concept' and were the justification for continued work on this topic. Many of the features used in these simulations are continued through each phase of the implementation process. However, as the phases get closer to the hardware implementation, the structure and system parameters were successively revised and reviewed.

The simulation process is comprised of three distinct phases each relying on the other two phases for information in order to produce well behaved and stable results, a detailed outline of the simulation is presented in Appendix F. First, the plant state is propagated to the next time step and a sub-step of this propagation phase is to calculate

the controller output. It is important to note that the control value is not based on the actual plant state at any time during the simulation, but rather it is determined using the current values of the estimated states. After plant state propagation is complete, the synthetic measurement process is performed. The object position is corrupted using a random noise from a zero-mean white Gaussian distribution with covariance R_k . The final portion of the simulation is to update the state estimate and covariance, and propagate the latest information available to the filter using the updated system values forward to the next time step. However, the state estimate and the covariance estimate are not integrated in the same manner due to some of the simulation infrastructure limitations. The state estimate is propagated forward using the same method as the plant state, a fixed step Runge-Kutta integration scheme. As previously mentioned, the covariance is propagated in a different manner; the simulation used in this portion of the research can not accommodate the 3×3 size of the covariance matrix, allowing for this limitation, only the covariance matrix diagonal terms are used to propagate forward to the next time step. While the plant and state estimates are cast into a continuous-time formulation, the covariance is cast into discrete time format allowing exact representation of the continuous-time covariance at the step time, albeit with only one third of the covariance information used in the propagation.

Table 3.1 Maglev simulation parameters

Simulation Parameter	Symbol	Value	Units
Levitated Object Mass	m	0.055066	Kg
Coil Inductance	L_c	0.59	H
Incremental Coil Inductance	L_0	0.02	H
Coil Resistance	R_c	25.0	Ω
Gravitational Constant	g	9.81	m/sec
Simulation Time Step	dt	0.001	sec
Measurement Noise Standard Deviation	v_k	0.001	m
Plant Initial Condition	x_1, x_2, x_3	0.0148, 0, 0.89409	$m, m/sec, A$
Estimator Initial Condition	$\hat{x}_1, \hat{x}_2, \hat{x}_3$	0.014367, 0, 0.9388	$m, m/sec, A$
Desired Closed-Loop Poles	η_1, η_2, η_3	-60, -80, -100	
Covariance Initial Condition	p_0	0.085 I	
Process Noise Covariance	$Q(t)$	0.025 $\begin{bmatrix} 0 & 0 & 0 \\ 0 & 1 & 0 \\ 0 & 0 & 1 \end{bmatrix}$	

The core structure of these simulations is based on example 5.5 found in [38], and the m-file can be found on the website maintained by the author [42]. The simulation parameters are based on the values determined by [45], and can be found in Table 3.1. These parameters will remain unchanged unless otherwise noted.

3.1.1 Fixed Step Numerical Integration

Many options are available for the integration of ordinary nonlinear differential equations. In particular, the widely accepted Runge-Kutta 4th-order fixed-step-size integration is considered for all phases of this work (m-file, Simulink and xPC). The script containing the m-file embodiment of this scheme can be found in Appendix F, while the version used for the simulations in Simulink and consequently xPC can be found in the Simulink documentation on the MathWorks website [44]. The selection of initial conditions and integration step-size are often critical selection parameters for successful simulations. These parameters must be adjusted during simulation and experimentation.

A variable-step Runge-Kutta integration scheme produces efficiencies over the fixed-step method upwards of several orders of magnitude; however, the controller and estimator equations are not setup for a variable-step approach. Additionally, the goal of the simulation was to stay true, in as many ways as possible, to how the actual hardware system would operate, thus, a fixed-step approach is consistent with the operation of an embedded microprocessor and the xPC environment used for hardware implementation.

3.1.2 Step Input Response

The Maglev response to a step input is discussed in this section. For the purposes of these simulations, the system is allowed to converge to a steady state after the initial filter and controller transient response, and then the step input is applied via the reference trajectory. The step trajectory used in this simulation is 2.0 mm change in the position of the levitated object. The measurement noise covariance used in the

simulations is shown in Table 3.1. The process noise, $Q(t)$, off diagonal terms are set to zero since the noise is assumed to be uncorrelated and zero mean Gaussian white-noise. The first term in the $Q_{1,1}$ position is also set to zero since an exact kinematic relationship is being represented, owing to the fact that the velocity is defined exactly as the position time rate of change. The coefficient preceding $Q(t)$ in Table 3.1 was found by iterating the simulations until a consistently stable state estimate was observed.

The simulated measured position, reference trajectory and estimated trajectory of the Maglev system responding to a 2.0 mm step input are illustrated in Figure 3.2. It is observed that the simulated measurement and filter estimated position of the object oscillate about the nominal trajectory after the transient response has decayed. As expected with simulated noisy measurements, the measured position of the levitated object will never correspond to the reference trajectory at any time in the simulation time. While the estimated position will exhibit much of the noisy tendency of the simulated measured position, it does exhibit smoother response, since the extended Kalman filter seeks to minimize the error state estimate. The simulated Maglev response to a step input presented in Figures 3.2 – 3.6 validate the controller, estimator and their interoperation structure represented in Figure 3.1.

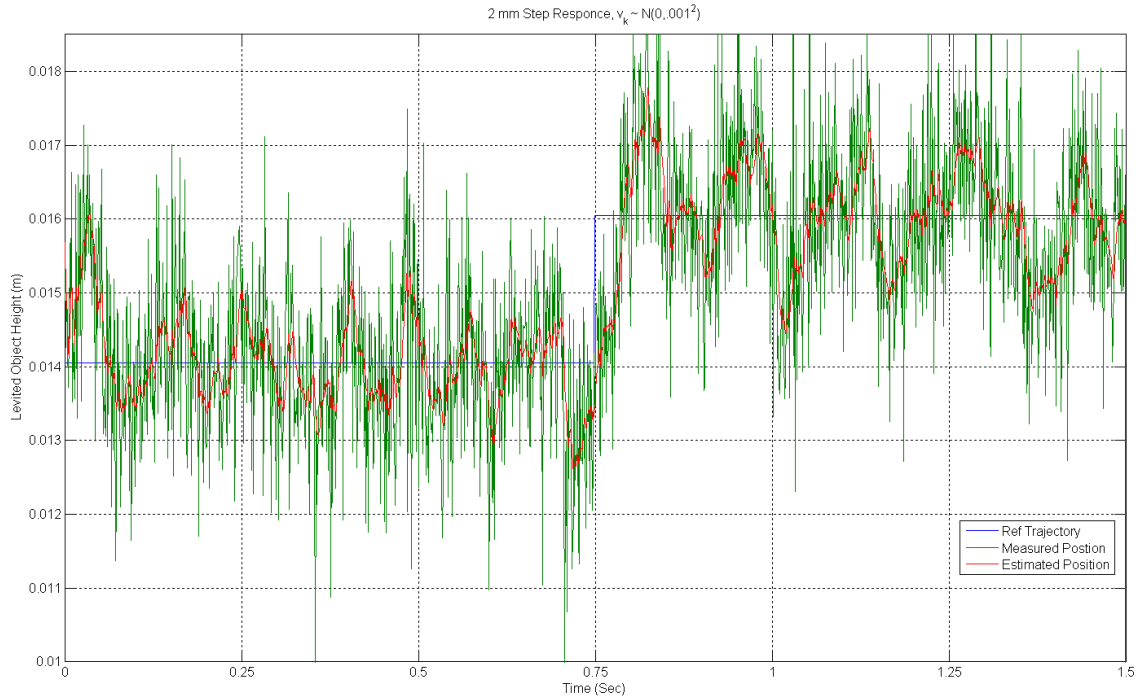


Figure 3.2 Maglev simulated system measured position response, estimated position response to a 2.0 mm step input

When comparing the quality of the estimates produced by an extended Kalman filter it is useful to compare the difference between the actual state value and the state estimate, as shown in equation 3.1.

$$\tilde{x}_1 = x_1 - \hat{x}_1 \quad (3.1)$$

The quality of the estimate can also be computed since it is directly used in the filtering scheme. The square root of the position error covariance produces the position error standard deviation and places a bound on the position error. A $\pm 3\sigma$ standard deviation bounds produced by the filter is plotted along with the position estimate error. This $\pm 3\sigma$ bounds is a confidence interval on the error estimate. The smaller $\pm 3\sigma$ bounds on position error, the higher quality estimate being generated by the

optimal state estimator. The position error of the Maglev when tracking a 2.0 mm step with the $\pm 3\sigma$ error bounds is presented in Figure 3.3. Two note worthy items of the position estimate error occur when the step change occurs at $t = 0.75$ sec . The first item is that the reference trajectory exhibits a singularity when the simulation time reaches the step time. When the filter is left to differentiate the step reference position trajectory a singularity does occur and the controller / estimator diverge. On the surface this violates the conditions for derivative continuity of the reference input developed in 2.3. To accommodate this situation the derivatives of the reference trajectory are defined equal to zero for this series of simulations, thereby eliminating the potential for the singularity to exist. The second item to note at this time is due to the position error and the standard deviation. The sudden change in the position does not cause the quality of the estimate to degrade and the position error is comparable to the rest of the filter performance.

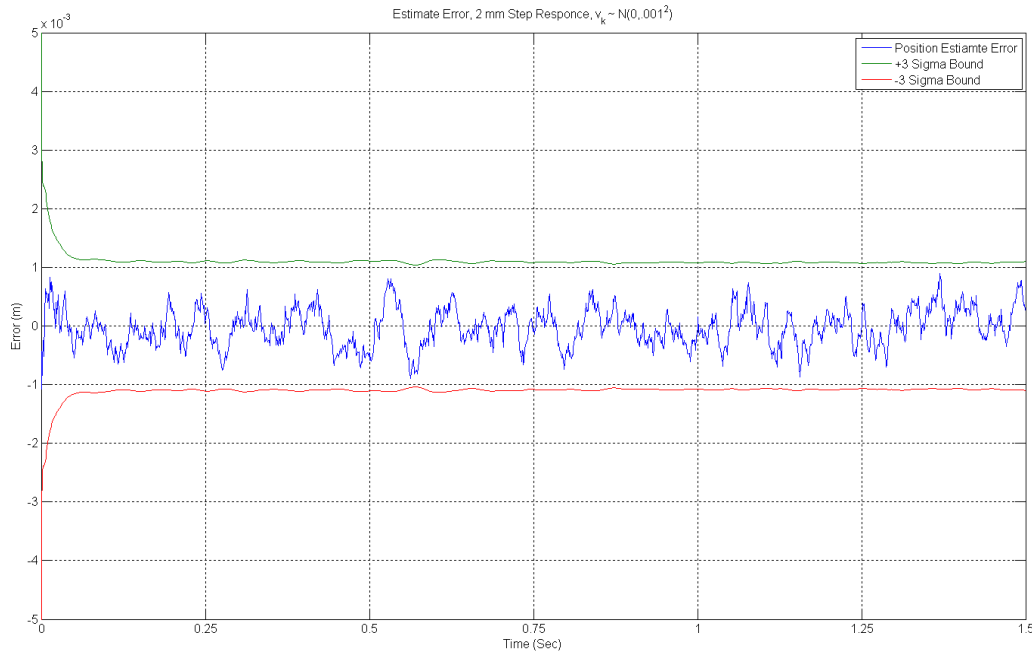


Figure 3.3 Maglev simulated position estimate error response and $\pm 3\sigma$ error bounds to a 2.0 mm step input

Figure 3.4 shows the performance of the extended Kalman filter for estimating the suspended object velocity although it can not be directly measured on the hardware and consequently is not synthetically measured in simulation. The differential velocity associated with the actual time instant of position change was omitted from the simulation as mentioned earlier since this discontinuity caused unbounded behavior in the simulation. Behaviorally speaking, the shape of the velocity estimate about the zero velocity reference trajectories corresponds with the position hunting about its trajectory.

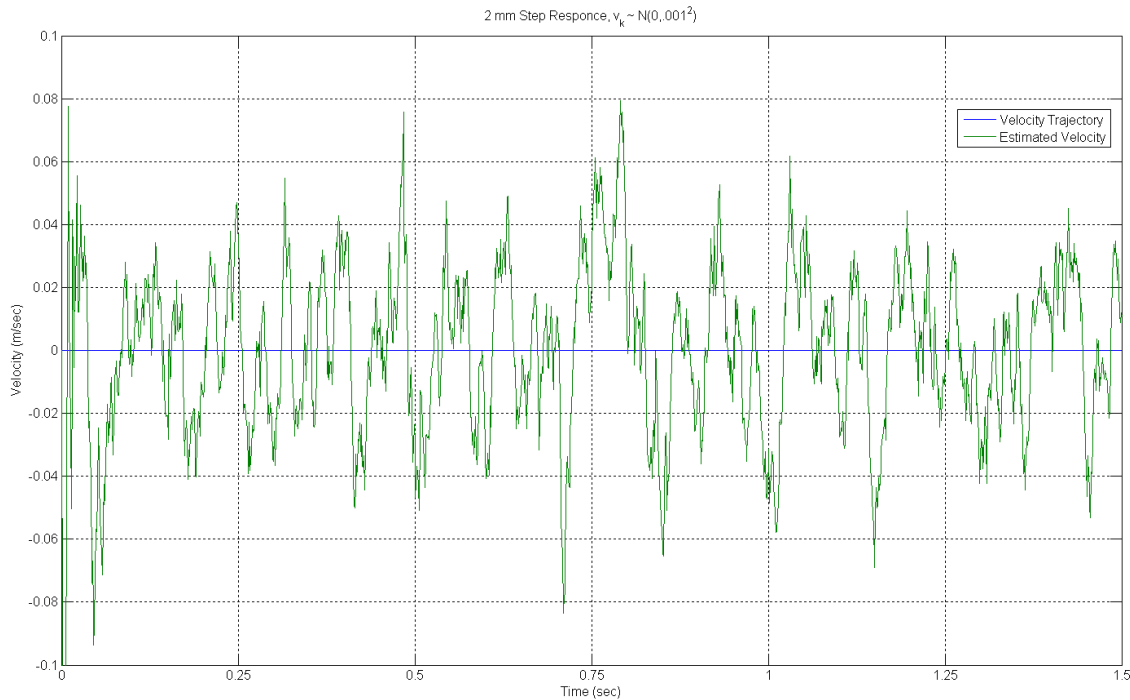


Figure 3.4 Maglev system estimated velocity response to a 2.0 mm step input

The velocity estimate error can be characterized in the same manner as the position estimate error. The simulated velocity error plotted along with the velocity error bounds at $\pm 3\sigma$ is shown in Figure 3.5. The bounds of the velocity error covariance when compared with the position error covariance are approximately an order of magnitude greater. Not measuring this state directly adds significantly to the degradation of the estimate quality.

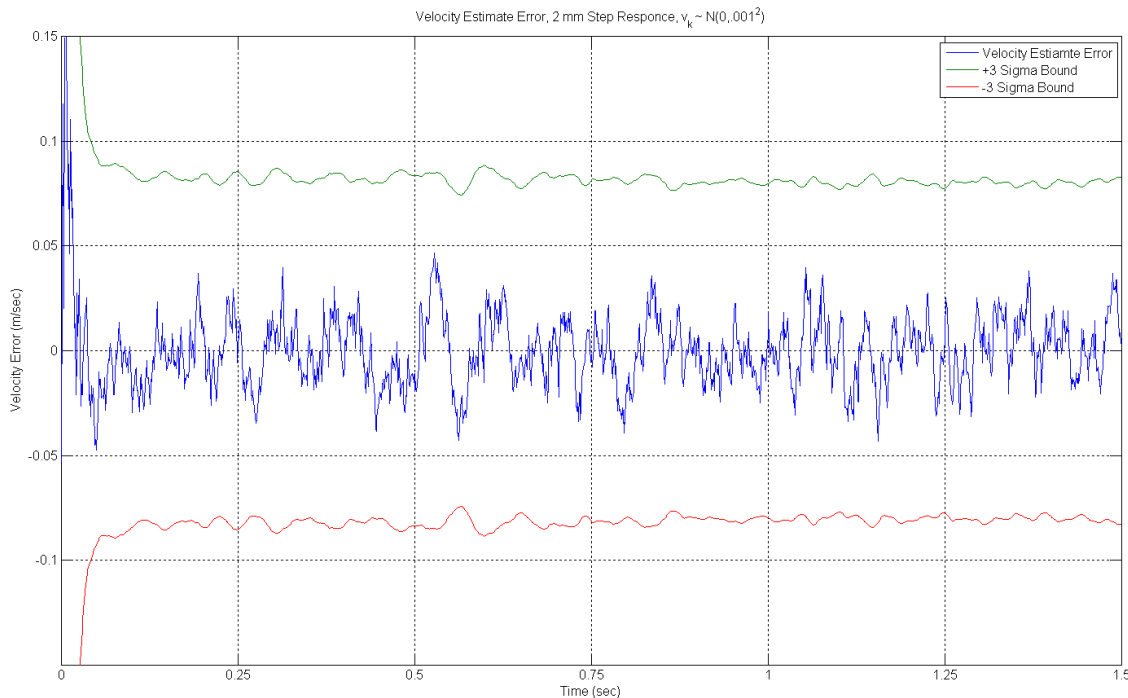


Figure 3.5 Maglev simulated velocity estimate error response and $\pm 3\sigma$ error bounds to a 2.0 mm step input

The extended Kalman filter also estimates the current used in the electromagnetic coil during the simulation. The change in coil current corresponding to the change in reference trajectory and simulated measured object position is illustrated in Figure 3.6. The oscillatory behavior of the coil current (and the other state estimates) is attributed to two significant types of behaviors. The first behavior stems from the control input calculated by the controller based on the estimated state of the system as mentioned earlier in this section. The second behavior lies in the inclusion of noise in the simulation process. In the unlikely event that the actual position is identically equal to the reference trajectory, the measurement noise will generate an error signal. Added to this effect is the plant noise that further complicates the estimate.

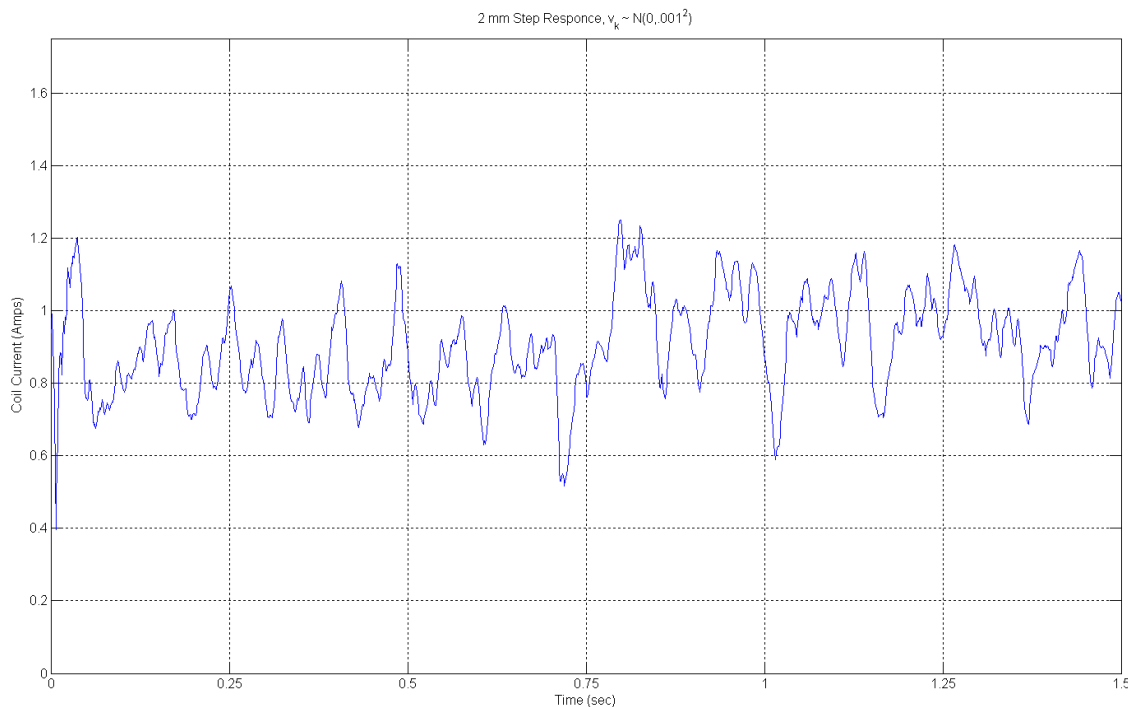


Figure 3.6 Maglev estimated current response to a 2.0 mm step input

3.1.3 Sine Wave Response

The performance of the feedback linearized controller and extended Kalman filter to track a sinusoidal trajectory about a nominal operating point is discussed in this section. The sine wave has amplitude of 1.0 mm and a frequency of 10 rad/sec with a nominal position of 14.8 mm yielding a nominal current of 0.894 A. The remaining simulation parameters remain unchanged from Table 3.1. Figure 3.7 shows the sinusoidal reference trajectory, measured position of the ferromagnetic object and the estimated position. The position estimate error along with the $\pm 3\sigma$ bounds illustrating the quality of the estimate is also presented in Figure 3.7 for completeness. It is observed that the controller can adequately track the reference signal.

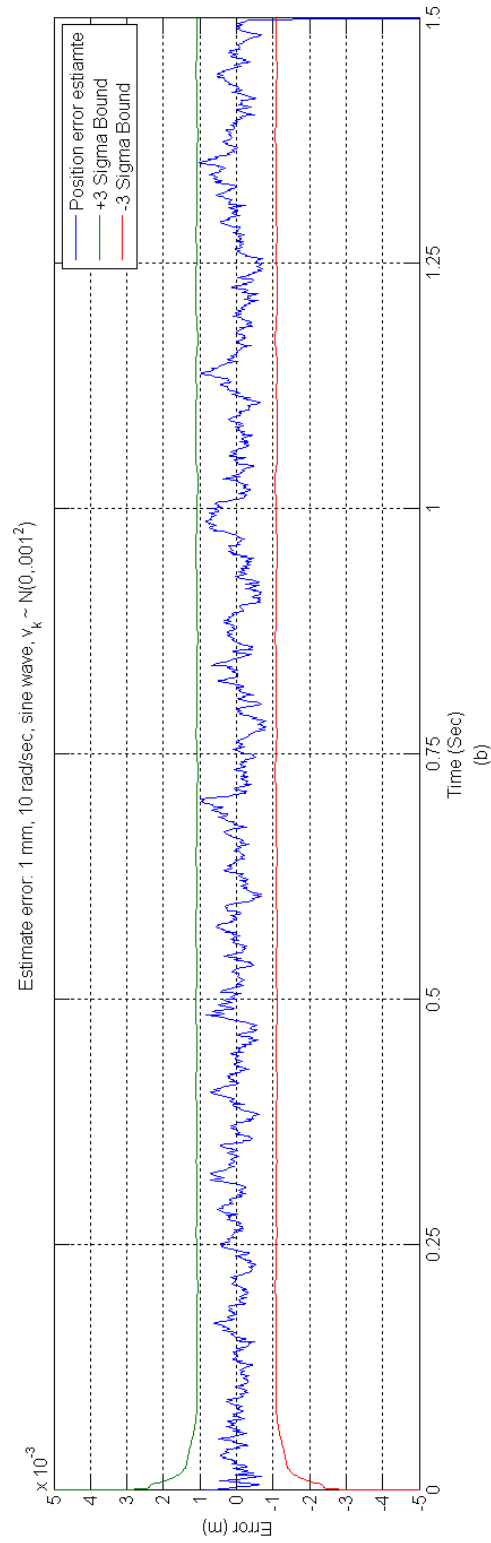
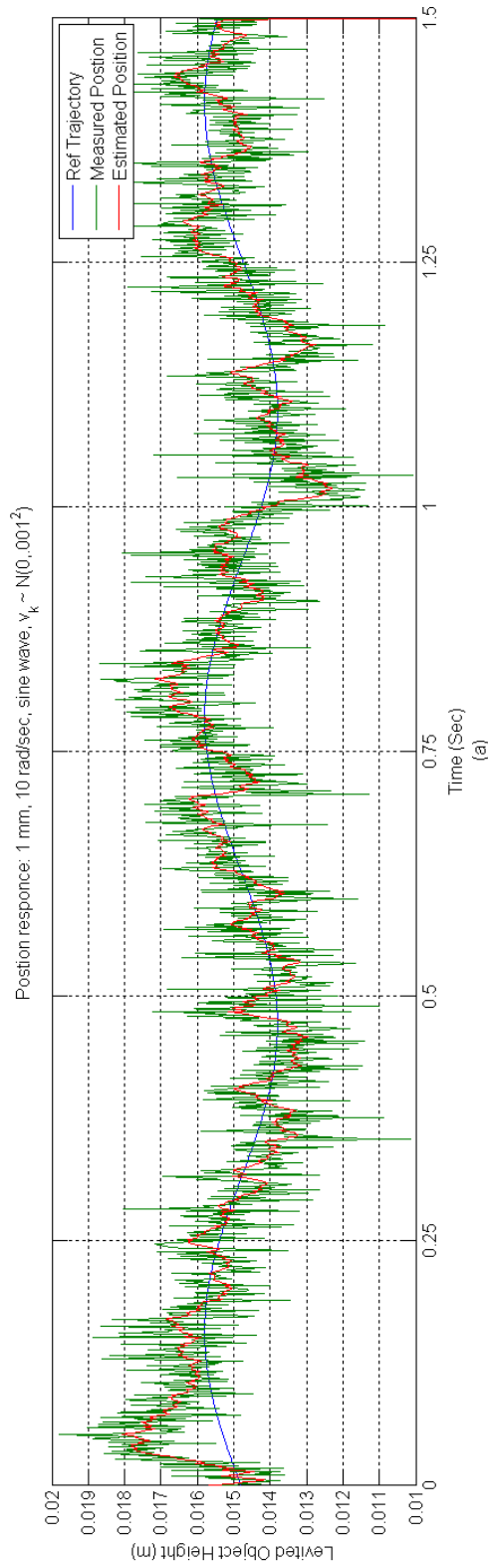


Figure 3.7 (a) Maglev simulated system measured position response, estimated position response to a 1.0 mm, 10 rad/sec sine wave and (b) position error estimate with error bounds

Figure 3.8 shows the performance of the extended Kalman filter for estimating the suspended object velocity when the position is tracking a 1.0 mm amplitude, 10 rad/sec sinusoidal reference trajectory. For this series of simulations the velocity has a nontrivial trajectory since the reference trajectory considered has well defined derivatives. This state variable can not be directly measured on the hardware and consequently is not synthetically measured in simulation but is estimated. The velocity estimate produces a lower quality estimate when compared with the position estimate. However, the velocity estimate error produces approximately the same quality of estimate when compared against the step input velocity estimate error illustrated in Figure 3.5. Behaviorally speaking, the shape of the velocity estimate about the reference velocity trajectory correlates with the position hunting about its trajectory. The velocity error estimate and its error bounds in addition to the velocity estimate and its reference trajectory are presented in Figure 3.8.

The extended Kalman filter also estimates the current used in the electromagnetic coil during the simulation. The current estimate corresponding to the simulated measured position tracking the reference trajectory is presented in Figure 3.9. The same behaviors discussed for the current estimate in section 3.1.2 are observed, with the notable exception that the state estimates have to constantly make adjustments in order to track the sinusoidal trajectory. It is important to note that in previous simulations the states were allowed to progress past the transient response before the step change is introduced, where in these simulations the system is forced to track the input signal and respond to the transient response.

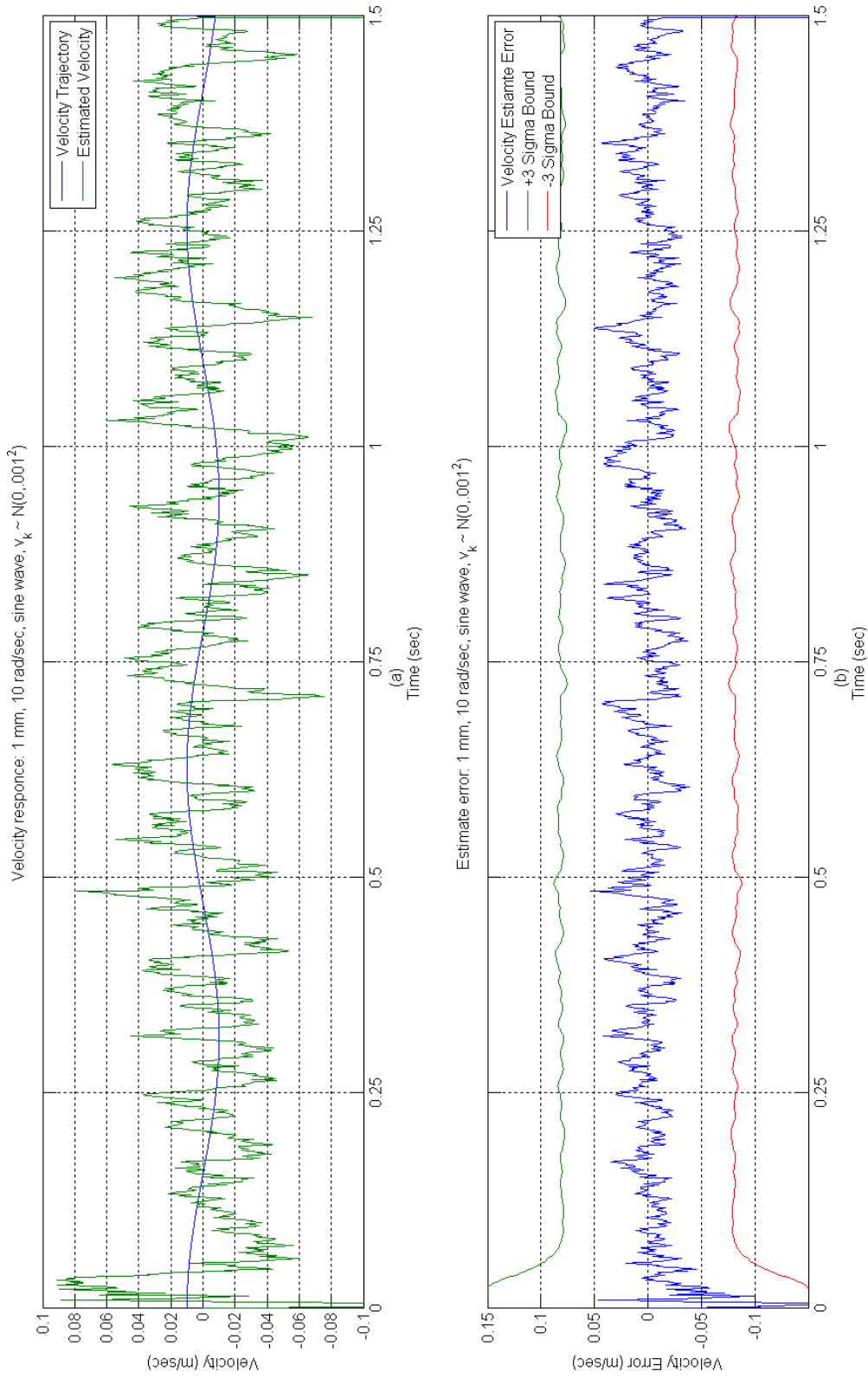


Figure 3.8 (a) Maglev simulated system velocity response, and estimated position response to a 1.0 mm, 10 rad/sec sine wave and (b) velocity error estimate with error bounds

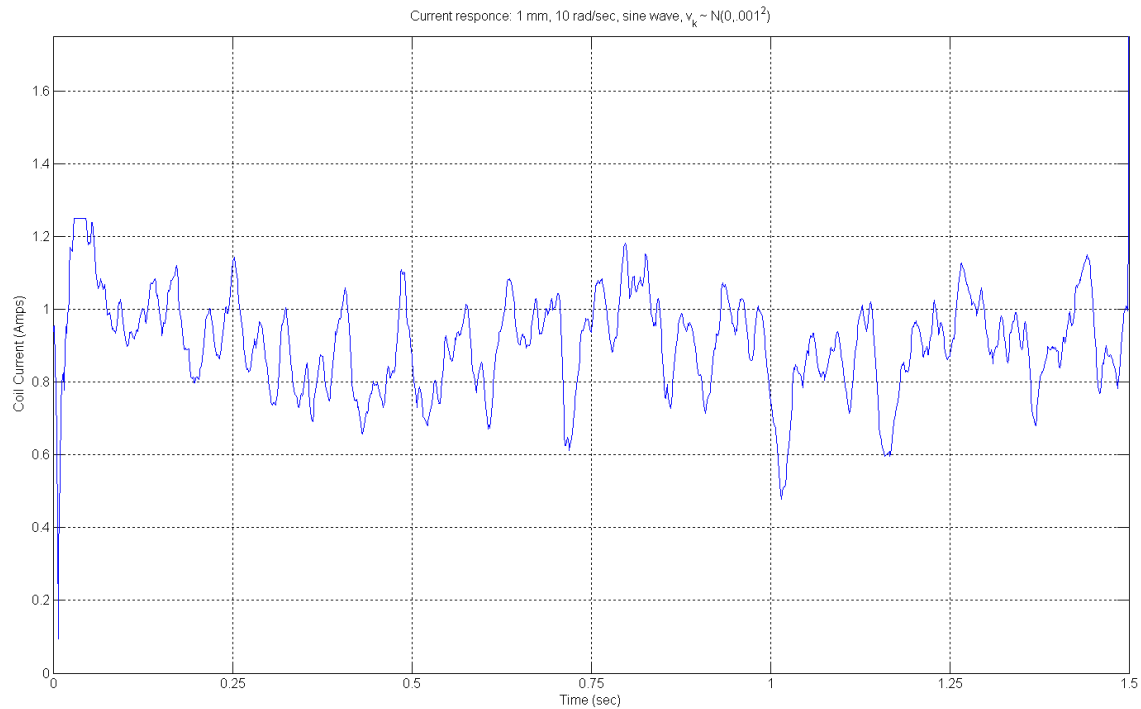


Figure 3.9 Maglev estimated current response to a 1.0 mm, 10 rad/sec sine wave

3.2 Enhanced Controller / Estimator Simulations

Validation of controller and estimator algorithm in section 3.1 is an important first step in the development process but to take this work closer to hardware implementation the algorithms proposed needed to be recast in the Simulink environment for xPC conformity.

3.2.1 Simulink Controller / Estimator Algorithm Structure

Several modifications had to be made to the structure of the simulation procedure outlined in Appendix E to accommodate the Simulink kernel. The first major departure is the method in which the controller, estimator and plant values are calculated. Taking full advantage of the Simulink Solver requires that the dynamics be

cast into the standard S-function format. All three major aspects of this work were appropriately cast in a S-function format but it was found that MATLAB's Real-Time Workshop (RTW) [43] could not compile these MEX based S-functions into an xPC executable. The controller and estimator were converted into an embedded m-file function [44] which can be compiled by RTW into an xPC executable. This allowed the code developed in these embedded m-files to be used in the implementation phase of this work. The embedded m-file function scripts used in these simulations are contained in Appendix G. The Simulink model used in these simulations is shown in figure 3.10. The values for the simulation parameters are contained in Table 3.1 and remain unchanged unless otherwise stated.

Recasting the m-file based simulation into the Simulink environment allowed the covariance to be reformulated. As mentioned in section 3.1 the state estimator proposed in these simulations is a continuous-time extended Kalman filter (CEKF). Due to the limitations of the m-file based simulations the covariance was changed to a discrete time formulation and only the diagonal elements of that matrix were propagated to the next time step. In the simulations presented in this section, the covariance is propagated in the same fashion as the plant and state estimate, using a standard 4th order Runge-Kutta fixed step solver found in Simulink xPC. Procedurally, the covariance being cast into a continuous-time formulation agrees with the embodiment of the plant, controller and state estimate which are all continuous-time representations. However, this change in the format and structure of the covariance allows for the off diagonal elements to have an impact on the state estimate.

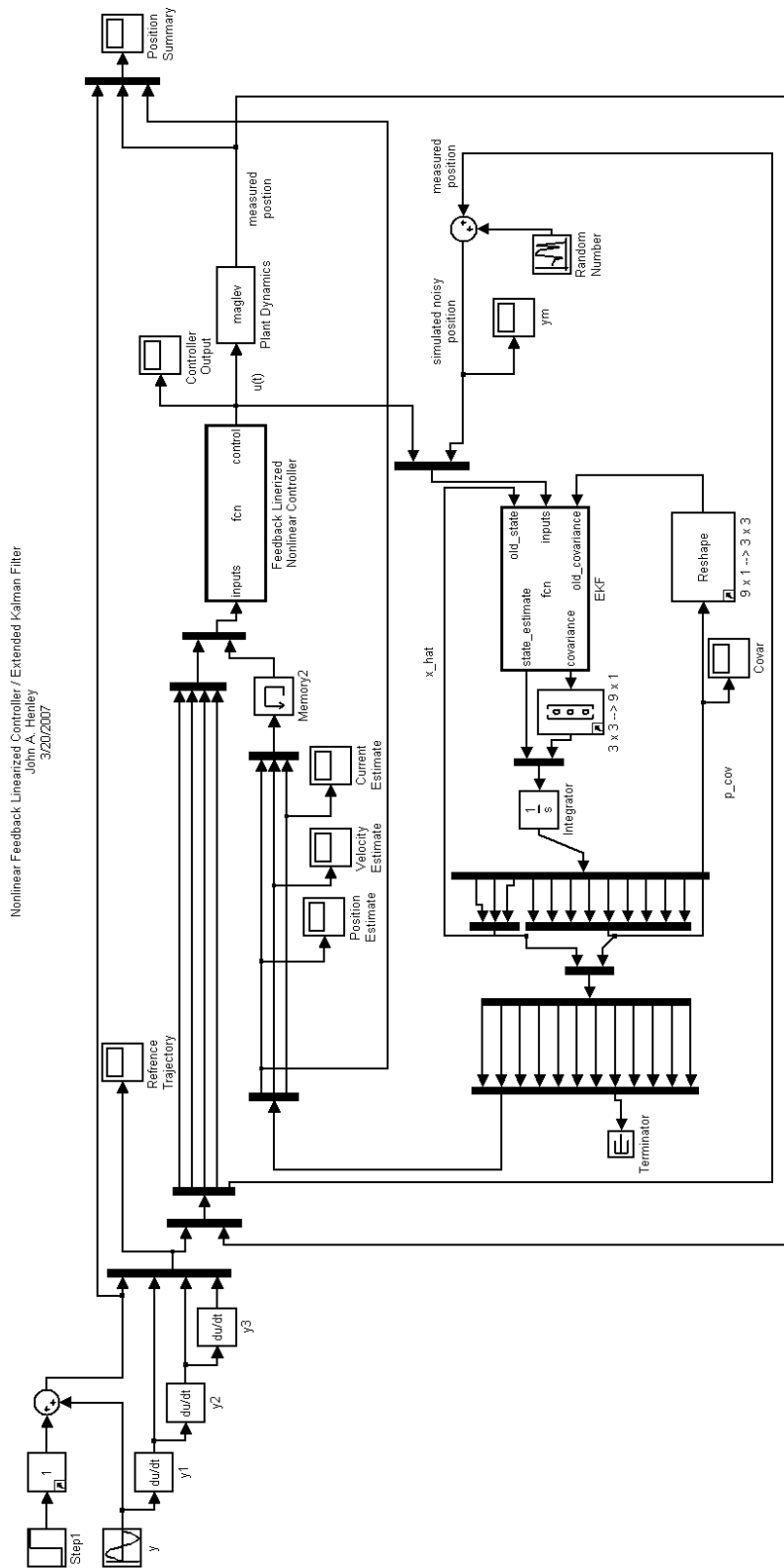


Figure 3.10 Simulink model for enhanced feedback linearized nonlinear controller and extended Kalman filter

3.2.2 Step Input Response

For consistency between the different simulations presented in this research, the same reference trajectory was applied to the enhanced Simulink simulations as the m-file based simulations. The simulated measured position, reference trajectory and estimated position are presented in Figure 3.11 as the Maglev responds to a 2.0 mm step input. Based on the simulated measurements, and the state estimate presented in the figure, the enhanced simulation produces acceptable results using the parameters presented in Table 3.1. The simulated system response is virtually indistinguishable from the simulated system response presented in Figure 3.2. While the simulated measured position appears to track the reference trajectory suitably well, this tracking performance does not address the quality of the estimate produced by the extended Kalman filter. The position estimate error along with a $\pm 1\sigma$ error bounds is presented in Figure 3.11. These error bounds were relaxed from $\pm 3\sigma$ used in the previous section to $\pm 1\sigma$ since the error standard deviation produced by the extended Kalman filter increased by a factor of 30. This difference is attributed to a higher fidelity model of the Simulink estimator; where the Simulink version propagates the entire covariance matrix but the m-file only propagates the diagonal elements of the error covariance. While the error bounds on the position estimate error have significantly increased, the actual error between the state estimate and the synthetic plant state has not increased by the same margin. Ideally the plant noise covariance should be tuned to reduce the bounds on the estimate error, but this parameter was left unchanged from the previous set of simulations in order to provide a baseline for comparing the two sets of simulations. In subsequent sections the actual plant noise will be tuned using actual hardware data.

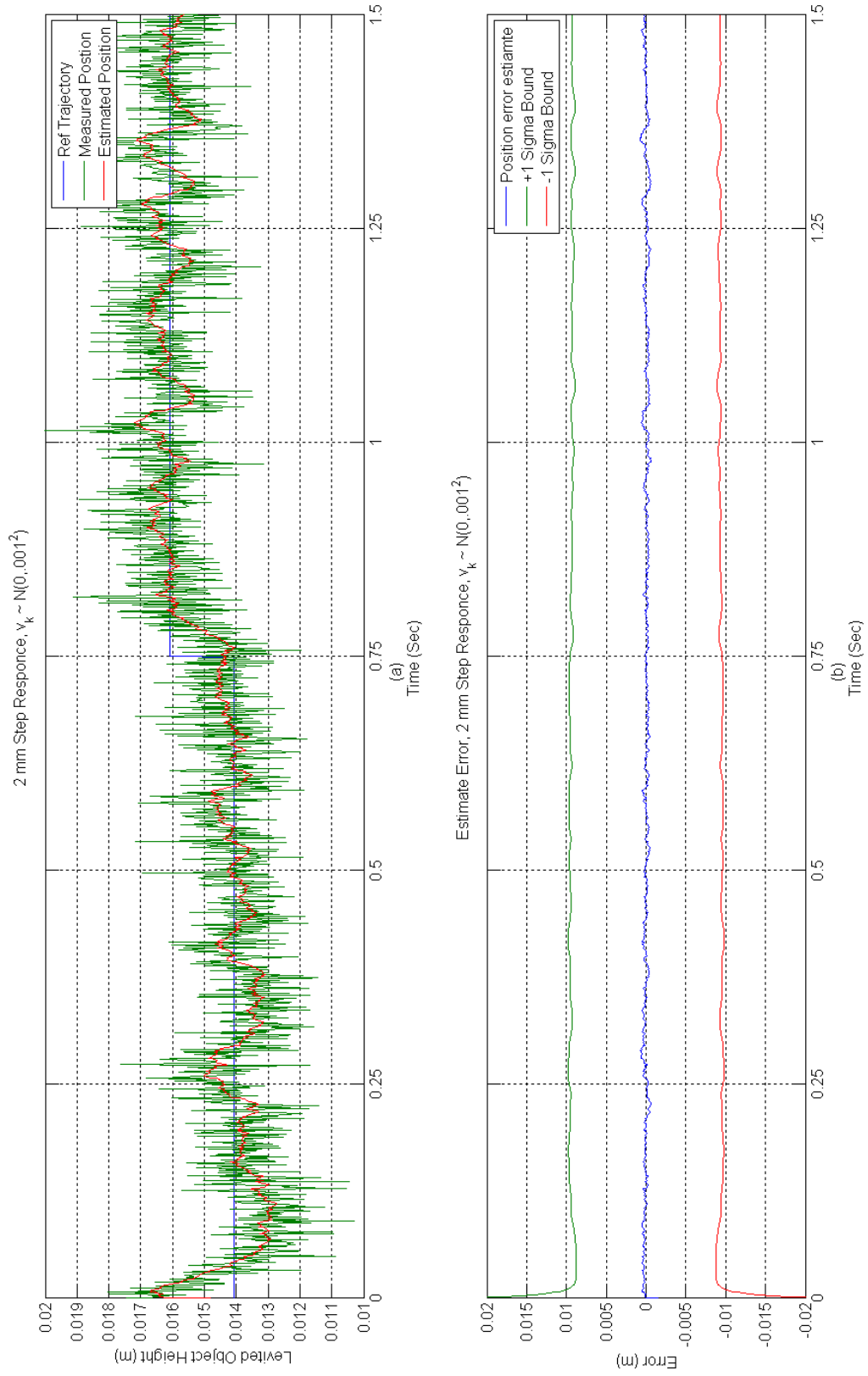


Figure 3.11 (a) Maglev simulated system measured position response, estimated position response to a 2.0 mm step input and (b) position error estimate with error bounds

The velocity estimate and velocity estimate error evaluated by the extended Kalman filter are shown in Figure 3.12. The velocity estimate error and the corresponding error bounds are shown as a gauge for the relative quality of the estimate. Note that the error bounds increase from the initial conditions and converge to a larger values. The error boundary illustrated in the figure was modified to reflect a $\pm 1 \sigma$ bound instead of the more conventional $\pm 3 \sigma$ bound. Although the error bounds are greater than the corresponding results produced by the m-file based simulation (see Figure 3.5), the actual estimate error does not increase accordingly. This behavior is also attributed to the higher fidelity in the Simulink model and the need to perform plant noise covariance tuning. As mentioned in section 3.1.2 the reference input needs to have a sufficiently differentiable form, and examination of the Simulink model presented in Figure 3.10 does not allow a singularity from a step change to cause an unbounded response.

The extended Kalman filter also estimates the current used in the electromagnetic coil during the simulation. The change in coil current corresponding to the change in reference trajectory and simulated measured object position is illustrated in Figure 3.13. The oscillatory behavior of the coil current is attributed to the controller tracking the reference input while the estimates are being perturbed by both the induced measurement and plant noise.

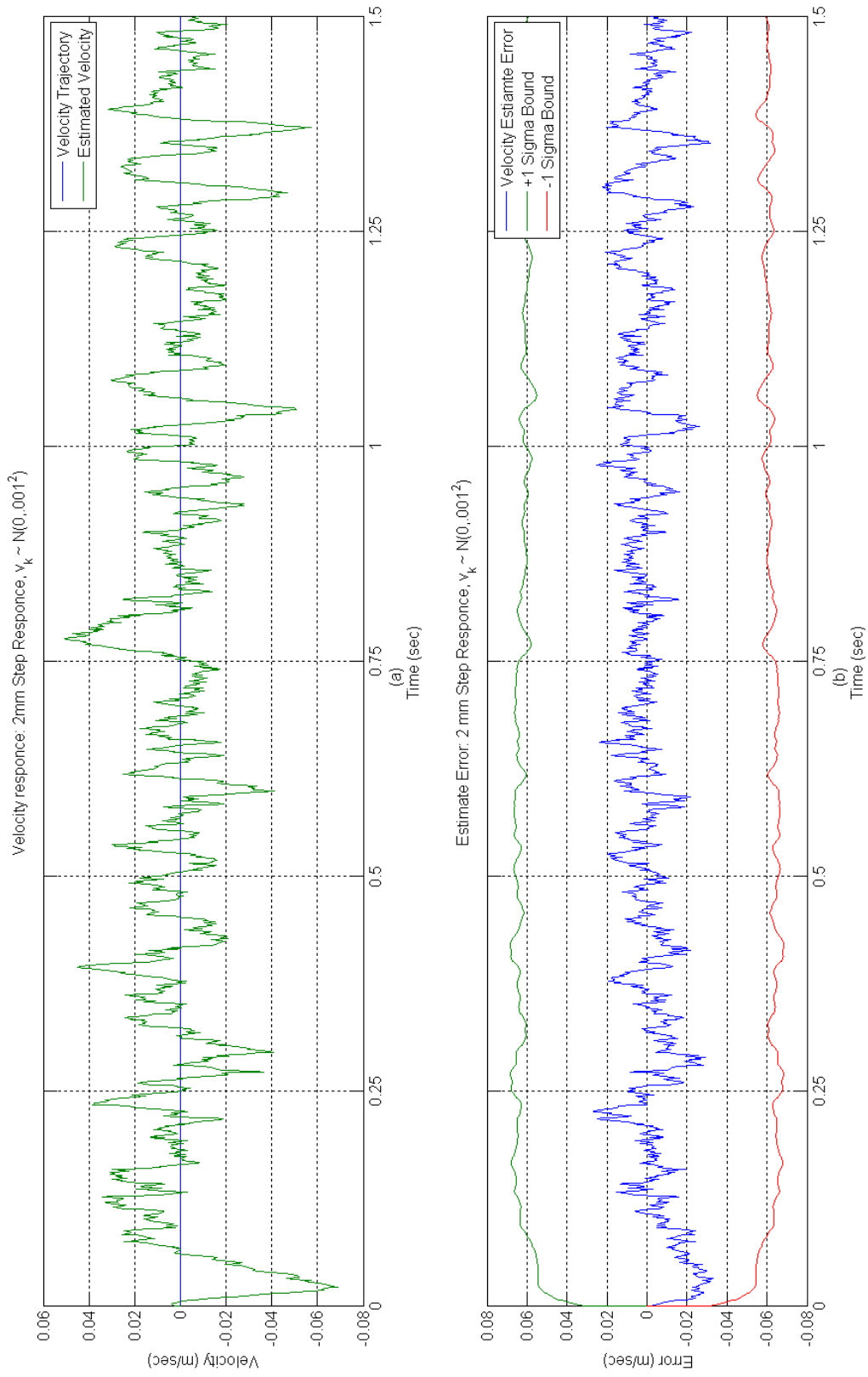


Figure 3.12 (a) Maglev simulated system velocity response, and estimated position response to a 2.0 mm, step input and (b) velocity error estimate with error bounds

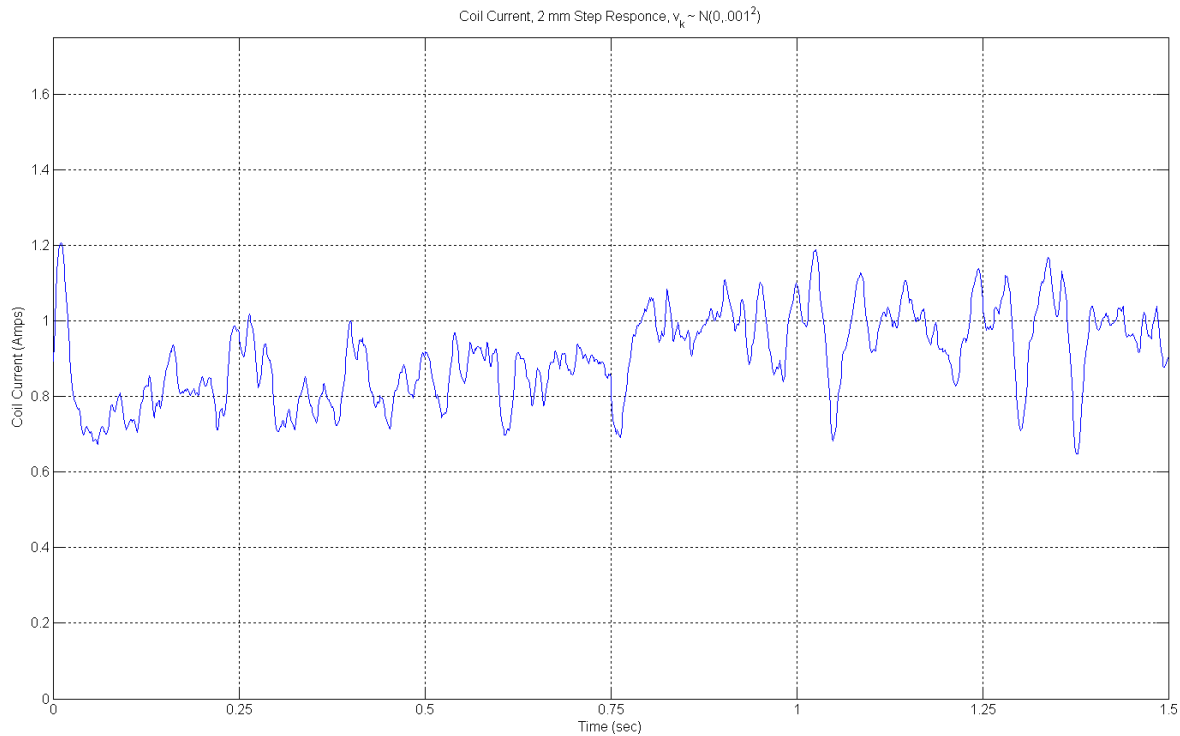


Figure 3.13 Maglev estimated current response to a 2.0 mm step input

3.2.3 Sine Wave Response

As mentioned in section 3.2.2 the same reference trajectory is supplied as an input in this set of simulations so that comparisons can be drawn between the simulations discussed in section 3.1.3. Figure 3.13 shows the measured position, estimated position and reference trajectory considered in this series of simulations. Figure 3.13 also shows the position estimate error and the associated position error bounds. The performance of the estimate error and the bounds on the estimate error agree with the results discussed in section 3.2.2.

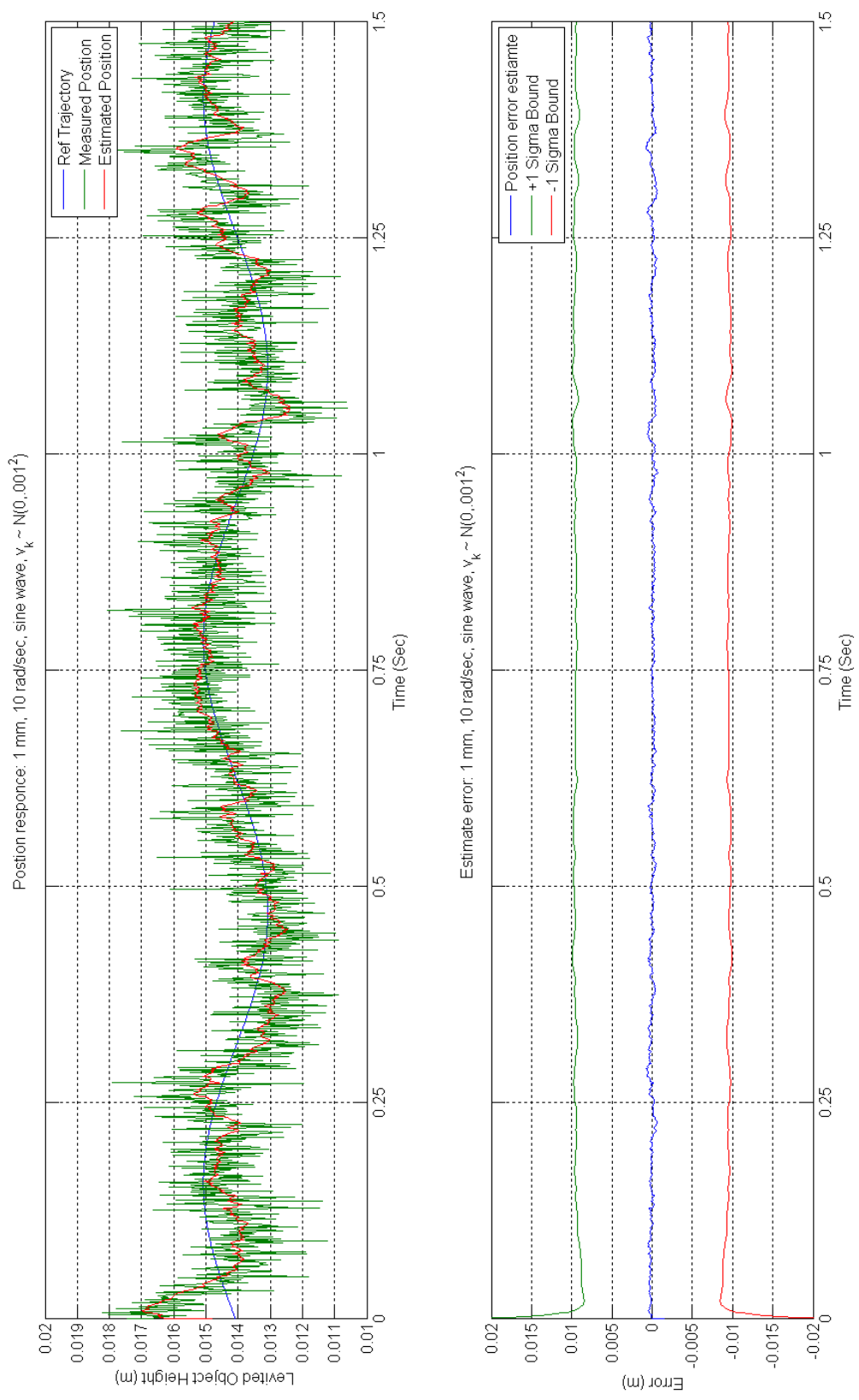


Figure 3.14 (a) Maglev simulated system measured position response, estimated position response to a 1.0 mm, 10 rad/sec sine wave and (b) position error estimate with error bounds

The estimated velocity and velocity trajectory associated with the sinusoidal input is presented in Figure 3.15. Note the relatively poor quality of the velocity estimate response in the simulation. This is expected since the velocity is not directly measured but is a synthetic state generated inside the filter. The velocity estimate error and the associated error bounds are also presented in Figure 3.15 as a means of comparing the relative filter performance. The velocity error bounds is quite significant; when compared to the m-file based simulation shown in Figure 3.8, the boundary is 27 times greater. This increased error bounds is attributed to the improved model of the filter covariance and the need to tune the plant noise covariance to suit the revised covariance formulation. While the error bounds significantly increased, the actual velocity estimate error had the same magnitude of response as the m-file based simulation as shown in Figure 3.8.

Figure 3.20 shows the simulated estimate response of the coil current to the levitated object tracking the sinusoidal reference trajectory. In the initial portion of the simulation the current briefly becomes negative. This small excursion of the current into negative values is attributed to transient response of the controller and state estimator. On the surface this does violate the conditions placed upon the region of state space that the system is allowed to operate without violating the necessary and sufficient conditions of the nonlinear controller. The actual state space region that must be observed is attributed to the actual state not the estimated state. This occurrence is not possible on the hardware due to the diode configuration across the coil, preventing a reversal of current.

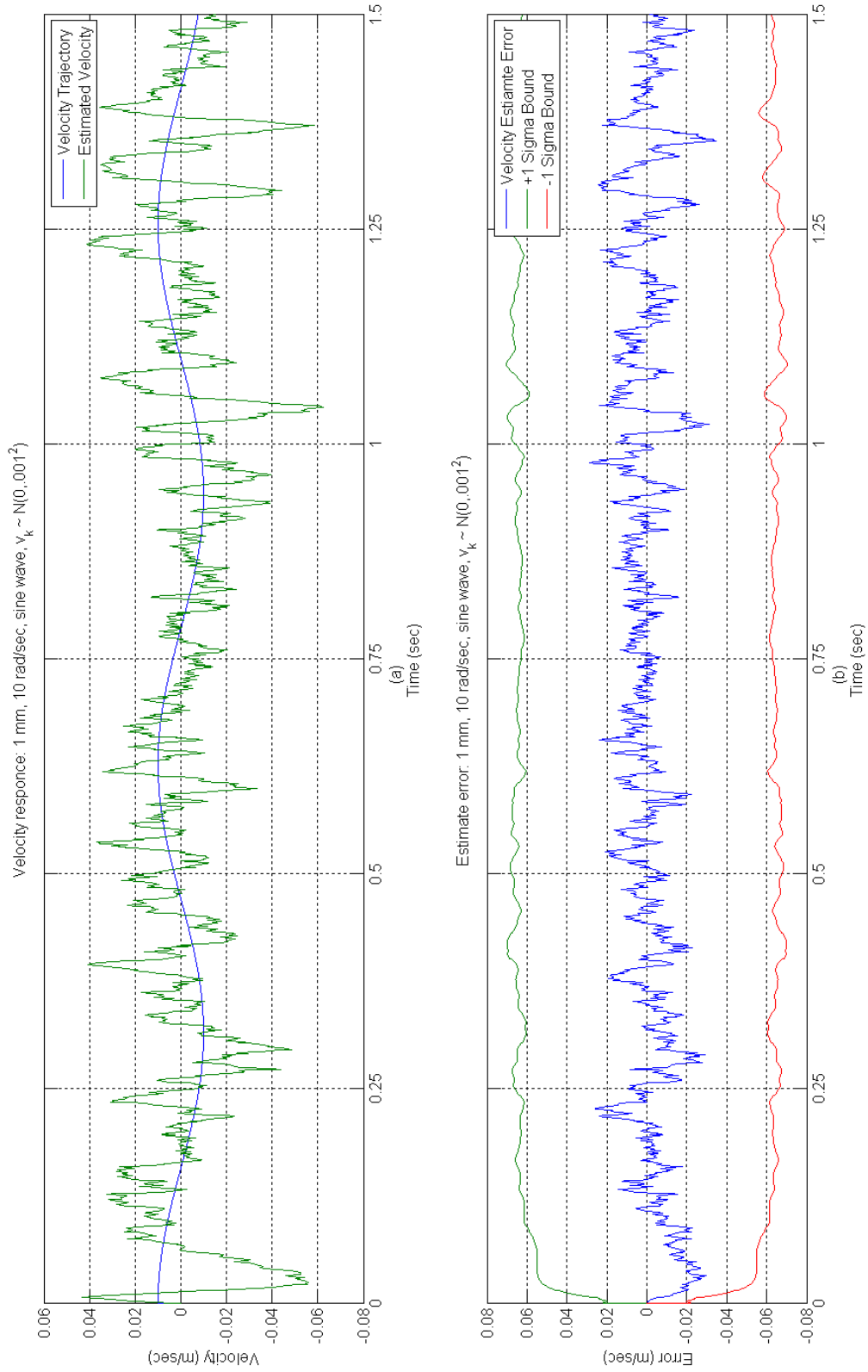


Figure 3.15 (a) Maglev simulated system velocity response, and estimated position response to a 1.0 mm, 10 rad/sec sine wave and (b) velocity error estimate with error bounds

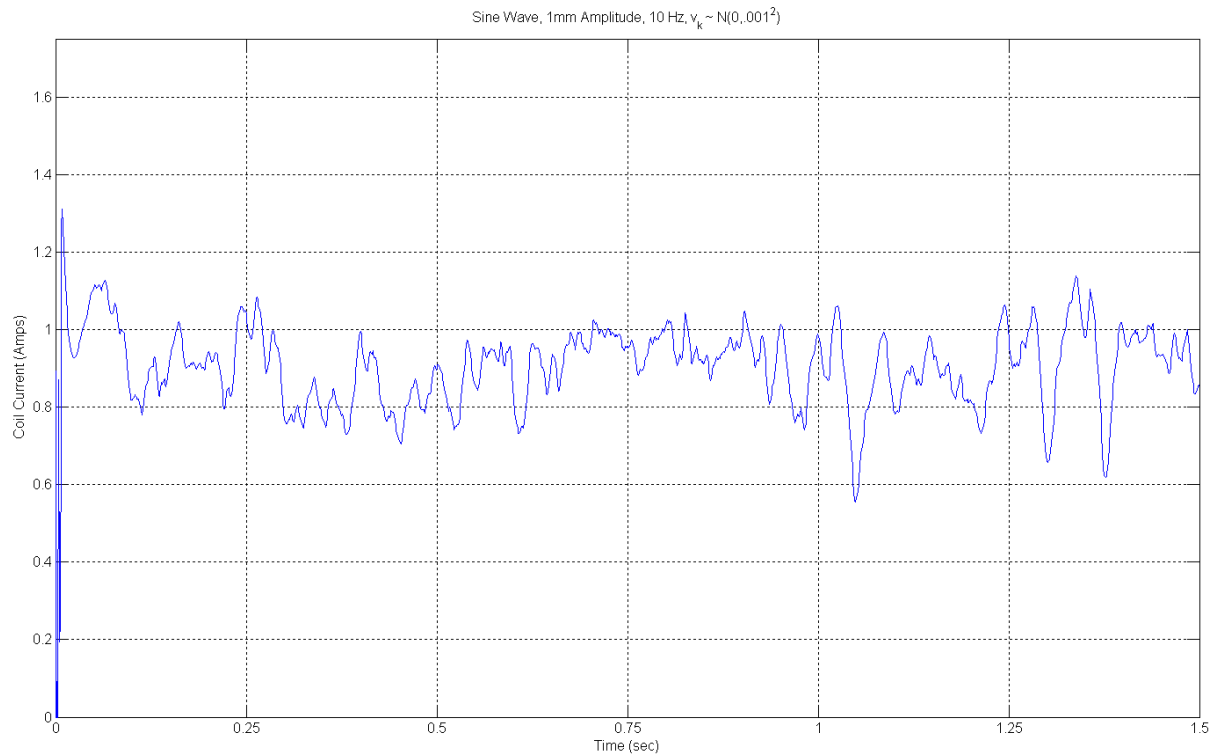


Figure 3.16 Maglev simulated system current response to a 1.0 mm, 10 rad/sec sine wave

3.3 Position Sensor Modeling

Sensor Modeling is required in order for the Simulink model to properly interpret the input from the hardware system. For the purposes of this research, the sensor measures the air gap between the levitated object and the bottom of the electromagnet coil. Proper understanding of the relationship between the levitated object position and the sensor output is required due to the fact that the position of the object is the state of the system being controlled. Therefore, the input-output relationship for the sensor in conjunction with the ferromagnetic object levitated in this research needs to be characterized.

The relationship between the sensor output voltage is easily determined experimentally. The ferromagnetic object levitated is a steel ball bearing with a measured diameter of 1.905 cm and a mass of 0.05506 Kg as shown in Figure 3.17.



Figure 3.17 Levitated object, steel ball bearing

To obtain the experimental sensor to voltage response the ball bearing will need to be positioned under the coil at known heights and the sensor output voltage recorded. The steel ball position is known since it is placed on top of the simple positioning device shown in Figure 3.18 attached to the Maglev hardware. This device is often referred to as the object positioning tool. The thread along the bolt section of the tool has a lead of 1.954 mm per revolution. As shown in Figure 3.18, the position tool has 16 subdivisions. The position resolution of the object positioning tool is 0.122 mm per subdivision. Using the ball bearing and the object positioning tool, the sensor response was characterized and shown in Figure 3.19. The linear portion of the response has a minimum bound of 14.0 mm and a maximum bound of 15.5mm along with a linear curve fit.

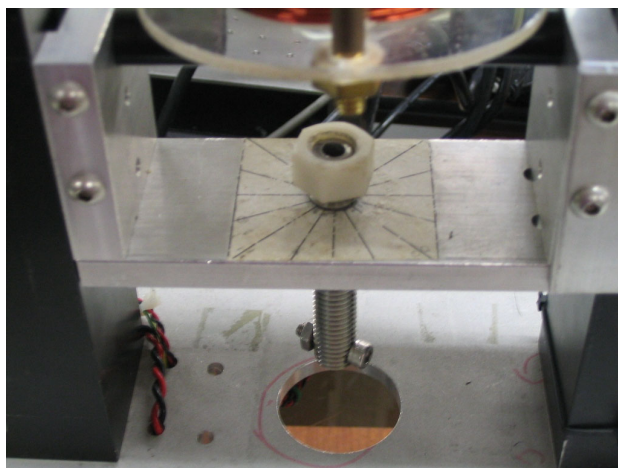


Figure 3.18 Object position tool attached to Maglev device

The nonlinear regions outside these bounds could be included as long as the output function has sufficient derivatives and is well defined so as not to present a singularity in the nonlinear controller calculations. However, this extended region of the sensor response is not considered due to the low signal to noise ratio the real-time hardware will experience during operation in this region.

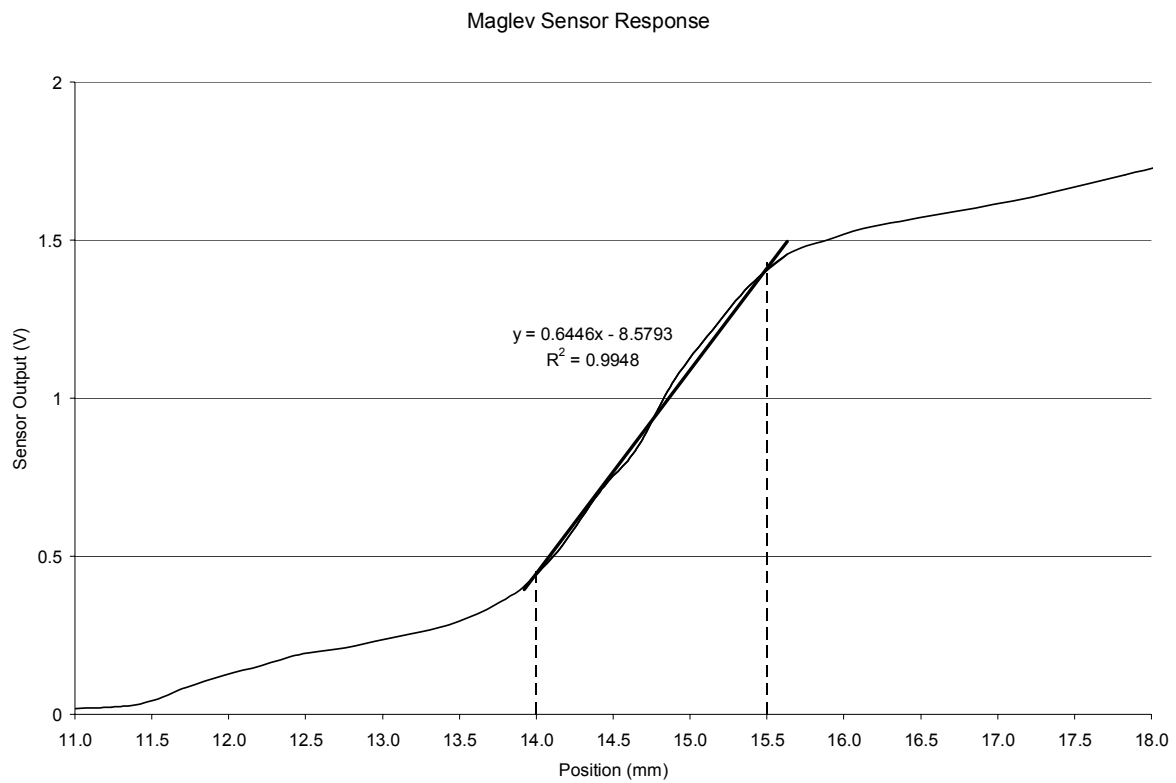


Figure 3.19 Input-output sensor response graph

The best fit line description for both the position-voltage and voltage-position will allow this sensor response to be properly modeled in the Simulink xPC model. The conversion blocks used in subsequent Simulink models for the position-voltage and voltage-position conversion are shown in Figures 3.20 *a* and *b* respectively.

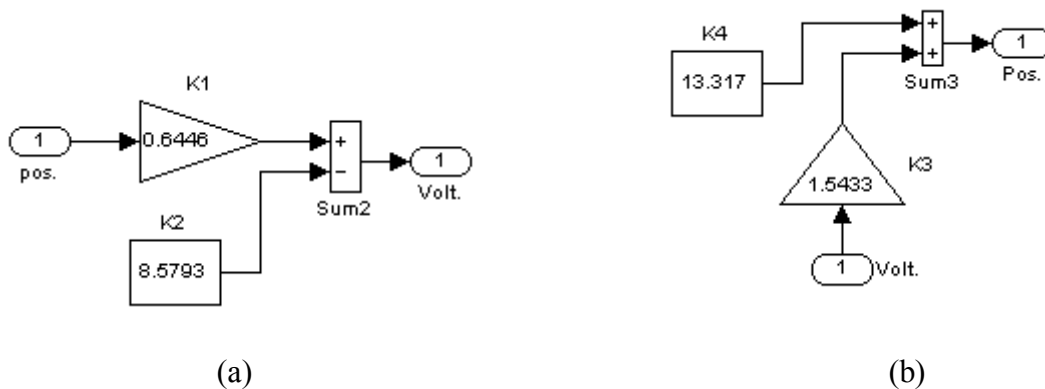


Figure 3.20 Simulink position sensor implementation (a) Position to voltage conversion and (b) voltage to position conversion

3.4 Measurement Noise Characterization

In order for the extended Kalman filter to properly operate and provide accurate estimates of the plant states, the sensor measurement noise must properly be accounted for in the filtering formulation. The measurement obtained by the sensor is assumed to be the actual value, y_k , plus some additive, random white Gaussian noise, v_k , with zero mean and known covariance, as shown in equation 3.2.

$$\tilde{y}_k = y_k + v_k \quad (3.2)$$

The object measurement tool was used to locate the metallic ball inside the position linear sensor range at a constant height, and data was collected via xPC target environment. Figure 3.21 shows the xPC Simulink model used to record the sensor values in order to determine the properties of the sensor noise.

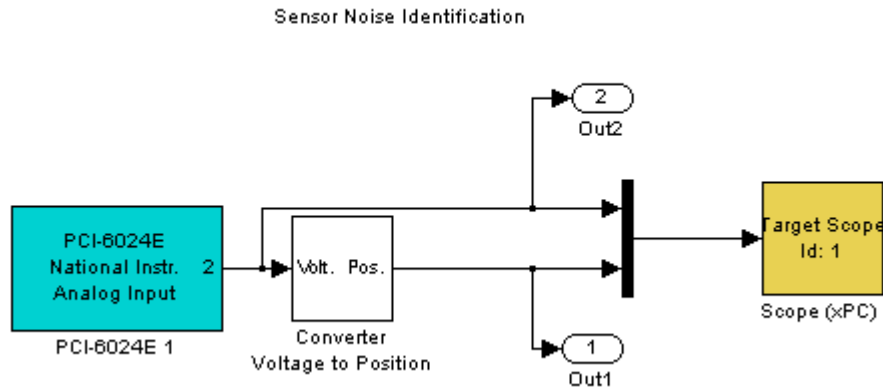


Figure 3.21 Simulink model used to determine the sensor noise covariance

The hardware data was logged in the MATLAB workspace for position sensor noise evaluation and the sensor noise covariance was determined. Equation 3.3 is used to determine sensor noise covariance, [46], where \tilde{y} is the measurement and μ is the measurement sample mean.

$$\sigma^2 = E[(\tilde{y} - \mu)^2] \quad (3.3)$$

The experimentally derived standard deviation, σ , and the covariance, σ^2 , of the position sensor employed in this research are presented in Table 3.2.

Table 3.2 Experimentally determined position sensor noise properties

Standard Deviation - σ <i>mm</i>	Covariance - σ^2 <i>mm²</i>
0.0034	1.156×10^{-5}

3.5 Kalman Filter Plant Noise Characterization

The next important step to complete in the implementation of the state estimator is to tune the process noise covariance matrix, $Q(t)$, since the values used for this parameter in previous sections of this research were arrived during the simulations and are not representative of the actual hardware. The first step in this process is accomplished with the use of an existing xPC Simulink digital lead-lag controller [16], as presented in figure 3.22, which stabilizes the levitating metallic object while the position and reference input are recorded in the MATLAB workspace for later analysis. Then, the recorded hardware response is used in an off-line manner to tune the plant noise covariance matrix. The recorded hardware position and reference trajectory are used as inputs in the nonlinear controller and the continuous-time extended Kalman filter used in the simulation sections 3.1 and 3.2. The Simulink model is modified such that the only inputs to the controller and state estimator model are those from the recorded hardware response stored in the MATLAB workspace, as presented in Figure 3.23. Iterations on the plant noise covariance candidates can then occur off-line and are quickly evaluated for some key attributes: quality of the estimate, relative errors and stability/ convergence of the covariance matrix. As a final validation step in the determination of the plant noise covariance the digital lead-lag controller and nonlinear controller / extended Kalman filter are run concurrently in the same model, where the lead-lag controller stabilizes the levitated object while the controller and estimator operate in a purely observation mode and evaluates the desired actuation signal as shown in Figure 3.24. This

type of configuration allows the successful candidate, determined in the off-line tuning, to be validated using the actual hardware in real-time.

3.5.1 Continuous-Time Extended Kalman Filter

As mentioned earlier in sections discussing the simulations of the nonlinear controller and extended Kalman filter, the specific type of Kalman filter used in those sections was a continuous-time extended Kalman filter. During the plant noise covariance determination carried out in support of this research, the quality of the estimates produced by this version of the state estimator was not suitable for hardware implementation. Many potential candidates were examined during the course of this tuning process. A successful candidate that produced simultaneously high quality position, velocity and current estimates while producing stable results on the hardware could not be determined. Many factors could have contributed to poor results with the foremost suspect in a list of reasons focusing on the discrete sampling of the output by the embedded microprocessor. A slightly different formulation of the extended Kalman filter was vetted against the recorded hardware data generated during this phase of the research. This formulation of the optimal state estimator was outlined in section 2.4. The results of these trials were promising enough that the continuous-time extended Kalman filter formulation was dropped from this research in favor of the discrete-time extended Kalman filter. The two different versions of the state estimator are identical in Simulink model structure, however, the difference is apparent when examining the estimator embedded m-function; this is available in Appendix G compared to the continuous version found in Appendix F.

Digital Control for Magnetic Levitation System by xPC Real-Time OS

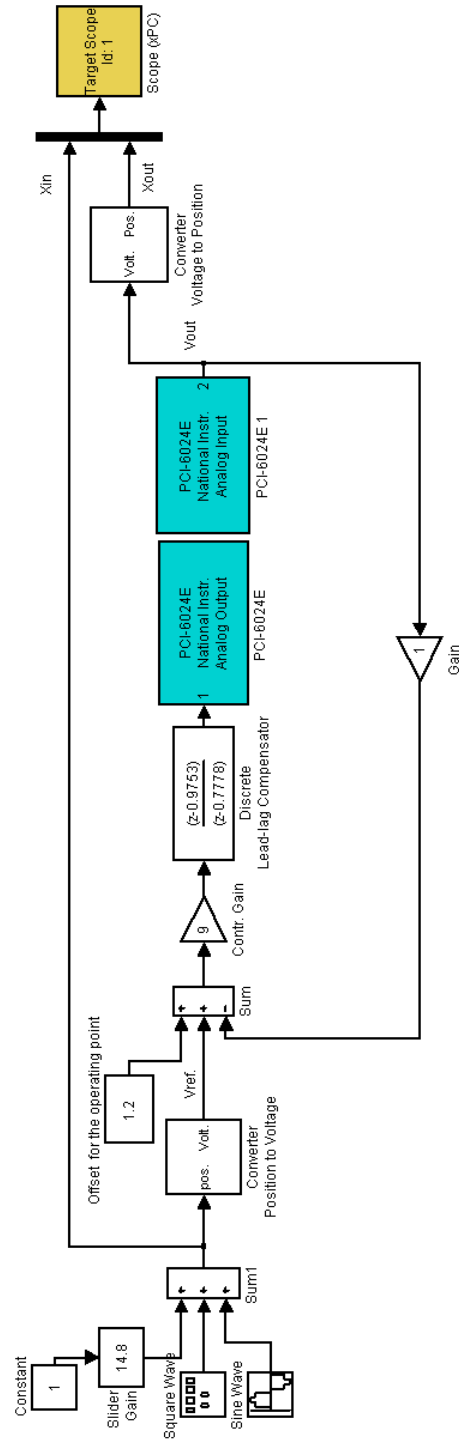


Figure 3.22 Simulink model for digital lead-lag controller

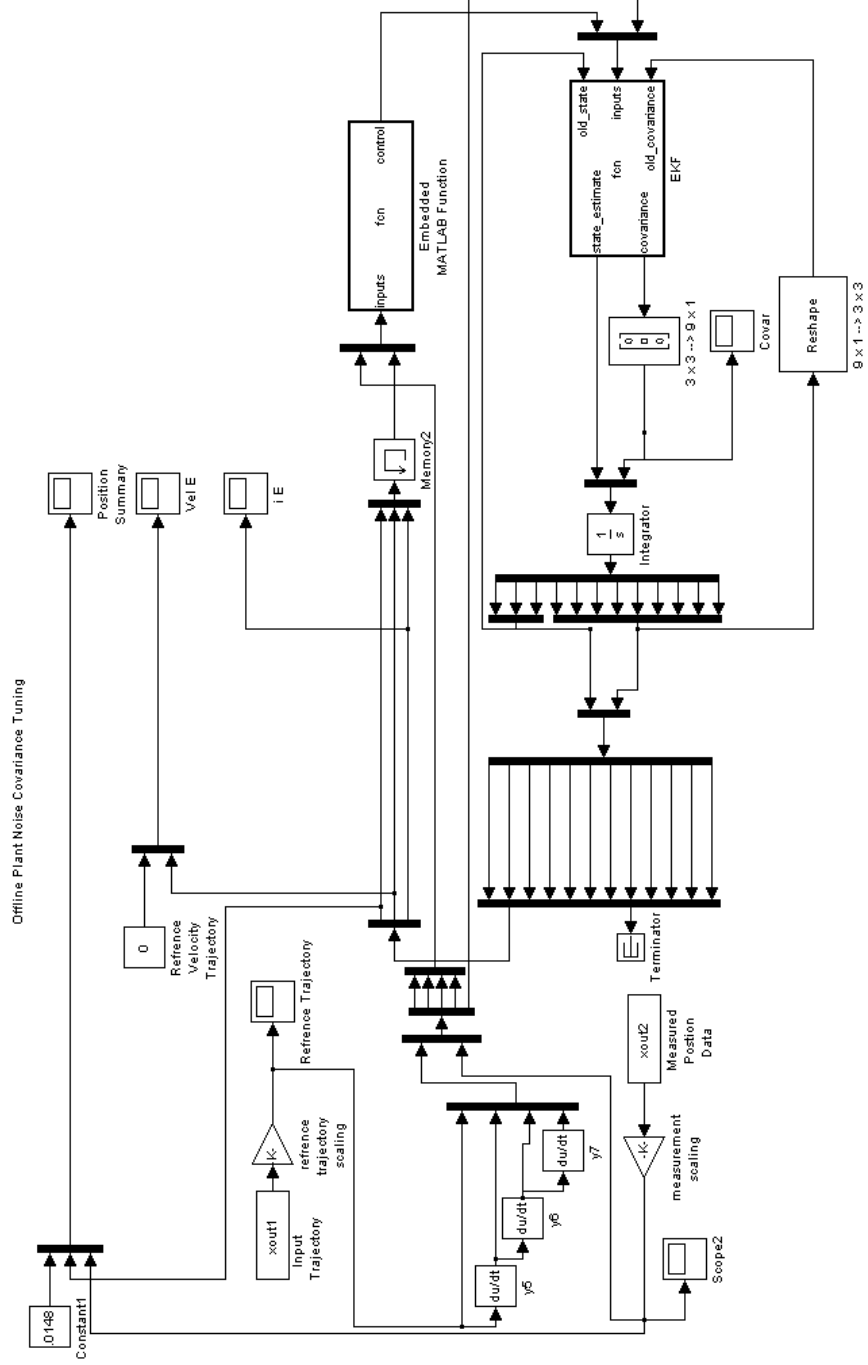


Figure 3.23 Simulink model used for off-line plant noise covariance tuning using hardware data

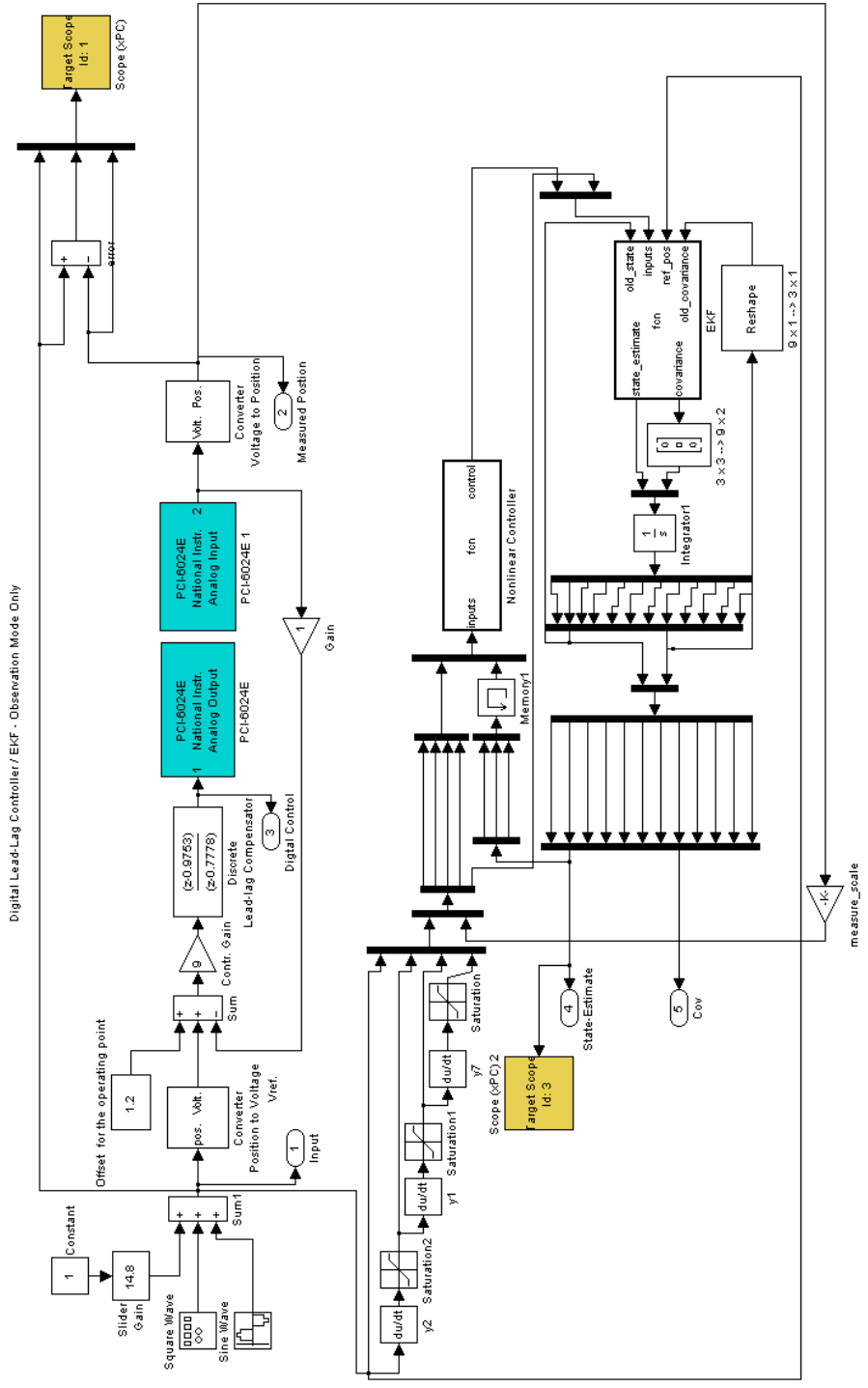


Figure 3.24 Digital lead-lag controller and continuous time extended Kalman filter for Maglev system plant noise covariance tuning

3.5.2 Continuous-Discrete Time Extended Kalman Filter

The digital lead-lag controller was compiled by MATLAB with the aid of RTW and xPC and then downloaded to the target computer. The reference input position of the levitated object was set in the middle of the sensor range at 14.8 mm. The object was placed under the coil and manually adjusted in the vertical axis until the controller successfully levitated the object. The offset for the operating block illustrated in Figure 3.22 was adjusted until the measured position was tracking the reference input. The results of digital lead-lag controller stabilizing the levitated object at 14.8 mm are presented in Figure 3.25. The 25 second time frame of the hardware data is sufficient time to determine filter performance and estimator state stability, due to the open-loop unstable behavior of the non-controller plant dynamics.

Once a suitable set of reference data was collected, it was used as input into Figure 3.23 where different plant noise covariance candidates were evaluated. After several iterations of potential candidates, a suitable set of covariance matrix parameters was determined and is presented in equation 3.4. These parameters represent a 'best fit' since trade-offs were made between the three states in such a manner to produce an overall high quality estimate.

$$Q(t) = \begin{bmatrix} 1*10^{-4} & 0 & 0 \\ 0 & .75*10^{-7} & 0 \\ 0 & 0 & 1*10^{-8} \end{bmatrix} \quad (3.4)$$

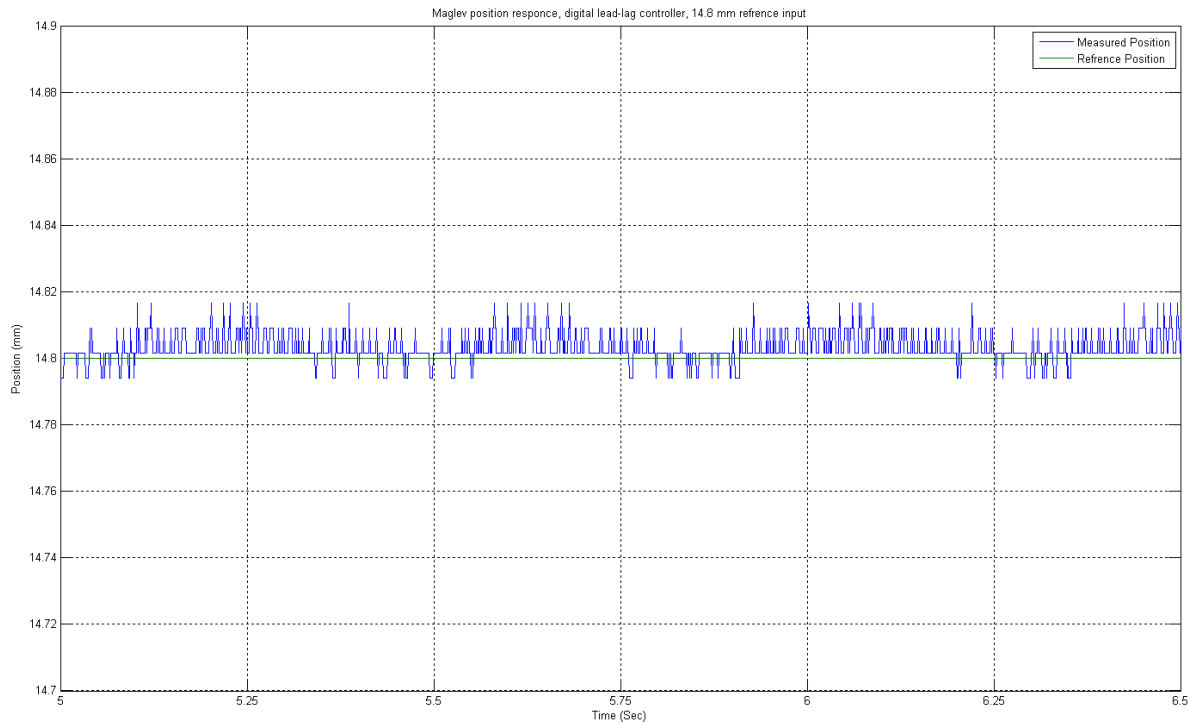


Figure 3.25 Digital lead-lag controller tracking 14.8 mm reference input

The measured hardware position, reference trajectory and position estimate produced by the simulation outlined in Figure 3.23 is presented in Figure 3.32. The performance of the position estimate will serve as a reliable representation of the state due to the high level of quality produced. The error between the measured and estimated position is also presented in Figure 3.23, along with a baseline representing the mean error. This mean error baseline is calculated on the difference between the measured position and the estimated position along the entire simulation time of 25 seconds and not on the 1.5 second representative simulation segment shown for clarity.

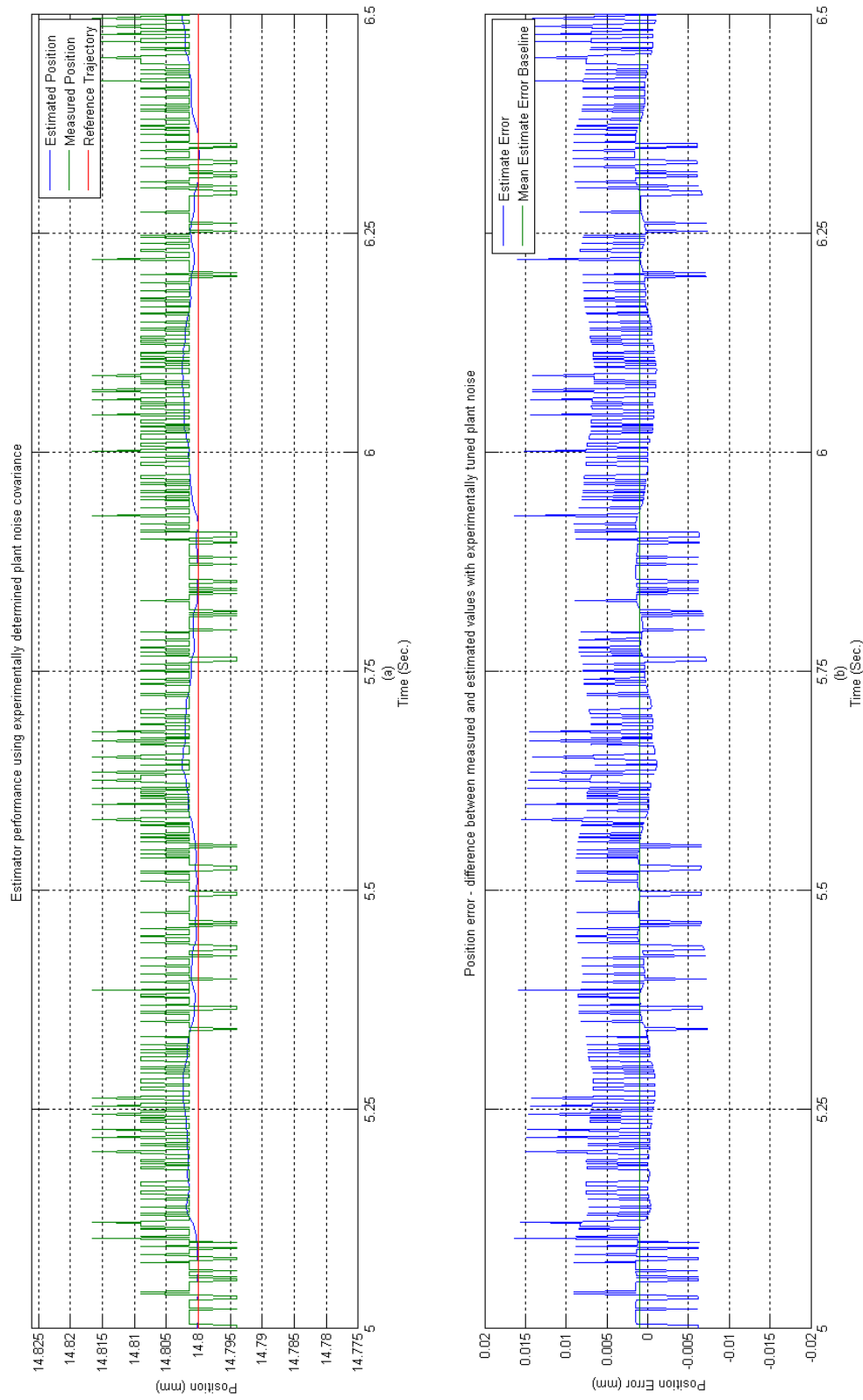


Figure 3.26 (a) Offline position estimate, hardware –measured position and reference trajectory using experimentally tuned plant noise covariance, (b) Position error between hardware-measured position and estimated position with mean estimate error baseline

The zero velocity reference trajectory and position estimate produced by the hardware data driven simulation is presented in Figure 3.27. The performance of the velocity estimate will serve as a reliable representation of the state due to the high level of quality produced. The error between the measured and estimated position is also presented in Figure 3.27, along with a baseline representing the mean velocity error. This mean error baseline is calculated on the difference between the measured position exactly the same as done with the mean position error, except that the time interval in this case is the 1.5 second interval shown in the simulation results from 5 to 6.5 seconds. As a note, the mean velocity error was determined to be 9.7571×10^{-7} mm/sec, during the 1.5 second simulation presented in Figure 3.27. Use of the entire simulation results would be misleading since there were many position fluctuations during the simulation sequence, namely the initial transient response of the extended Kalman filter converging to and then tracking the state trajectory. In sections 3.1 and 3.2 special considerations were made during the simulation process so singular behavior would be avoided in the simulated system response. In the present simulation, the possibility of a singularity existing due to step change in the reference trajectory is avoided since the controller and extended Kalman filter are given the constant position from the start of the simulation. The time derivative of the measured position is not presented, since it serves as a poor source of velocity information due to very low signal to noise ratio.

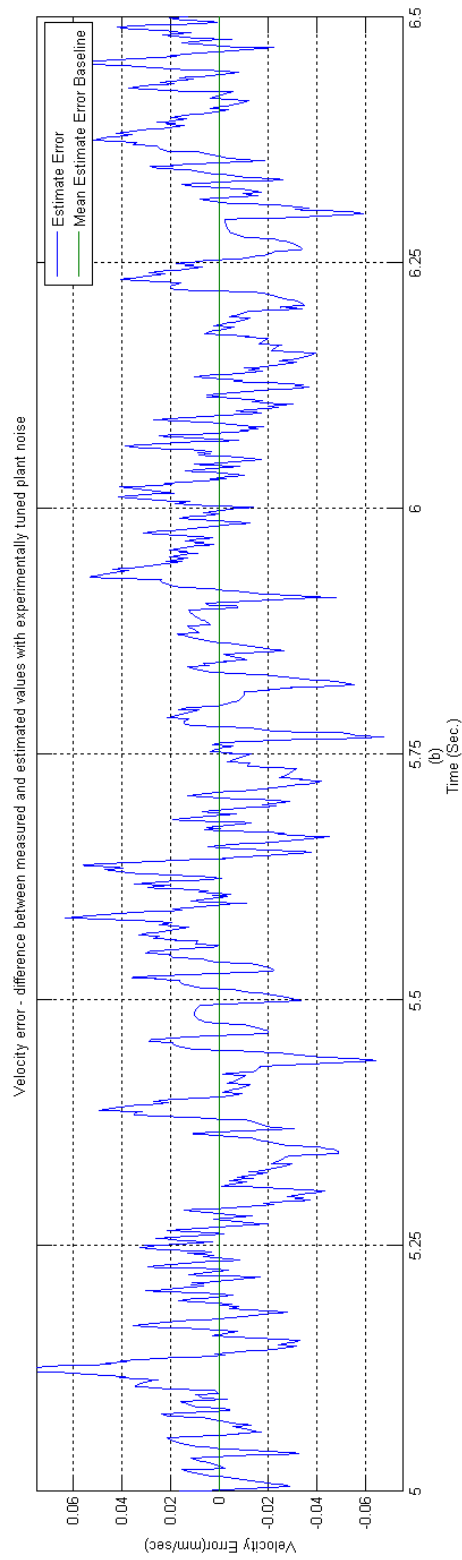
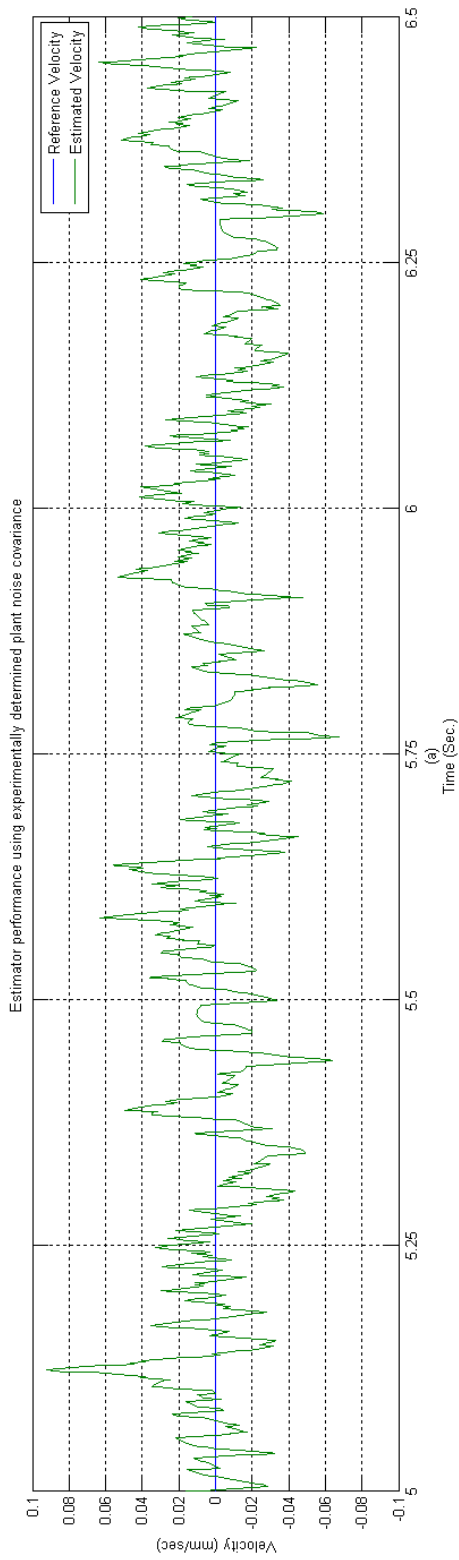


Figure 3.27 (a) Offline velocity estimate, and reference velocity trajectory using experimentally tuned plant noise covariance, (b) Velocity error between estimated velocity and reference velocity trajectory with mean estimate error baseline

The current estimate produced by the hardware data driven simulation along with the mean current estimate is presented in Figure 3.28. The response of the current estimate tracks the measured position of the levitated object very closely. The mean current estimate is presented as a reference for the average current estimated during the simulation.

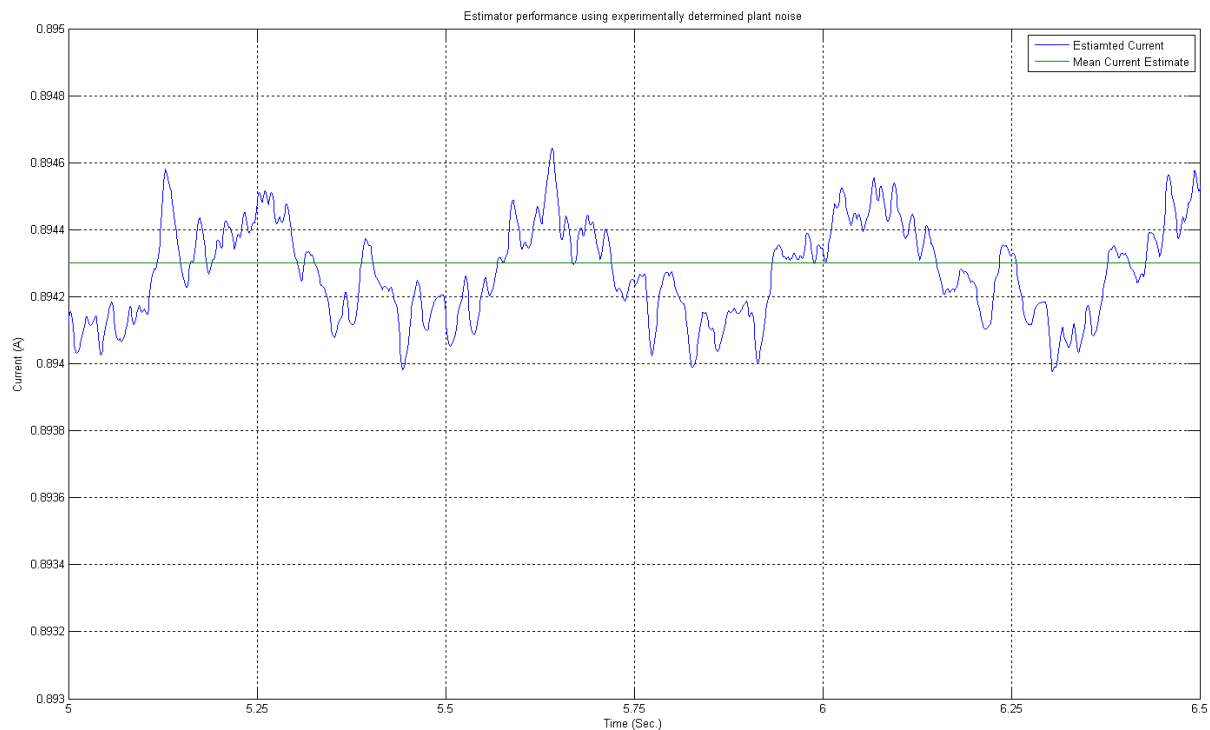


Figure 3.28 Offline current estimate using experimentally tuned plant noise covariance and mean estimate current

The response of the covariance is an important feature in the determination of a suitable candidate for the plant noise covariance. Since the stability of the extended Kalman filter is difficult to prove, if not impossible, the only real methods available for the determination of 'good' results lies in the convergence and tracking results produced by the state estimates and the convergence and relative error of the covariance matrix. The

covariance matrix response to the hardware-driven data is shown in Figure 3.29. Of particular importance is the response associated with diagonal elements of the covariance matrix, since it is assumed that the states are not correlated with each other, see section 2.4. However, when the simulation is driven by real data this assumption is not valid in the strictest sense. Since the diagonal and off-diagonal elements converge to relatively small numbers when compared with the magnitude of the estimate errors presented in Figure 3.32-3.27 any correlation is weak and can be neglected.

The estimated states of the Maglev system produced from the experimentally tuned plant noise covariance are quite suitable to be discussed as inputs for the feedback linearized nonlinear controller. As a unit of estimated states that are driven from the hardware data they are closely aligned with simulation results presented in sections 3.1 and 3.2.

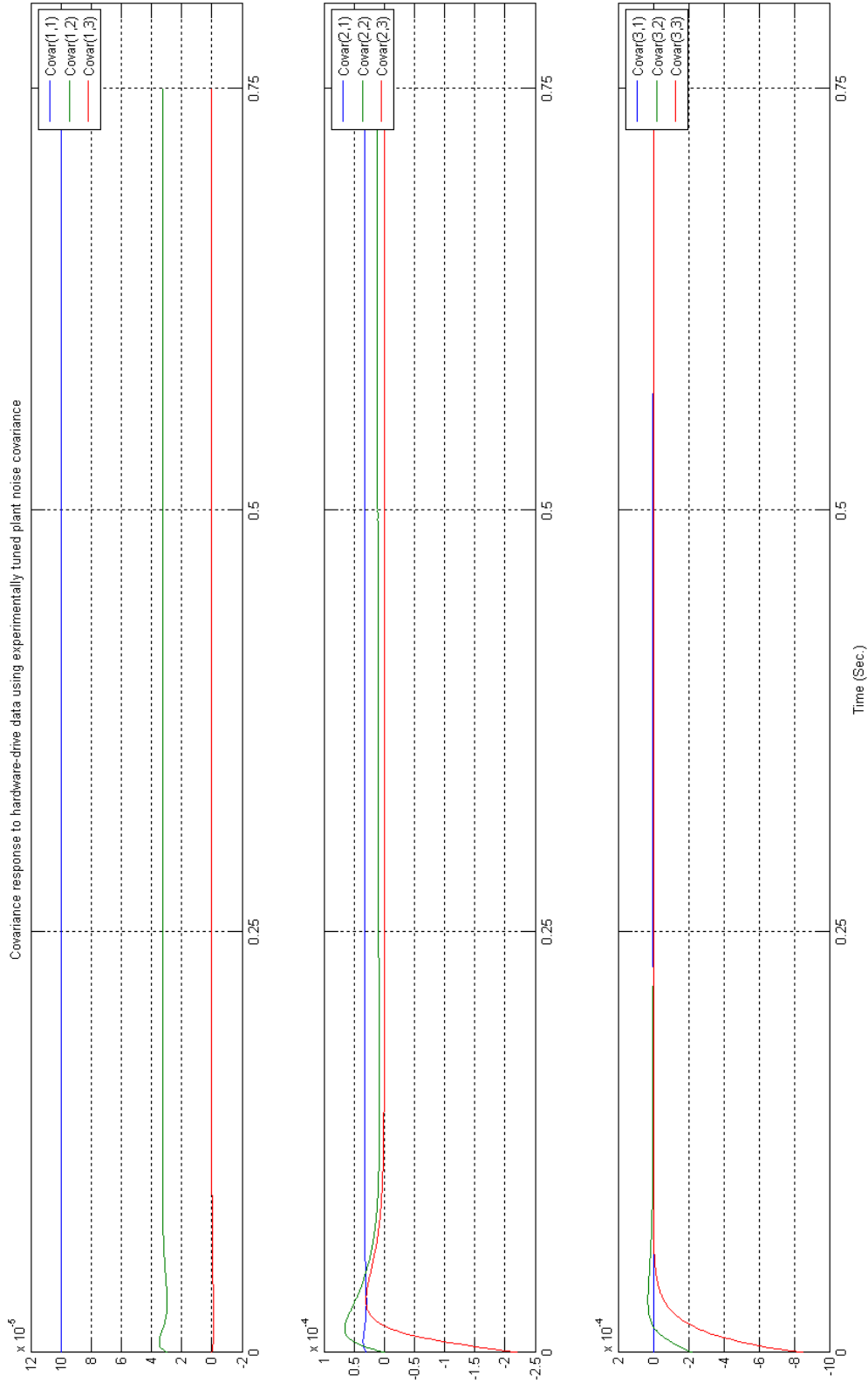


Figure 3.29 Offline covariance responses using experimentally tuned plant noise covariance

As final validation, the plant noise covariance determined thus far was implemented on the Maglev hardware using the continuous-discrete time extended Kalman filter illustrated in Figure 3.24, while the digital lead-lag controller stabilized the system and the nonlinear controller / extended Kalman filter operated in an observer role.

The reference trajectory, measured and estimated position for the extended Kalman filter using the experimentally determined plant noise covariance is presented in Figure 3.30. Due to the large amount of data recorded when this model was run on the hardware only a 1.5 second interval of the results are presented here. The state estimate produces a very strong estimate and tracks the measured position well when the levitated object experiences a disturbance as shown at the 77.5 second marker.

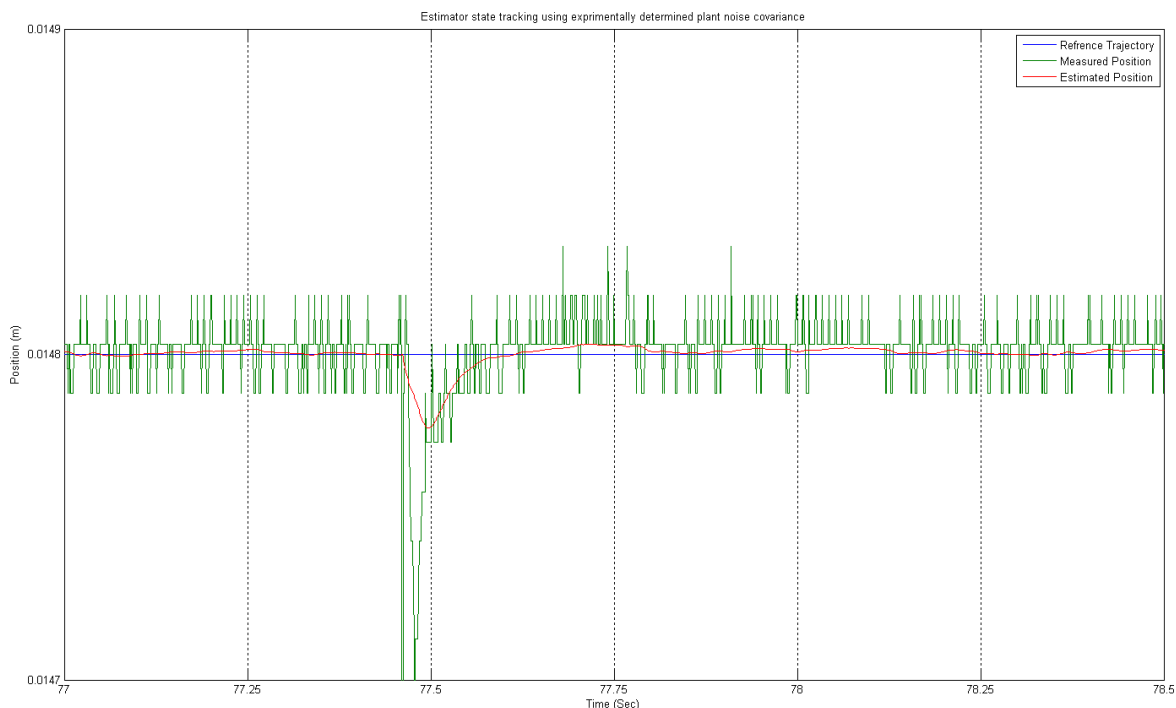


Figure 3.30 On-line position estimate produced by the extended Kalman filter with experimentally tuned plant noise covariance

The on-line estimated velocity and the reference velocity trajectory produced by the extended Kalman filter operating as a pure observer are presented in Figure 3.31. The performance of the estimated velocity closely correlates to the hardware position response illustrated in Figure 3.30. However, the estimated velocity responds much more quickly to the disturbance than the position estimate. The difference in response can be attributed to the plant noise tuning. Throughout the off-line tuning process performance of the position estimate had to be sacrificed in order to receive acceptable estimated velocity estimates.

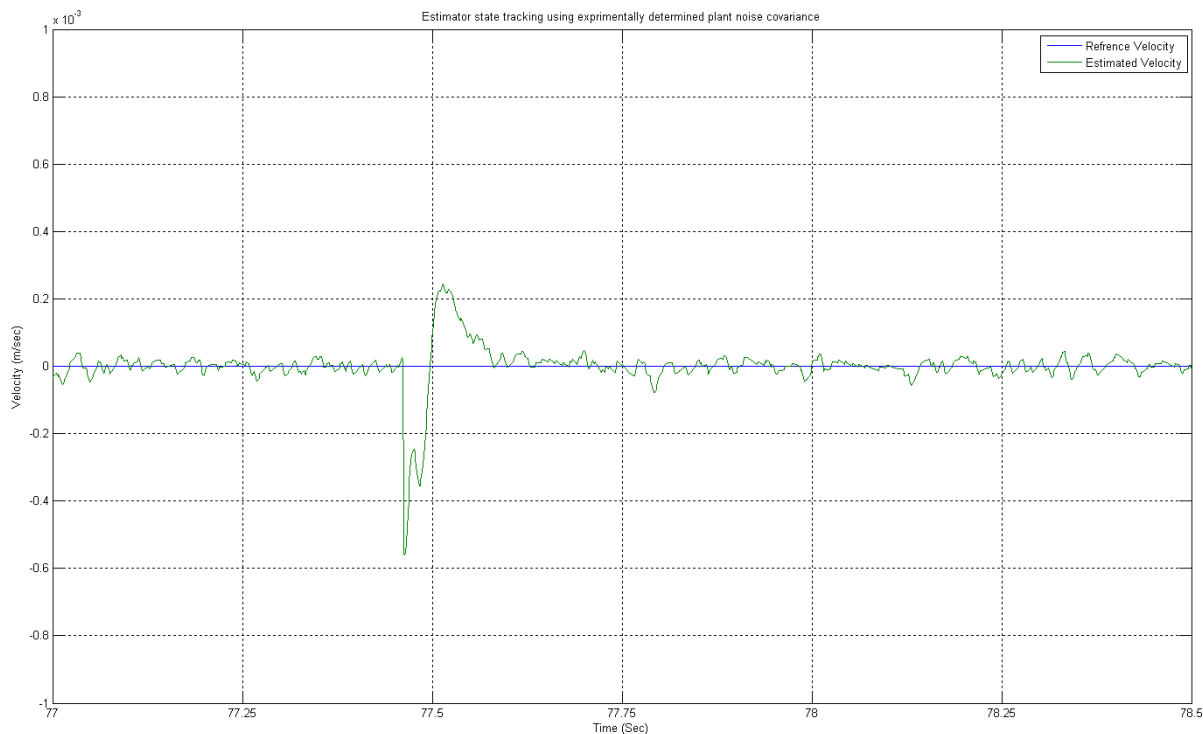


Figure 3.31 On-line velocity estimate produced by the extended Kalman filter with experimentally tuned plant noise covariance

The on-line estimated current produced by the extended Kalman filter operating as a pure observer is presented in Figure 3.32. As with the estimated velocity, the current is very

quick to respond to the disturbance compared to the position estimate. However and as expected, the overall response of the current estimate is closely correlated with the position response shown in Figure 3.30.

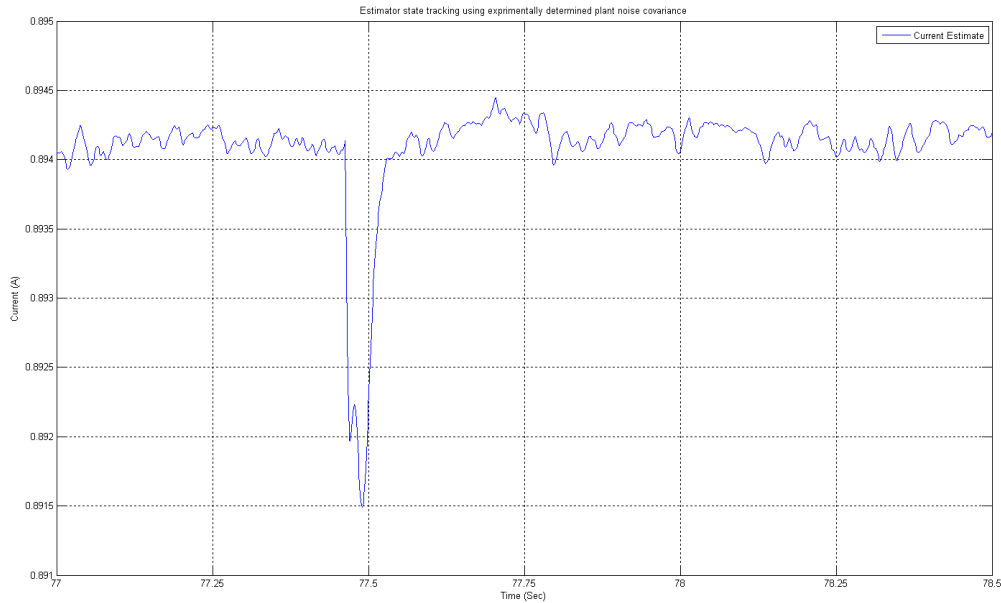


Figure 3.32 On-line velocity estimate produced by the extended Kalman filter with experimentally tuned plant noise covariance

3.6 Nonlinear Controller Output Mapping

As outlined in section 2.2.2 the control input to the system is the voltage drop across the electromagnet coil. The Simulink file must communicate this desired voltage drop across a series of interconnects, first the PCI-6024E Digital Acquisition Card (DA card) and then through the power amplification electronics to deliver this voltage to its intended location on the hardware. This section discusses the mapping of the nonlinear control effort through

these interconnects that would allow the Simulink based Kalman Filter to control the coil voltage.

3.6.1 Software and Hardware Interconnects

The difference between the hardware and the theoretical model lies in their respective outputs, note the difference between the detail shown in Appendix A and Figure 2.4. The electric circuit model used in this research is very simple and is easily characterized by a Kirchhoff's voltage law while the actual hardware devices are much more complicated. A mapping between the linear controller output and the nonlinear controller output will allow the system output to be properly scaled to produce the desired changes in the levitated object position. The Simulink model of the controller and state estimator along with a linear mapping function that allows the nonlinear control output to be appropriately mapped to a usable output by the system to control the levitated object is presented in Figure 3.33. This model is similar to the model shown in Figure 3.24; the only real difference being the mapping function and the manual switch which determines whether the linear or nonlinear controller output is used to control the hardware.

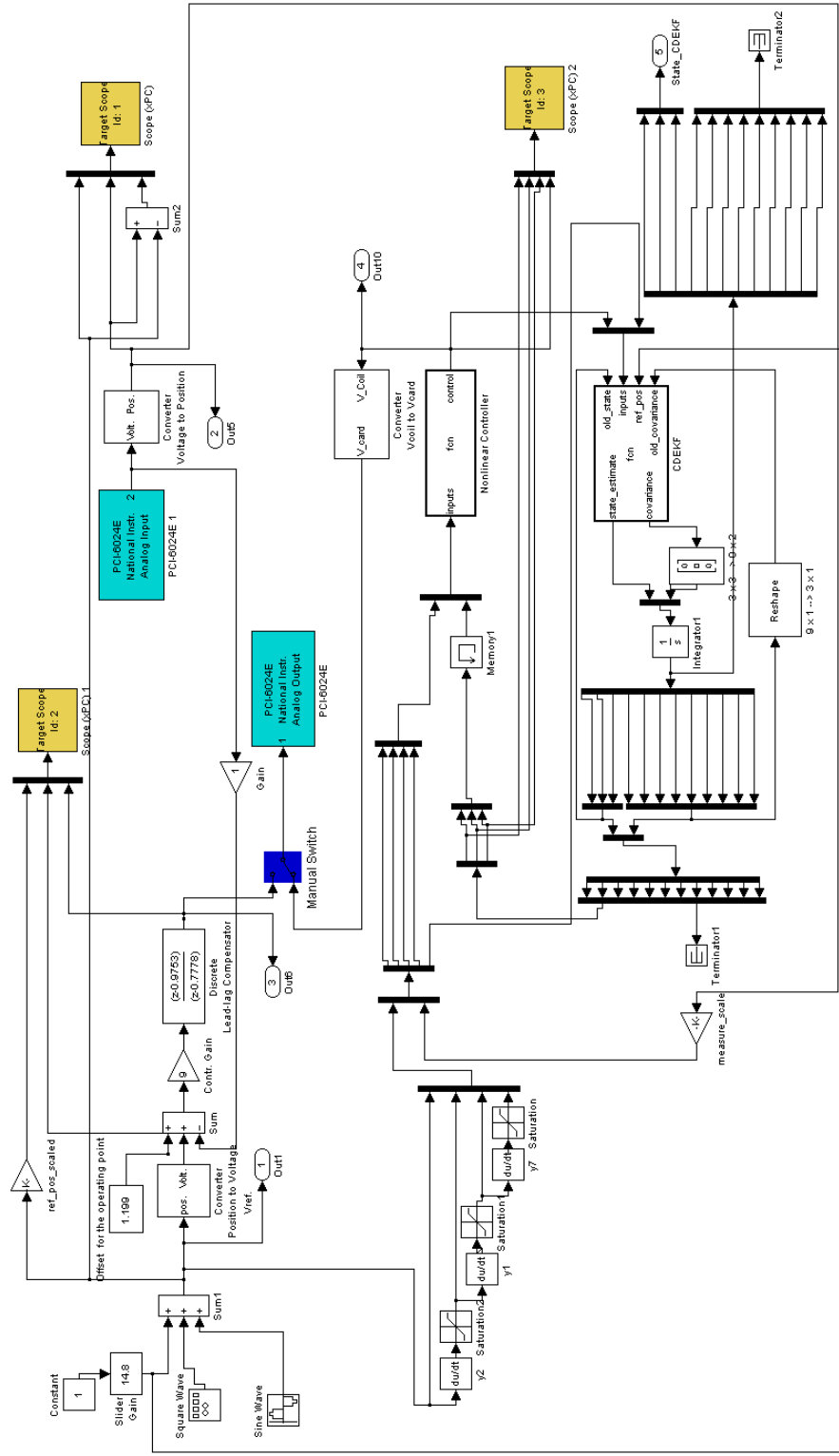


Figure 3.33 Simulink model allowing scaled nonlinear control output or digital lead-lag controller output to control the Maglev system

3.6.2 Output Mapping

The digital lead-lag controller is used to determine a suitable conversion between the two controllers. This mapping is accomplished by changing the set point of the digital controller (between 14.2 mm to 15.2 mm) and recording the output of the two controllers as well as the coil voltage and resistance. These results are presented in Appendix H. Then, the measured nonlinear controller output is plotted against the measured output from the digital lead-lag controller, along with a linear curve fit as illustrated in Figure 3.34.

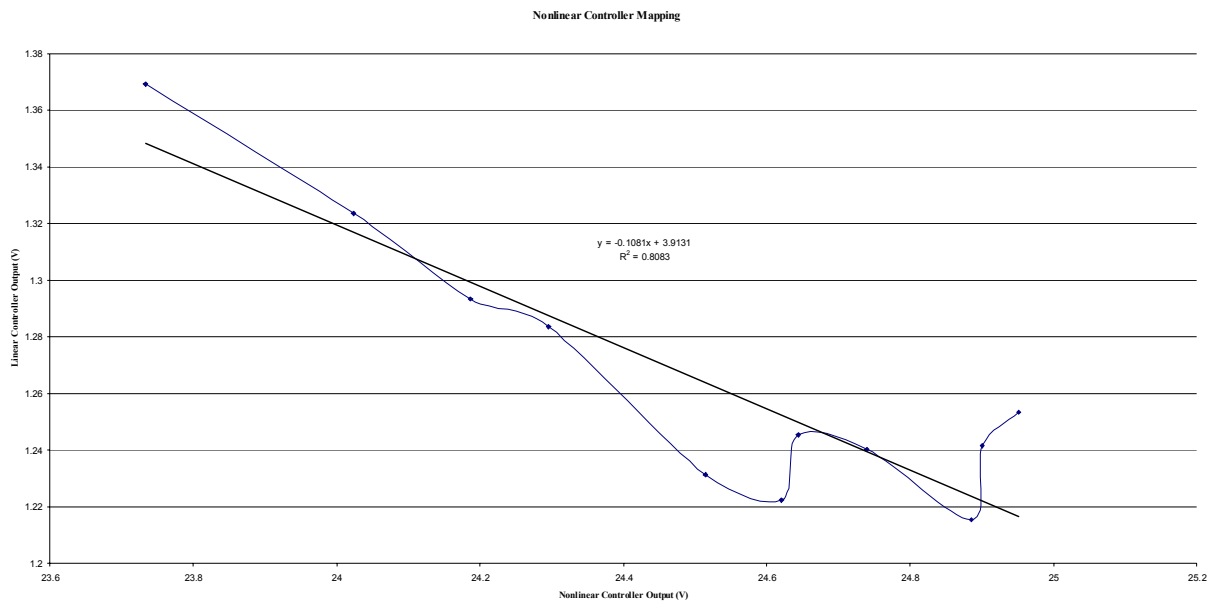


Figure 3.34 Nonlinear controller output versus linear controller output, along with linear best fit

The linear mapping relationship identified in Figure 3.34 is implemented in Simulink by the output conversion block shown in Figure 3.35, which will allow the nonlinear output to be properly scaled for use by the hardware.

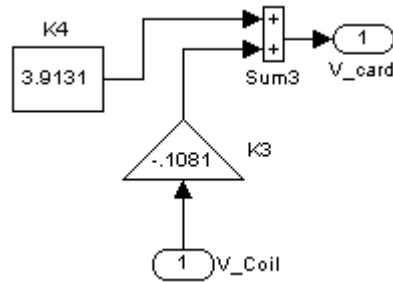


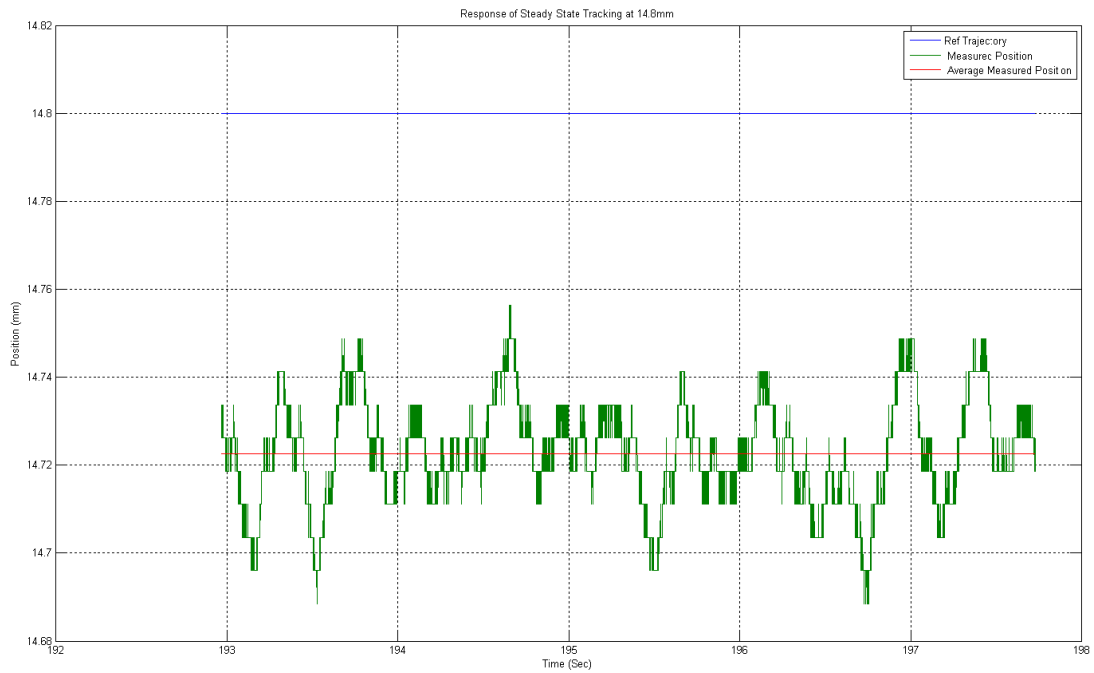
Figure 3.35 Nonlinear output to linear output scaling block

3.7 Experimental Hardware Results

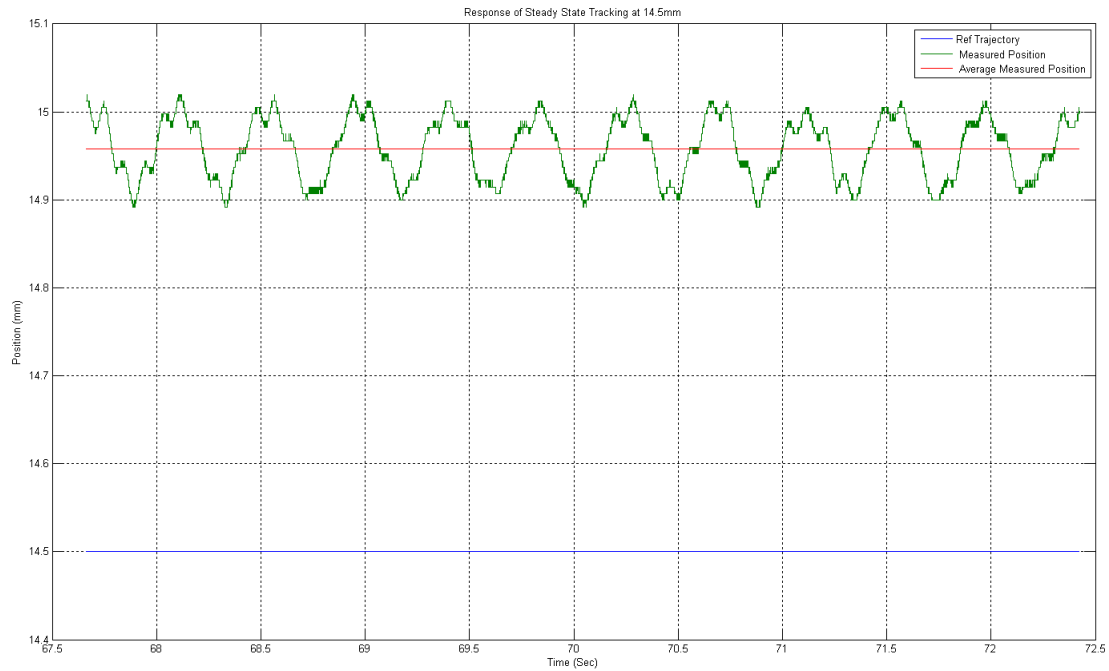
The feedback linearized nonlinear controller and continuous-discrete extended Kalman filter are implemented in a Simulink model as shown in Figure 3.33. The Simulink model, related plant noise and output mapping have been experimentally adjusted specifically for the levitated object considered in this research. Attempts to levitate similar objects using the parameters previously discussed were unsuccessful. Therefore, it is assumed that any additional objects would need to have the filter parameters tuned specifically for that object. This is a reasonable assumption since a different sized object will induce different inductance due to its presence in the electromagnet's field and the sensor response characterization will also change due to the shape of the object. The results of this hardware implementation are presented in three different sections, Steady State Tracking, Square Wave Response, and Sine Wave Response. These responses represent the behavior of the Maglev interaction with the nonlinear controller and state estimator proposed in this research.

3.7.1 Steady State Tracking

Two different set points were considered in this research to demonstrate the ability of the nonlinear controller and extended Kalman filter to track a constant reference trajectory. The first set point is in the middle of the linear region of the position sensor range at 14.8 mm. The steady state tracking of the levitated object, mean levitated position and the corresponding reference trajectory are presented in Figure 3.36a. As illustrated in the simulation results in section 3.1 and 3.2 the measured position also oscillates about a nominal value. The mean value of the measured position is also shown in this figure allowing the -0.078 mm static offset to be more apparent. The second reference trajectory chosen was 14.5 mm with the results of the position tracking shown in Figure 3.36b. The measured position oscillates about the nominal trajectory as in the 14.8mm case, but the oscillation is much more periodic than the first case. The oscillations for both trajectories are attributed to the unmodeled plant dynamics or even a consequence of the output mapping discussed in section 3.6 having poor correlation near 14.5 mm. However the constant periodic nature of the Maglev response also points to an external disturbance to the system. All of these factors being accounted for results in a mean measurement showing a static offset of almost 0.5 mm.



(a)



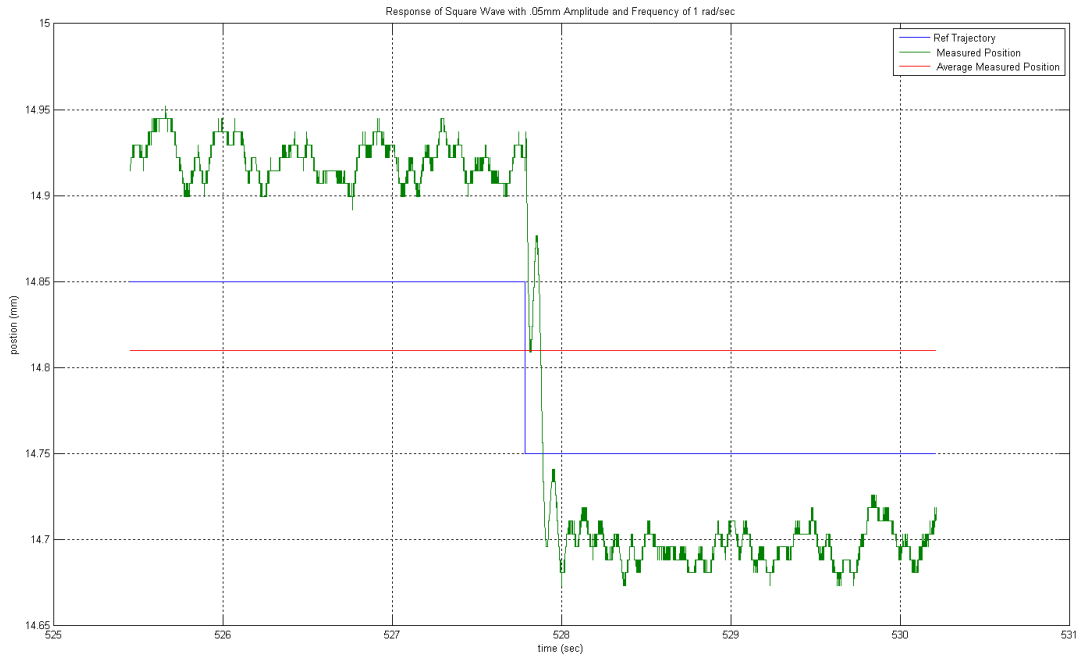
(b)

Figure 3.36 Steady state tracking of the Maglev with levitated object to a reference trajectory 14.8 mm and 14.5 mm

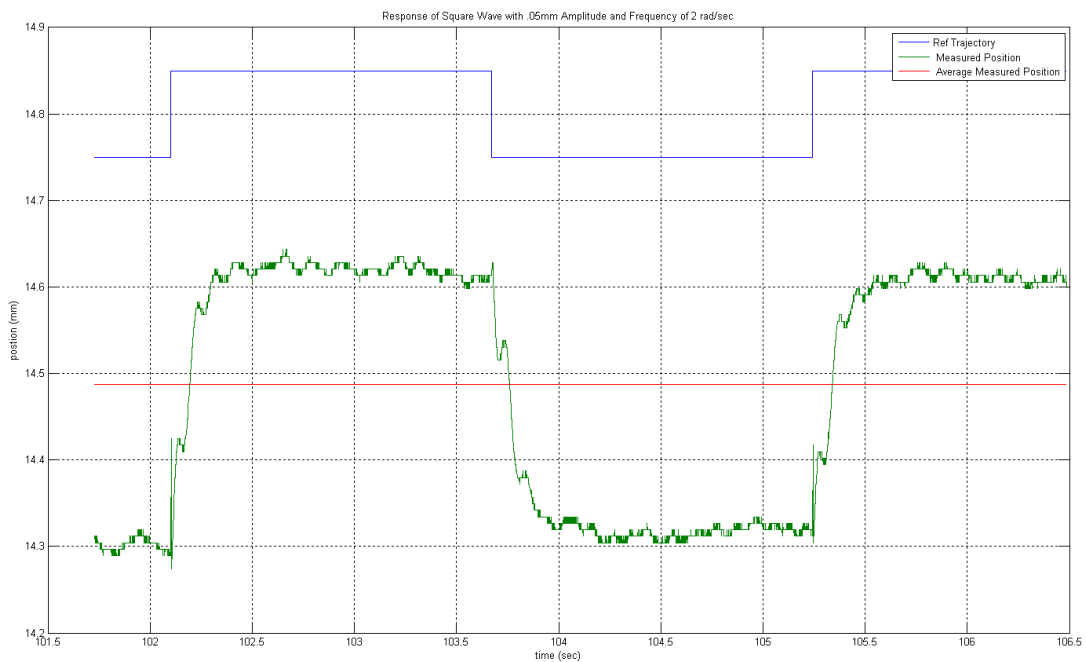
3.7.2 Square Wave Tracking

Two different set points were considered in this research to demonstrate the ability of the nonlinear controller and extended Kalman filter to track a square wave reference trajectory. To prevent singularities and consequently unbounded response in both the controller output and/or the extended Kalman filter saturation blocks were placed on the output of the derivative elements shown in Figure 3.33. A nominal trajectory of 14.8 mm was selected allowing the levitated object to be best placed in the middle of the linear response region of the position sensor. To the nominal trajectory, a 0.05 mm amplitude square wave is added with frequency of 1.0 rad/sec and 2.0 rad/sec respectively. The measured position of the levitated object to each square wave trajectory, mean measured position and reference trajectory are presented in Figure 3.37. The response of the levitated object to the 1.0 rad/sec input frequency closely correlates with the simulation results. The initial offset between the measured output and the reference trajectory is approximately 0.05 mm below the desired position and after change in position, the measured position is approximately 0.05 mm above the desired reference trajectory. These results correlate very well with the simulated results for two reasons: the first being that the mean measured position is very close to the nominal reference trajectory of 14.8 mm, and the second reason is that the sinusoidal disturbance experienced in Figure 3.36b is not significant. Tracking results for 2.0 rad/sec frequency represent a slightly different response for the hardware. The levitated object tracked the square wave quite well with the exception of the offset error associated with mean measured position and static offset associated with steady state

region before or after the step change. The mean measured error is observed to be at 14.49 mm, approximately 0.31 mm above the nominal reference trajectory. The measured wave height is 0.31 mm and the reference trajectory wave height is 0.1 mm, approximately 3 times greater wave height.



(a)

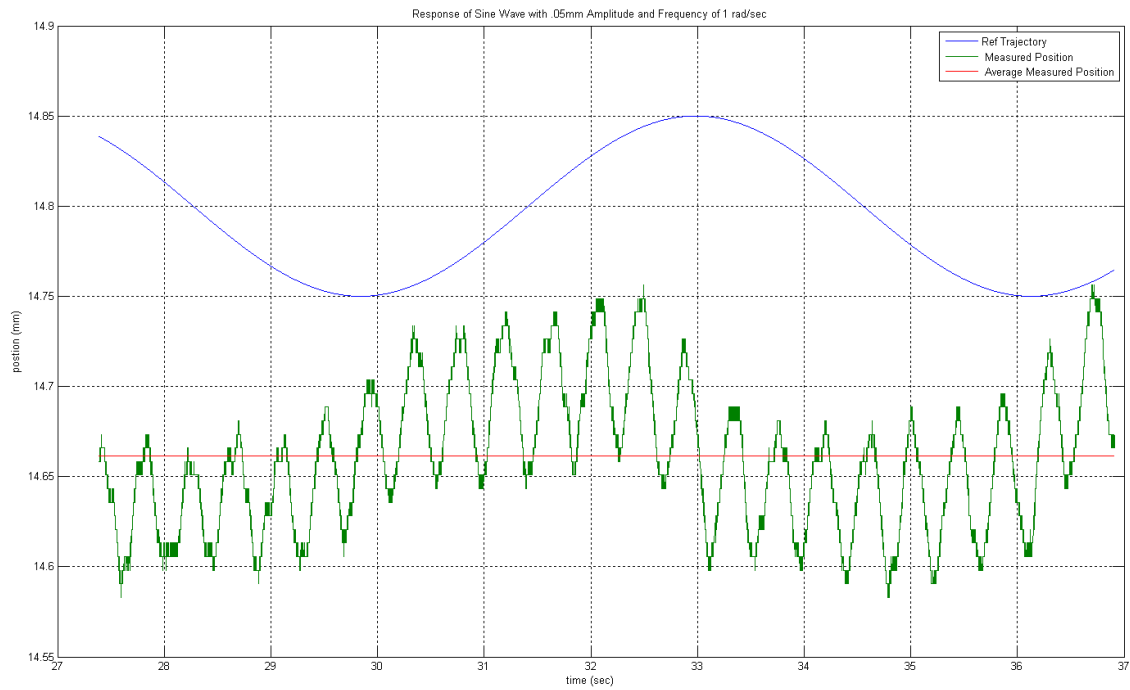


(b)

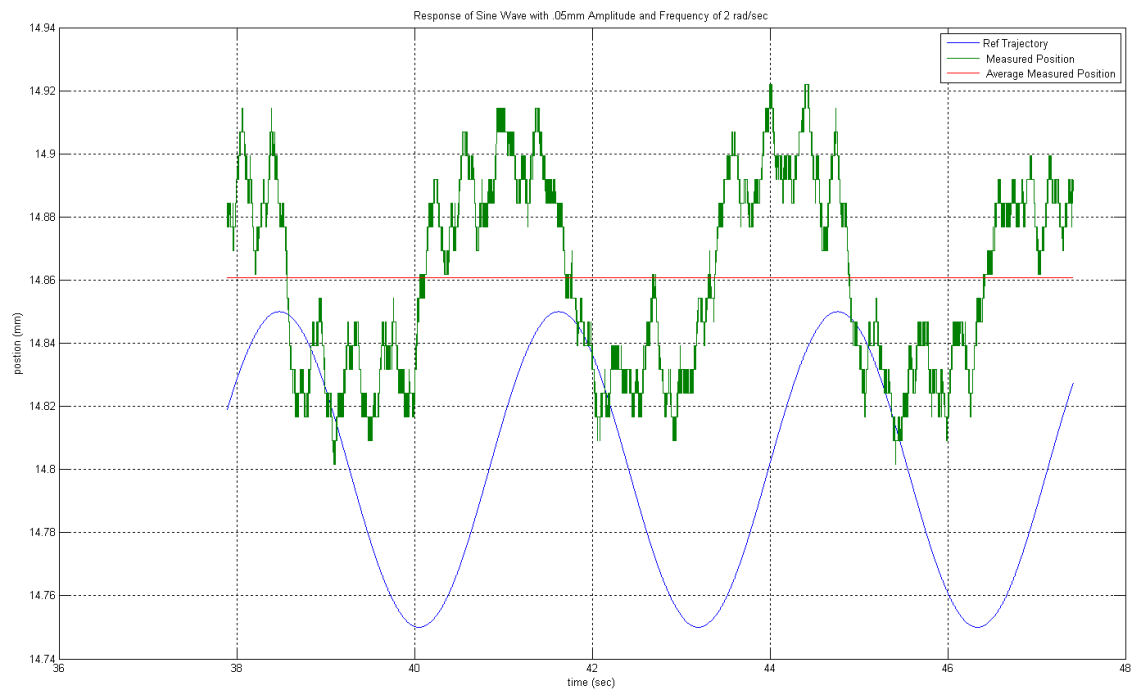
Figure 3.37 Square wave tracking for the Maglev with an amplitude of 0.05mm and frequency of (a) 1.0 rad/sec and (b) 2.0 rad/sec

3.7.3 Sine Wave Tracking

Two different set points were considered in this research to demonstrate the ability of the nonlinear controller and extended Kalman filter to track a sinusoidal reference trajectory. The nominal trajectory of 14.8 mm was selected in order to place the levitated object in the center of the position sensor linear response region. Two wave forms were added to this nominal trajectory of 0.05 mm amplitude sine wave with frequency of 1.0 rad /sec and 2.0 rad /sec. The measured position, mean measured position and the reference trajectory for both cases considered are presented in Figure 3.38. The mean measured position of the Maglev hardware to the 1.0 rad/sec frequency input showed a 0.13 mm offset when compared to the reference trajectory. While the mean measured position of the Maglev hardware to the 2.0 rad/sec input showed an offset of 0.06 mm, the position of the levitated object did track the input trajectory suitably well when considering the persistent sinusoidal disturbance. This disturbance can most definitely be attributed to un-modeled plant dynamics, output mapping issues associated with poor correlation and sinusoidal disturbance.



(a)



(b)

Figure 3.38 Sine wave tracking for the Maglev with an amplitude of 0.05mm and frequency of (a) 1.0 rad/sec and (b) 2.0 rad/sec.

CHAPTER 4

CONCLUSIONS AND FUTURE WORK

In this research, a feedback linearizing nonlinear controller with an extended Kalman filter was studied for implementation on a Maglev system which served as hardware in the loop using a MATLAB/Simulink-based development environment. A nonlinear feedback linearizing controller was developed to control the open-loop unstable, highly nonlinear plant dynamics. Additionally, a continuous-discrete extended Kalman filter was developed to provide suitable state estimates to the controller for proper operation. The extended Kalman filter and nonlinear controller concept was validated in simulation using m-file and Simulink-based methods. The extended Kalman filter was tuned using data taken from the hardware in an offline method. Then, the output of the nonlinear controller was mapped back to a suitable level so existing data-acquisition Simulink blocks and power electronics could control the levitated objects trajectory. Experimental validation of the closed-loop response of the Maglev system was also presented.

4.1 Conclusions

To better address the actual behavior of the Maglev system a nonlinear dynamical model was constructed based on the understood dynamics of the system. For the control method to be successfully implemented, a coordinate transformation needed to be constructed that would convert the nonlinear system into an equivalent linear

system. Then, the equivalent linear system would be controlled by any linear method, and the control effort communicated back to the plant with the use of nonlinear feedback. A few system details needed to be verified, and then the system needed to be shown as feedback linearizable by means of a set of necessary and sufficient conditions.

The dynamical model was first analyzed to determine if there were any hidden dynamics. In linear system theory this is analogous to determining if the system has any pole/zero cancellations. Once the relative degree of the nonlinear system was verified the necessary and sufficient conditions were checked to ensure that a coordinate change could be constructed. Finally, a linearizing coordinate transformation and nonlinear feedback were constructed that converted the original plant into an equivalent linear system.

Next, the problem of pole placement and asymptotic output tracking was considered. Arbitrary placement of the closed-loop system poles allowed the performance of the system to be tailored for this specific purpose. The linearizing coordinate transformation allowed for an augmented form of the controller that would asymptotically track certain reference trajectories.

For the purposes of state estimation, an extended Kalman filter was constructed such that reliable and accurate state values could be utilized by the controller in a timely manner. The Kalman filter is a state estimation method that seeks to optimally minimize the error between the actual and estimated states. Although the formulation in this work is “near” optimal, this method is robust enough that parameter changes and un-modeled plant dynamics do not have a large effect on the results.

A first series of simulations was developed in MATLAB m-file format which allowed the structure of the nonlinear controller and extended Kalman filter to be validated. The performance of the controller and estimator were promising enough that implementation on hardware was then pursued.

The m-file simulations were first converted into S-function based Simulink models but it was discovered that MATLAB's Real Time Workshop can not create an xPC executable from these types of models. The simulations had to be recast into a more suitable format using embedded m-files. While these simulations were being reformulated, the covariance equation was also updated from the simple format used in the m-file based simulations to the actual version that was implemented on hardware. The simulations produced promising results that strengthened the confidence in the original simulations. They showed that the higher fidelity covariance model, while allowing for higher standard deviations in estimation error, did not degrade the performance of the estimates or the controller performance.

Implementation of the controller and estimator could be carried out on the hardware after the sensor noise, plant noise covariance and nonlinear controller output mapping was performed using the Maglev hardware.

The sensor noise was determined empirically by fixing the position of the levitated object in the middle of the position sensors range and recording position values. These values were then used off-line to determine the appropriate sensor noise covariance.

Making use of an existing Lead-Lag controller, measurements were taken of the levitated object suspended by the hardware. The Simulink simulation model was modified to allow off-line plant noise covariance tuning. During the tuning process the state values produced by the estimator were not sufficient enough to allow for closed-loop control. The format of the state estimator was changed from a continuous-time extended Kalman filter to a continuous-discrete time extended Kalman filter. The utility of the Simulink environment allowed only some minor code changes to occur and the state estimator was converted. After several iterations a likely plant noise covariance was determined using the actual hardware data. As a final test, another Simulink model was constructed that allowed the state estimator to operate in an observation only mode. The state estimates produced by the extended Kalman filter were strong enough that hardware implementation could continue.

The next challenge was to adequately scale the output of the nonlinear controller so that the hardware could make use of it. Again, a linear controller was used to map the output of the nonlinear controller to the output of the linear controller. This mapping was very sensitive to changes in mass of the levitated object and the sensor curve used. Any changes to the system parameters beyond this point in the development would require a full system 're-tune'.

Several reference trajectories were considered for the Maglev hardware to track. In general, the Maglev tracked the reference trajectory with the exception that a static offset is present in all cases considered. Furthermore, there was strong evidence of a sinusoidal disturbance and/or a combination of un-modeled plant dynamics.

4.2 Future Work

4.2.1 Feedback Linearized Nonlinear Controller

At the core of this nonlinear control technique was the linearizing coordinate transformation and feedback. One of the many assumptions that this process drew upon was that the plant dynamics were known exactly. Once the system had been converted into a linear equivalent, a more robust controller could be used instead of a pole placement design to reduce the sensitivity to parameter changes and un-modeled plant dynamics.

4.2.2 State Estimation

Determination of the plant noise covariance was by far the most difficult portion of this research. The question for the designer was often, "what is a good enough state estimate?" Without adequate knowledge of the task to be performed or of how the hardware will actually perform, this question was difficult, if not impossible, to answer. An adaptive filtering scheme [38] would seek to alleviate the large and difficult tuning process. Post-measurement signal processing might also be implemented to improve performance and help reduce some of the persistent disturbances.

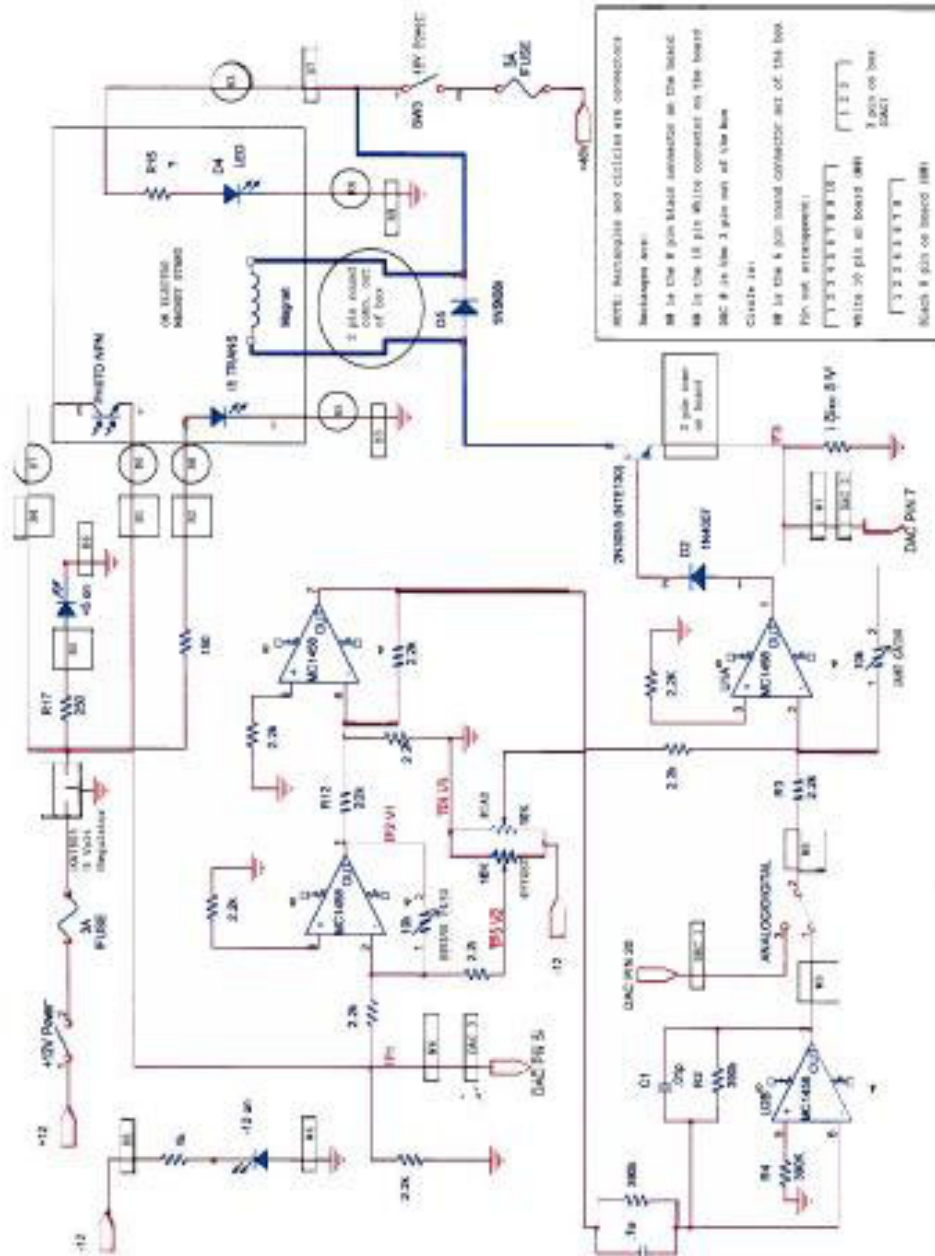
4.2.3 Hardware

Three hardware issues prohibited this system from being an outstanding platform for the future development of advanced control and state estimation techniques. First, the range of the position sensor, 1.0 mm, was not enough of a dynamic range to fully demonstrate the power of the nonlinear controller. A sensor with a larger operating range would greatly enhance this hardware.

Second, use of a commercially available electromagnet would further reduce the potential for un-modeled plant dynamics to exist, since the quality of construction and material construction are higher quality. Material selection and construction technique will help prevent the existence of distributed capacitance effects during electromagnet operation.

Third, the use of a commercially available power amplifier to drive the electromagnet would enable a more accurate plant model to be constructed. The present hardware requires the use of an operational amplifier and power transistor to boost the control input.

APPENDIX A
POWER ELECTRONICS SCHEMATIC



APPENDIX B

LIE DERIVATIVES AND LIE BRACKETS

Two types of operations are outlined in this section that will further the main body of this work as it pertains to the required math operations.

Lie Derivatives:

The first type of operation involving a real-valued function $h(x)$ and a vector field $f(x)$ is called a Lie Derivative. It involves taking the derivative of $h(x)$ along $f(x)$ and is often expressed as $L_f h$ [23].

$$\langle dh(x), f(x) \rangle = \frac{\partial h}{\partial x} f(x) = \sum_{i=1}^n \frac{\partial h}{\partial x_i} f_i(x) \quad (\text{B.1})$$

Lie Brackets can be used multiple times along the same vector field and on more than one different vector field. An example of a Lie Derivative taken twice of $h(x)$, first along $f(x)$ then along $g(x)$.

$$L_g L_f h(x) = \frac{\partial (L_f h)}{\partial x} g(x) \quad (\text{B.2})$$

This process is very straight forward. Simply start at the right-most Lie Derivative and work back towards the left. An example of a Lie Derivative taken twice of $h(x)$, both times along $f(x)$.

$$L_f^k h(x) = \frac{\partial (L_f^{k-1})}{\partial x} f(x) \quad (\text{B.3})$$

Lie Brackets:

The second type of operation involves two smooth vector fields $f(x)$ and $g(x)$ that produce another vector field. This new vector field is commonly called a Lie Bracket, $[f, g]$ and is defined as

$$[f, g] = \frac{\partial g}{\partial x} f(x) - \frac{\partial f}{\partial x} g(x) \quad (\text{B.4})$$

where $\frac{\partial g}{\partial x}$ and $\frac{\partial f}{\partial x}$ are the Jacobians of $g(x)$ and $f(x)$ respectively.

As with the Lie Derivative, the Lie Bracket, also called a Lie product, can be determined in successive iterations.

$$ad_f^k g(x) = [f, ad_f^{k-1} g](x) \quad (\text{B.5})$$

Allowing for any $k \geq 1$, when $ad_f^0 g(x) = g(x)$.

APPENDIX C
RELATIVE DEGREE CALCULATIONS

In order to determine the relative degree, following Definition 2.1, k is set to 0 and the Lie derivatives are taken. Then this process will continue until the Lie Derivative result is nonzero, when taken at the equilibrium state, x_0 .

$k = 0$:

$$L_g h(x) = [1 \ 0 \ 0] \begin{bmatrix} 0 & 0 & \frac{1}{L_c} \end{bmatrix}^T = 0 \quad (\text{C.1})$$

$k = 1$:

First taking the derivative of $h(x)$ along $f(x)$.

$$L_f h(x) = [1 \ 0 \ 0] \begin{bmatrix} x_2 & g - \frac{C}{m} \left(\frac{x_3}{x_1} \right)^2 & -\frac{R_c}{L_c} x_3 \end{bmatrix}^T = x_2 \quad (\text{C.2})$$

Then taking the derivative of $L_f h(x)$ along $g(x)$.

$$L_g L_f h(x) = [0 \ 1 \ 0] \begin{bmatrix} 0 & 0 & \frac{1}{L_c} \end{bmatrix}^T = 0 \quad (\text{C.3})$$

It is clear from C.3 that the process must progress to $k = 2$ since $L_g L_f h(x) \neq 0$

$k = 2$:

Instead of starting back with having to take the derivative $h(x)$ of along $f(x)$, the next step in this process can proceed directly from C.2. Starting with $L_f h(x)$ and take the derivative of it along $f(x)$.

$$L_f^2 h(x) = [0 \quad 1 \quad 0] \begin{bmatrix} x_2 & g - \frac{C}{m} \left(\frac{x_3}{x_1} \right)^2 & -\frac{R_c}{L_c} x_3 \end{bmatrix}^T = g - \frac{C}{m} \left(\frac{x_3}{x_1} \right)^2 \quad (\text{C.4})$$

As in the previous step take $L_f^2 h(x)$ and take its derivative along $g(x)$.

$$L_g L_f^2 h(x) = \begin{bmatrix} \frac{2C}{m} \left(\frac{x_3^2}{x_1^3} \right) & 0 & -\frac{2C}{m} \left(\frac{x_3}{x_1^2} \right) \end{bmatrix} \begin{bmatrix} 0 & 0 & \frac{1}{L_c} \end{bmatrix}^T = -\frac{2C}{mL_c} \left(\frac{x_3}{x_1^2} \right) \quad (\text{C.5})$$

$L_g L_f^2 h(x)$ being non-zero is not enough to finish the process; it will have to be non-zero at the equilibrium point x_0 . Since the region of state space has been restricted to $x_1 > 0$ and $x_3 > 0$ the relative degree of the system is simply computed relying on the equality $r - 1 = k$. By simple inspection the relative degree of the Maglev system at x_0 is 3.

APPENDIX D

NECESSARY AND SUFFICIENT CONDITION CALCULATIONS

Noting that the first vector of the matrix $g(x_0)$ is nothing more than a condensed version of $ad_f^0 g(x_0)$ there are no computations required other than establishing the Lie Product at the equilibrium point, x_0 .

$$g(x_0) = \begin{bmatrix} 0 & 0 & \frac{1}{L_c} \end{bmatrix}^T \quad (D.1)$$

Calculating $ad_f g(x)$:

$$ad_f g(x) = \frac{\partial g}{\partial x} f - \frac{\partial f}{\partial x} g \quad (D.2)$$

Note that $g(x)$ and $f(x)$ can be found defined in equation 2.10:

$$\frac{\partial g}{\partial x} = \begin{bmatrix} 0 \end{bmatrix} \quad (D.3) \quad \frac{\partial f}{\partial x} = \begin{bmatrix} 0 & 1 & 0 \\ \frac{2C}{m} \left(\frac{x_3}{x_1} \right)^2 & 0 & -\frac{2C}{m} \left(\frac{x_3}{x_1} \right) \\ 0 & 0 & -\frac{R_c}{L_c} \end{bmatrix} \quad (D.4)$$

$$ad_f g(x) = \begin{bmatrix} 0 \end{bmatrix} \begin{bmatrix} x_2 \\ g - \frac{C}{m} \left(\frac{x_3}{x_1} \right)^2 \\ -\frac{R_c}{L_c} x_3 \end{bmatrix} - \begin{bmatrix} 0 & 1 & 0 \\ \frac{2C}{m} \left(\frac{x_3}{x_1} \right)^2 & 0 & -\frac{2C}{mL_c} \left(\frac{x_3}{x_1} \right) \\ 0 & 0 & -\frac{R_c}{L_c} \end{bmatrix} \begin{bmatrix} 0 \\ 0 \\ \frac{1}{L_c} \end{bmatrix} \quad (D.5)$$

$$ad_f g = \begin{bmatrix} 0 & \frac{2C}{mL_c} \left(\frac{x_3}{x_1} \right) & \frac{R_c}{L_c^2} \end{bmatrix}^T \quad (D.6)$$

Calculating $ad_f^2 g(x)$ involves:

$$ad_f^2 g(x) = [f, ad_f g(x)] = \frac{\partial ad_f g}{\partial x} f - \frac{\partial f}{\partial x} ad_f g \quad (D.7)$$

Determining the Jacobian of D.6 produces:

$$\frac{\partial ad_f g}{\partial x} = \begin{bmatrix} 0 & 0 & 0 \\ -4C \left(\frac{x_3}{x_1^3} \right) & 0 & \frac{2C}{mL_c} \left(\frac{1}{x_2} \right) \\ 0 & 0 & 0 \end{bmatrix} \quad (D.8)$$

$$ad_f^2 g(x) = \begin{bmatrix} 0 & 0 & 0 \\ -4C \left(\frac{x_3}{x_1^3} \right) & 0 & \frac{2C}{mL_c} \left(\frac{1}{x_2} \right) \\ 0 & 0 & 0 \end{bmatrix} \begin{bmatrix} x_2 \\ g - \frac{C}{m} \left(\frac{x_3}{x_1} \right)^2 \\ -\frac{R_c}{L_c} x_3 \end{bmatrix}$$

$$- \begin{bmatrix} 0 & 1 & 0 \\ \frac{2C}{m} \left(\frac{x_3^2}{x_1^3} \right) & 0 & -\frac{2C}{m} \left(\frac{x_3}{x_1^2} \right) \\ 0 & 0 & -\frac{R_c}{L_c} \end{bmatrix} \begin{bmatrix} 0 \\ \frac{2C}{mL_c} \left(\frac{x_3}{x_1^2} \right) \\ \frac{R_c}{L_c^2} \end{bmatrix} \quad (D.9)$$

$$ad_f^2 g = \begin{bmatrix} -2Cx_3 & -4Cx_2x_3 & R_c^2 \\ mL_c x_1^2 & mL_c x_1^3 & L_c^3 \end{bmatrix}^T \quad (D.10)$$

Once $[g \quad ad_f g \quad ad_f^2 g]$ is constructed its rank can be determined at x_0 .

$$\text{rank}\{g(x_0), ad_f g(x_0), ad_f^2 g(x_0)\} = \text{rank} \left\{ \begin{array}{ccc} 0 & 0 & \frac{-2C}{mL_c} \left(\frac{x_3}{x_1^2} \right) \\ 0 & \frac{2C}{mL_c} \left(\frac{x_3}{x_1^2} \right) & \frac{-4C}{mL_c} \left(\frac{x_2 x_3}{x_1^3} \right) \\ \frac{1}{L_c} & \frac{R_c}{L_c^2} & \frac{R_c^2}{L_c^3} \end{array} \right\} \Bigg|_{x_0} \quad (\text{D.11})$$

$$= 3$$

Checking Condition II:

The center piece of condition II involves the Frobenius Theorem, which allows for the span to be involutive if it is completely integrable. This condition is easily checked by noting the Lie Product of any two column vectors in the span is said to be involutive if that product can be constructed as a linear combination of those two vectors.

$$[g(x), ad_f g(x)] = \delta g(x) + \gamma ad_f g(x) \quad (\text{D.12})$$

Calculating $[g(x), ad_f g(x)]$:

$$[g(x), ad_f g(x)] = \frac{\partial ad_f g(x)}{\partial x} g(x) - \frac{\partial g(x)}{\partial x} ad_f g(x) \quad (\text{D.13})$$

All of the required Jacobians for this product have already been calculated, substituting D.1, D.3, D.6 and D.8 into D.13 produces

$$[g(x), ad_f g(x)] = \begin{bmatrix} 0 \\ \frac{2C}{mL_c^2} \left(\frac{1}{x_1^2} \right) \\ 0 \end{bmatrix} \quad (\text{D.14})$$

Equation D.14 can also be constructed with the linear combination of $g(x)$ and $ad_f g(x)$.

$$[g(x), ad_f g(x)] = \begin{bmatrix} 0 \\ \frac{2C}{mL_c^2} \left(\frac{1}{x_1^2} \right) \\ 0 \end{bmatrix} = \frac{-R_c}{L_c x_3} \begin{bmatrix} 0 \\ 0 \\ 1 \\ \frac{1}{L_c} \end{bmatrix} + \frac{1}{x_3} \begin{bmatrix} 0 \\ \frac{2C}{mL_c} \left(\frac{x_3}{x_1^2} \right) \\ \frac{R_c}{L_c^2} \end{bmatrix} \quad (\text{D.15})$$

Note that $\delta = \frac{-R_c}{L_c x_3}$ and $\gamma = \frac{1}{x_3}$ thus making the second condition true and making the

existence of a linearizing coordinate transformation and nonlinear feedback possible.

APPENDIX E

CONSTRUCTION OF THE COORDINATE CHANGE AND NONLINEAR
FEEDBACK

Take the derivative of the output $h(x)$ along the dynamics of the system until the input appears [24]. Looking back at the relative degree determination, the input $u(t)$ is not expected to appear until third iteration of this process.

$$\dot{y} = \nabla h(x)(f(x) + g(x)u(t)) = L_f h(x) + L_g h(x)u(t) \quad (\text{E.1})$$

$$L_g h(x) = [1 \ 0 \ 0][0 \ 0 \ 1/L_c]^T = 0 \quad (\text{E.2})$$

Substituting C.2 and E.2 into E.1

$$\dot{y} = x_2 + 0 \cdot u(t) \quad (\text{E.3})$$

Repeating this process for E.3.

$$\ddot{y} = L_f^2 h(x) + L_g L_f h(x) u(t) \quad (\text{E.4})$$

Taking advantage of C.3 and C.4 and substituting them into E.4

$$\ddot{y} = g - \frac{C}{m} \left(\frac{x_3}{x_1} \right)^2 + 0 \cdot u(t) \quad (\text{E.5})$$

Again for equation E.5

$$\ddot{\ddot{y}} = L_f^3 h(x) + L_g L_f^2 h(x) u(t) \quad (\text{E.6})$$

Building on the results of C.4

$$L_f^3 h(x) = \begin{bmatrix} \frac{2C}{m} \left(\frac{x_3^2}{x_1^3} \right) & 0 & -\frac{2C}{m} \left(\frac{x_3}{x_1^2} \right) \end{bmatrix} \begin{bmatrix} x_2 & g - \frac{C}{m} \left(\frac{x_3}{x_1} \right)^2 & -\frac{R_c}{L_c} x_3 \end{bmatrix}^T \quad (\text{E.7a})$$

$$L_f^3 h(x) = \frac{2C}{m} \left(\frac{x_2 x_3^2}{x_1^3} \right) + \frac{2C R_c}{m L_c} \left(\frac{x_3^2}{x_1^2} \right) \quad (\text{E.7b})$$

Again using C.4 except its derivative is taken along $g(x)$

$$L_g L_f^2 h(x) = \begin{bmatrix} \frac{2C}{m} \left(\frac{x_3^2}{x_1^3} \right) & 0 & -\frac{2C}{m} \left(\frac{x_3}{x_1^2} \right) \end{bmatrix} \begin{bmatrix} 0 & 0 & 1/L_c \end{bmatrix}^T \quad (\text{E.8a})$$

$$L_g L_f^2 h(x) = -\frac{2C}{m L_c} \left(\frac{x_3}{x_1^2} \right) \quad (\text{E.8b})$$

Equation E.6 can be rewritten substituting in E.8a and E.8b

$$\ddot{y} = \frac{2C}{m} \left(\frac{x_2 x_3^2}{x_1^3} \right) + \frac{2C R_c}{m L_c} \left(\frac{x_3^2}{x_1^2} \right) - \frac{2C}{m L_c} \left(\frac{x_3}{x_1^2} \right) u(t) \quad (\text{E.9})$$

The input has appeared as part of the output. Now a coordinate transformation between $y(t)$ and $u(t)$ can be defined.

$$z = \Phi(x) = \begin{bmatrix} y \\ \dot{y} \\ \ddot{y} \end{bmatrix} \quad (\text{E.10a})$$

An alternative definition can be expressed in terms of the dynamic system parameters.

Note that the position, velocity and acceleration of the levitated object are represented in the coordinate transformation.

$$z = \Phi(x) = \begin{bmatrix} x_1 & x_2 & g - \frac{C}{m} \left(\frac{x_3}{x_1} \right)^2 \end{bmatrix}^T \quad (\text{E.10b})$$

Casting E.10b into a set of first order differential equations the coordinate change picks up the input $u(t)$ allows the definition of the new input $v(t)$.

$$\begin{bmatrix} \dot{z}_1 \\ \dot{z}_2 \\ \dot{z}_3 \end{bmatrix} = \begin{bmatrix} \dot{y} \\ \ddot{y} \end{bmatrix} = \begin{bmatrix} x_2 \\ g - \frac{C}{m} \left(\frac{x_3}{x_1} \right)^2 \\ \frac{2C}{m} \left(\frac{x_2 x_3^2}{x_1^3} \right) + \frac{2C R_c}{m L_c} \left(\frac{x_3^2}{x_1^2} \right) - \frac{2C}{m L_c} \left(\frac{x_3}{x_1^2} \right) u(t) \end{bmatrix} \quad (\text{E.11})$$

Calling the last derivative taken \ddot{y} , the new input to the linear system E.11 can be rewritten in a $\dot{z} = Az + bv$ format. Where A is 3x 3 matrix and b is a 3x1 vector.

$$\dot{z} = \begin{bmatrix} z_2 \\ z_3 \\ v \end{bmatrix} = \begin{bmatrix} 0 & 1 & 0 \\ 0 & 0 & 1 \\ 0 & 0 & 0 \end{bmatrix} \begin{bmatrix} z_1 \\ z_2 \\ z_3 \end{bmatrix} + \begin{bmatrix} 0 \\ 0 \\ 1 \end{bmatrix} v(t) \quad (\text{E.12})$$

The format of equation E.12 is commonly known as a Bruvonsky form. The last row of E.12 is of special interest since it is the nonlinear feedback. Examining it closer one finds that a relationship exists between the nonlinear system's input $u(t)$ and the linear system's input v .

$$v = L_f^3 h(x) + L_g L_f^2 h(x) u(t) \quad (\text{E.13})$$

Solving for $u(t)$ determines what the relationships is between the two inputs using nonlinear feedback.

$$u(t) = \frac{-L_f^3 h(x) + v}{L_g L_f^2 h(x)} \quad (\text{E.14})$$

In much of the literature equation E.14 is written in a different format [22], [23]

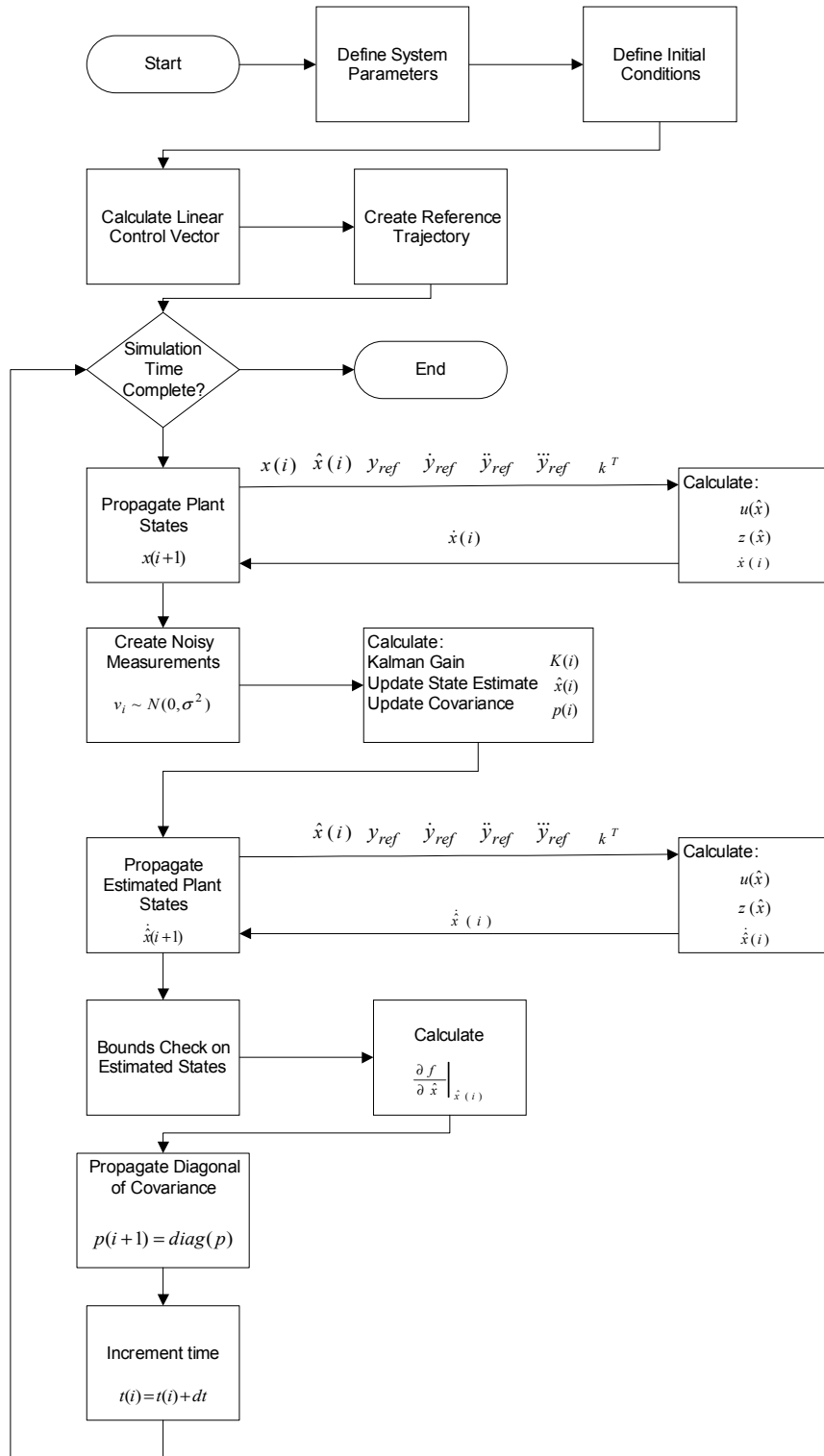
$$u(t) = \frac{\alpha(x) + v}{\beta(x)} \quad (\text{E.15})$$

Where the elements of α and β are shown in equation E.14.

APPENDIX F

CONTROLLER / ESTIMATOR SIMULATION CODE

Simulation Flow Schematic:



M-file Based Simulation for Step Response:

```

%John A. Henley
%22 May 2005
% Feedback Linearized Controller / Extended Kalman Filter
% Simulation via M-file for concept validation
%This file requires that the m-file real_state_track.m and
%estimate_fun_track.m
%close and reset
clear all; close all;
%System Parameters
x10=.0148; L0=.02; C0=x10*L0/2;
mass=.05506; g=9.81; L1=.59;
r=.001^2; R=25;
%Time Step
dt=.001;
%Time Vector
t=[0:dt:1.5];
m=length(t);
%Define State Vector Size and Length
xt=zeros(m,3); ym=zeros(m,1);p_cov=zeros(m,3);xe=zeros(m,3);
%define Initial Conditions
x10=.0148; x20=0; x30=x10*sqrt(g*mass/C0);
x0=[1*x10;0;1*x30]
%Setting Initial Conditions of Plant & Estimate
xt(1,:)=x0';
xe(1,:)=[1.05*x10;0;1.05*x30]';
%Define initial conditions for covaraince
p0=.085*eye(3); p=p0; p_cov(1,:)=diag(p0)';
%Define Process Noise Covaraince
q=.025*[ 0 0 0;
        0 1 0;
        0 0 1];
%define measurement equation
h=[1 0 0];
%linearization and pole placement
b=[ 0;
    0;
    1];
A=[ 0 1 0;
    0 0 1;
    0 0 0];
%desired poles
p1=[-100,-60,-80];
%Closed Loop Poles based on [-100,-60,-80]
l=[240 18800 480000];
%Open Loop Poles
a=[0 0 0];
%Teoplitz Matrix
T=[1 0 0; 0 1 0; 0 0 1];
%Controbality Matrix

```

```

C=[0 0 1;0 1 0;1 0 0];
%Bass-Gura Formula
k=(1-a)*inv(T')*inv(C)
%Load workspace with 2mm step change
load reftraj0140501605
yr=yref;
%velocity is set to zero to help avoid singularity in the response
yr1=zeros(m,1);
yr2=yr1;
yr3=yr2;
%start of simulation
for i=1:m-1;
%i-th portion of the reference trajectory
y=yr(i);
y1=yr1(i);
y2=yr2(i);
y3=yr3(i);
%Plant State Propagation
%fixed step 4th Order Runge-Kutta Integration
f1=dt*real_state_track(xt(i,:),k,y,y1,y2,y3,xe(i,:));
f2=dt*real_state_track(xt(i,)+0.5*f1',k,y,y1,y2,y3,xe(i,:));
f3=dt*real_state_track(xt(i,)+0.5*f2',k,y,y1,y2,y3,xe(i,:));
f4=dt*real_state_track(xt(i,)+f3',k,y,y1,y2,y3,xe(i,:));
xt(i+1,:)=xt(i,)+1/6*(f1'+2*f2'+2*f3'+f4');
%create artificial measurement bases on reference trajectory with
%standard deviation r
ym(i)=xt(i,1)+sqrt(r)*randn;
% Kalman Update
gain=p*h'*inv(h*p*h'+r);
p=(eye(3)-gain*h)*p;
xe(i,:)=xe(i,)+gain*(ym(i)-xe(i,1));
%State Estimate Propagation
%fixed step 4th Order Runge-Kutta Integration
f1=dt*estimate_fun_track(xe(i,:),k,y,y1,y2,y3);
f2=dt*estimate_fun_track(xe(i,)+f1',k,y,y1,y2,y3);
f3=dt*estimate_fun_track(xe(i,)+f2',k,y,y1,y2,y3);
f4=dt*estimate_fun_track(xe(i,)+f3',k,y,y1,y2,y3);
xe(i+1,:)=xe(i,)+1/6*(f1'+2*f2'+2*f3'+f4');
%Bounds Check
if xe(i,3)<0
    xe(i,3)=0;
end
if xe(i,3)>1.25
    xe(i,3)=1.25;
end
%Jacobian of open loop plant
fpart =[0, 1,0;
3*(C0/mass)*(xe(i,3))^2/xe(i,1)^3,0,2*(C0/mass)*xe(i,3)/xe(i,1)^2;
0,0,-(R/L1)];
%propagation of covariance
phi=c2d(fpart,[0;0;1],dt);
p=phi*p*phi'+q*dt;

```



```

p_cov(i+1,:) = diag(p)';
end
%calculation of sigma bounds
sig3 = p_cov.^ (0.5) * 3;
M-file Based Plant Propagation:
function f = real_state_track(xt, k, y, y1, y2, y3, xe)
x1d = .0148;
x10 = .0148;
L0 = .02;
C0 = x10 * L0 / 2;
mass = .05506;
g = 9.81;
L = .59;
R = 25;
Ks = 1;
%transformed states
z1 = Ks * (xe(1));
z2 = Ks * xe(2);
z3 = Ks * (g - C0 / mass * xe(3) ^ 2 / xe(1) ^ 2);
%componets of nonlinear feedback
b = 2 * Ks * C0 / mass * xe(3) ^ 2 / xe(1) ^ 3 * xe(2) + 2 * Ks * C0 / mass * xe(3) ^ 2 / xe(1) ^ 2 * R / L;
a = -2 * Ks * C0 / mass * xe(3) / xe(1) ^ 2 / L;
v = -(k(1) * (z1 - Ks * y) + k(2) * (z2 - Ks * y1) + k(3) * (z3 - Ks * y2));
u = (-b + v + y3) / a;
%controlled plant
f = [ xt(2);
      g - (C0 / mass) * (xt(3) / xt(1)) ^ 2;
      - (R / L) * xt(3) + (1 / L) * u];

```

M-file Based Estimate Propagation:

```

function f = estimate_fun_track(xe, k, y, y1, y2, y3)
x1d = .0148;
x10 = .0148;
L0 = .02;
C0 = x10 * L0 / 2;
mass = .05506;
g = 9.81;
L = .59;
R = 25;
Ks = 1;
%transformed states
z1 = Ks * (xe(1));
z2 = Ks * xe(2);
z3 = Ks * (g - C0 / mass * xe(3) ^ 2 / xe(1) ^ 2);
%componets of nonlinear feedback
b = 2 * Ks * C0 / mass * xe(3) ^ 2 / xe(1) ^ 3 * xe(2) + 2 * Ks * C0 / mass * xe(3) ^ 2 / xe(1) ^ 2 * R / L;
a = -2 * Ks * C0 / mass * xe(3) / xe(1) ^ 2 / L;
v = -(k(1) * (z1 - Ks * y) + k(2) * (z2 - Ks * y1) + k(3) * (z3 - Ks * y2));
u = (-b + v + y3) / a;
f = [ xe(2);
      g - (C0 / mass) * (xe(3) / xe(1)) ^ 2;

```

$-(R/L) * x_e(3) + (1/L) * u];$

M-file Based Simulation for Sine Wave Response:

```
%John A. Henley
%22 May 2005
% Feedback Linearized Controller / Extended Kalman Filter
% Simulation via M-file for concept validation
%This file requires that the m-file real_state_track.m and
%estimate_fun_track.m
%close and reset
clear all; close all;
%System Parameters
x10=.0148; L0=.02; C0=x10*L0/2;
mass=.05506; g=9.81; L1=.59;
r=.001^2; R=25;
%Time Step
dt=.001;
%Time Vector
t=[0:dt:1.5];
m=length(t);
%Define State Vector Size and Length
xt=zeros(m,3); ym=zeros(m,1);p_cov=zeros(m,3);xe=zeros(m,3);
%define Initial Conditions
x10=.0148; x20=0; x30=x10*sqrt(g*mass/C0);
x0=[1*x10;0;1*x30]
%Setting Initial Conditions of Plant & Estimate
xt(1,:)=x0';
xe(1,:)= [1.05*x10;0;1.05*x30]';
%Define initial conditions for covariance
p0=.085*eye(3); p=p0; p_cov(1,:)=diag(p0)';
%Define Process Noise Covariance
q=.025*[ 0 0 0;
        0 1 0;
        0 0 1];
%define measurement equation
h=[1 0 0];
%linearization and pole placement
b=[ 0;
    0;
    1];
A=[ 0 1 0;
    0 0 1;
    0 0 0];
%desired poles
p1=[-100,-60,-80];
%Closed Loop Poles based on [-100,-60,-80]
l=[240 18800 480000];
%Open Loop Poles
a=[0 0 0];
%Teoplitz Matrix
```

```

T=[1 0 0; 0 1 0; 0 0 1];
%Controbality Matrix
C=[0 0 1;0 1 0;1 0 0];
%Bass-Gura Formula
k=(1-a)*inv(T')*inv(C)

%reference signal
yr=.0148*ones(m,1)+0.001*sin(20*t');
yr1=diff(yr)/dt;
yr1(m)=yr(m-1); %First Time Derivative of Trajectory
yr2=diff(yr1)/dt;
yr2(m)=yr1(m-1); %Second Time Derivative of Trajectory
yr3=diff(yr2)/dt;
yr3(m)=yr2(m-1); %Third Time Derivative of Trajectory
%start of simulation
for i=1:m-1;
%i-th portion of the reference trajectory
y=yr(i);
y1=yr1(i);
y2=yr2(i);
y3=yr3(i);
%Plant State Propagation
%fixed step 4th Order Runge-Kutta Integration
f1=dt*real_state_track(xt(i,:),k,y,y1,y2,y3,xe(i,:));
f2=dt*real_state_track(xt(i, :)+0.5*f1',k,y,y1,y2,y3,xe(i,:));
f3=dt*real_state_track(xt(i, :)+0.5*f2',k,y,y1,y2,y3,xe(i,:));
f4=dt*real_state_track(xt(i, :)+f3',k,y,y1,y2,y3,xe(i,:));
xt(i+1,:)=xt(i, :)+1/6*(f1'+2*f2'+2*f3'+f4');
%create artificial measurement bases on reference trajectory with
%standard deviation r
ym(i)=xt(i,1)+sqrt(r)*randn;
% Kalman Update
gain=p*h'*inv(h*p*h'+r);
p=(eye(3)-gain*h)*p;
xe(i, :)=xe(i, :)+gain*(ym(i)-xe(i,1));
%State Estimate Propagation
%fixed step 4th Order Runge-Kutta Integration
f1=dt*estimate_fun_track(xe(i,:),k,y,y1,y2,y3);
f2=dt*estimate_fun_track(xe(i, :)+f1',k,y,y1,y2,y3);
f3=dt*estimate_fun_track(xe(i, :)+f2',k,y,y1,y2,y3);
f4=dt*estimate_fun_track(xe(i, :)+f3',k,y,y1,y2,y3);
xe(i+1,:)=xe(i, :)+1/6*(f1'+2*f2'+2*f3'+f4');
%Bounds Check
if xe(i,3)<0
    xe(i,3)=0;
end
if xe(i,3)>1.25
    xe(i,3)=1.25;
end
%Jacobian of open loop plant
fpart =[0,1,0;
3*(C0/mass)*(xe(i,3))^2/xe(i,1)^3,0,-2*(C0/mass)*xe(i,3)/xe(i,1)^2;

```

```
0,0,-(R/L1)];  
%propigation of covariance  
phi=c2d(fpart,[0;0;1],dt);  
p=phi*p*phi'+q*dt;  
p_cov(i+1,:)=diag(p)';  
end  
%calculation of sigma bounds  
sig3=p_cov.^(0.5)*3;
```

APPENDIX G

EMBEDDED M-FUNCTION CODE

Nonlinear Controller:

```

function control = fcn(inputs)
    y = inputs(1);
    y1 = inputs(2);
    y2 = inputs(3);
    y3 = inputs(4);
    x1 = inputs(5);
    x2 = inputs(6);
    x3 = inputs(7);
    x1d=.0148;
    x10=.0148;
    L0=.02;
    C0=x10*L0/2;
    mass=.05506;
    g=9.81;
    L=.59;
    R=25;
    Ks=1;
    k=[480000, 18800, 240];
    z1 = Ks*(x1);
    z2 = Ks*x2;
    z3 = Ks*(g- (C0/mass) * (x3/x1)^2);
    b=2*Ks*C0/mass*x3^2/x1^3*x2+2*Ks*C0/mass*x3^2/x1^2*R/L;
    a=-2*Ks*C0/mass*x3/x1^2/L;
    v=-(k(1)*(z1-Ks*y)+k(2)*(z2-Ks*y1)+k(3)*(z3-Ks*y2));
    u1=(-b+v+y3)/a;
control = u1;

```

Extended Kalman Filter:

```

function [state_estimate,covariance] = fcn(old_state,inputs,
old_covariance)
p0 = 1e-5*eye(3);
p = p0 ;
p_cov = diag(p0)';
q = [0 0 0;
      0 1*10^-5 0;
      0 0 1*10^-5];
gamma=.25* [0,0,0;
            0,1,0;
            0,0,1];
x10=.0148; L0=.02; C0=x10*L0/2;
mass=.05506; g=9.81; L=.59; R=25;
h = [1 0 0];
r = 0.001^2;
u1 = inputs(1);
ym = inputs(2);
p=old_covariance;
x=old_state;
gain=p*h'/r;

```

```

fpart = [ 0, 1,
0;
3*(C0/mass)*(x(3))^2/x(1)^3, 0, -2*(C0/mass)*x(3)/x(1)^2;
0, 0, -(R/L)];
dx=[ x(2);
g-(C0/mass)*(x(3)/x(1))^2;
-(R/L)*x(3)+(1/L)*u1] + gain*(ym - x(1));
pdot = fpart*p + p*fpart' -p*h'*(1/r)*h*p+ gamma*q*gamma';
state_estimate=dx;
covariance=pdot;

```

Maglev Plant Dynamics:

```

function [sys,x0] = maglev_3(t,x,u,flag)
switch flag,
case 0
    sizes = simsizes;
    sizes.NumContStates = 3;
    sizes.NumDiscStates = 0;
    sizes.NumOutputs = 1;
    sizes.NumInputs = 1;
    sizes.DirFeedthrough = 0;
    sizes.NumSampleTimes = [];
    sys = simsizes(sizes);
    x0 = [1.10*.0148;0;1.1*.8921];

case 1
    u1=u(1);
    x10=.0148;
    L0=.02;
    C0=x10*L0/2;
    mass=.05506;
    g=9.81;
    L=.59;
    R=25;
    dx=[ x(2);
        g-(C0/mass)*(x(3)/x(1))^2;
        -(R/L)*x(3)+(1/L)*u1];
    sys=dx;

case 3
    sys = [x(1)];

case {2, 4, 9 }
    sys = []; % Unused flags

otherwise
    error(['Unhandled flag = ',num2str(flag)]); % Error handling
end;

```

Continuous - Discrete Extended Kalman Filter:

```

function [state_estimate,covariance] =
fcn(old_state,inputs,ref_pos,old_covariance)
q = [ 1*10^-4      0      0;
      0      .75*10^-7      0;
      0      0      1*10^-8 ];
gamma=[ 1,0,0;
        0,1,0;
        0,0,1];
x1d=ref_pos/1000;
x10=x1d;
L0=.02;
C0=x10*L0/2;
mass=.05506;
g=9.81;
L=.59;
R= 27.6;
Ks=1;
h=[1 0 0];
r = 0.0034^2;
u1=inputs(1);
ym=inputs(2);
p=old_covariance;
x=old_state;
%Continuous-Discrete Extended Kalman Filter
k=p*h'*inv(h*p*h'+r);
%State Update
x=x+k'*(ym-x(1));
%Covariance Update
p=(eye(3,3)-k*h)*p;
%propigation of state
dx=[x(2);
     g-(C0/mass)*(x(3)/x(1))^2;
     -(R/L)*x(3)+u1/L];
%propigation of covariance
fpart =[0, 1, 0;
        3*(C0/mass)*(x(3))^2/x(1)^3, 0, -2*(C0/mass)*x(3)/x(1)^2;
        0, 0, -(R/L)];
pdot=fpart*p+p*fpart'+gamma*q*gamma';
state_estimate=dx;
covariance=pdot;

```


APPENDIX H

NONLINEAR CONTROL OUTPUT MAPPING

Table H.1 Nonlinear control output mapping results

Ref Position	Offset		Digital Controller Out		Nonlinear Controller Out		Measured Position		Position Estimate		Velocity Estimate		Current Estimate		Coil Voltage		Coil Resistance		Coil Current	
	<i>mm</i>	<i>V</i>	<i>V</i>	<i>V</i>	<i>V</i>	<i>V</i>	<i>m</i>	<i>m</i>	<i>m</i>	<i>m</i>	<i>m/sec</i>	<i>A</i>	<i>A</i>	<i>V</i>	<i>V</i>	Ω	Ω	<i>A</i>	<i>A</i>	
14.2	1.2	1.369	23.734	0.0139	0.0141	6.037E-05	0.860	25.74	26.7	0.964										
14.3	1.2	1.423	23.716	0.0140	0.0142	4.929E-05	0.859	25.35	26.4	0.960										
14.4	1.2	1.324	24.024	0.0142	0.0143	4.392E-05	0.870	25.97	26.2	0.991										
14.5	1.2	1.293	24.187	0.0144	0.0144	3.326E-05	0.876	26.29	26.2	1.003										
14.6	1.2	1.284	24.296	0.0145	0.0145	2.992E-05	0.880	26.15	25.8	1.014										
14.7	1.2	1.231	24.515	0.0147	0.0147	1.076E-05	0.888	26.85	25.9	1.037										
14.8	1.2	1.222	24.620	0.0148	0.0148	1.370E-05	0.892	26.88	25.9	1.038										
14.9	1.2	1.245	24.644	0.0148	0.0149	1.667E-05	0.893	26.84	26	1.032										
15.0	1.2	1.240	24.740	0.0149	0.0150	1.450E-05	0.896	27.16	26.1	1.041										
15.1	1.2	1.215	24.885	0.0151	0.0151	5.250E-06	0.902	27.31	26.1	1.046										
15.2	1.2	1.241	24.901	0.0151	0.0152	1.615E-05	0.902	27.33	26	1.051										
15.3	1.2	1.253	24.952	0.0152	0.0153	2.022E-05	0.904	27.69	26.5	1.045										
15.4	1.2	1.385	24.964	0.0152	0.0153	4.768E-04	0.903	27.44	26.5	1.035										
15.5	1.2	2.027	23.588	0.0148	0.0153	-1.575E-03	0.887	27.15	26.3	1.032										

REFERENCES

- [1] I. Busch-Vishniac, et. al, "Magnetic Levitation-Based Micro-Automation of Mechanical Processes in Semiconductor Fabrication," *Proceedings of IEEE MEMS '90*, Napa Valley, CA, pp 144-146, 1990.
- [2] T. Nakagawa, M. Hama and T. Furukawa, "Study of Magnetic levitation technique Applied to Steel Plate Production Line," *IEEE Transactions on Magnetics*, Vol. 36, No. 5, pp 3686-3689, 2000.
- [3] D. Cho, Y. Kato, and F. Spilman, "Sliding mode control and classical control magnetic levitation systems," *IEEE Control Systems Magazines*, Vol. 13, pp 42-28, 1993
- [4] L Li, T. Shinshi and A. Shimokohbe, "Asymptotically Exact Linearizations for Active Magnetic Bearing actuators in Voltage Control Configuration," *IEEE Transactions on Control Systems Technology*, Vol. 11, No. 2, pp 185-195, 2003
- [5] H. Gutierrez and P. Ro, " Sliding-Mode Control of a Nonlinear-Input System: application to a Magnetically Levitated Fast-Tool Servo," *IEEE Transactions on Industrial Electronics*, Vol. 45, No. 6, 1998.
- [6] A. El Hajjaji and M. Ouladsine, "Modeling and Nonlinear Control of Magnetic Levitation Systems," *IEEE Transactions on Industrial Electronics*, Vol. 48, No. 8, pp. 831-838, 2001.
- [7] F. Zhang and K. Suyama, "Nonlinear Feedback of Magnetic Levitation System by Exact Linearization Approach," *Proceedings of the 4th IEEE Conference on*, pp. 327- 328, 1995.
- [8] M.R Filho and E. Munaro, "A Design Methodology of Tracking Controllers for Magnetic Levitation Systems," *Proceedings of the 2001 IEEE International Conference on Control Applications*, September 2001.
- [9] F.J.Lin, H.J. Shieh, L.T. Teng and P.H Shieh, "Hybrid Controller with Recurrent Neural Network for Magnetic Levitation System," *IEEE Transactions on Magnetics*, Vol. 41, No. 7, pp. 2320-2329, 2005.
- [10] N.F. Al-Muthairi and M. Zribi, "Sliding Mode Control of a Magnetic Levitation System," *Mathematical Problems in Engineering 2004:2*, pp. 93-107, 2004.
- [11] J. Phuah, J. Lu, M. Yasser and T. Yahagi, "Neuro-Sliding Mode Control for Magnetic Levitation Systems," *Circuits and Systems, IEEE International Symposium*, pp. 23-32, 2005.
- [12] C.J. Munaro, M.R. Filho, R.M. Borges, S. Munareto and W.T. Costa, "Modeling and Observer-Based Nonlinear Control of a Magnetic Levitation System," *Proceedings of the 2002 IEEE International Conference on Control Applications*, pp.162-167, September 2002.

- [13] W. Barie and J. Chiasson, "Linear and Nonlinear State-Space Controllers for Magnetic Levitation," *International Journal of Systems Science*, Vol. 27, No. 11, pp. 1153-1163, 1996.
- [14] *6023E/6024E/6025E Families*, National Instruments Corp., Austin.
- [15] *xPC Target User's Guide*, MathWorks Inc., MA, 1999.
- [16] D. Piyabongkarn, "Digital Control of a Magnetic Levitation System Through xPc Real-Time Operating System: Classical, Feedforward and Artificial Neural Network," *Masters Thesis*, Mechanical and Aerospace Engineering, UT-Arlington, 2000.
- [17] O. Taghavi-Zargar, "Fuzzy Logic Control of a Magnetic Levitation System with Hardware Implementation," *Masters Thesis*, Mechanical and Aerospace Engineering, UT-Arlington, 2003.
- [18] P.S. Shiakolas, S.R. an Schneck, D. Piyabongkarn, and I. Frangeskou, "Magnetic Levitation Hardware-in-the-Loop and MATLAB-Based Experiments for Reinforcement of Neural Network Control Concepts," *IEEE Transactions on Education*, Vol. 47, No. 1, pp. 33-41, 2004.
- [19] A.R. Hambley, *Electrical Engineering & Applications*, Upper Saddle River, NJ: Prentice Hall, 1997.
- [20] L. Sun, H. Ohmori, and A. Sano, "Direct Closed-loop Identification of Magnetic Suspension System," *Proceeding of the 1999 IEEE International Conference on Control Applications*, Hawaii, pp. 749-754, August 1999.
- [21] T.H. Wong, "Design of a Magnetic Levitation Control System – An Undergraduate Project," *IEEE Transactions on Education*, Vol. E-29, No. 4, pp. 196-200, November 1986.
- [22] W. Barie and J. Chiasson, "Linear and Nonlinear State-Space Controllers for Magnetic Levitation," *International Journal of Systems Science*, Vol. 27, No. 11, pp. 1153-1163, 1996.
- [23] A. Isidori, *Nonlinear Control Systems*, Third Edition, London, UK: Springer, 2002.
- [24] J.E. Slotine and W. Li, *Applied Nonlinear Control*, Upper Saddle River, NJ: Prentice Hall, 1991.
- [25] L.R. Hunt, G. Meyer and R. Su, "Driven Dynamics of Time-Varying Linear Systems," *IEEE Transactions on Automatic Control*, Vol. 42, No. 9, pp. 1313-1317, 1997.
- [26] G. Meyer, L.R. Hunt and R. Su, "Nonlinear System Guidance in the Presence of Transmission Zero Dynamics", *NASA Technical Memorandum 4661*, 1995.
- [27] L.R. Hunt, G. Meyer and V. Ramakrishna, "Guidance and Stable and Unstable Manifolds with Input," *International Journal of Robust and Nonlinear Control*, Vol. 9, pp. 85-99, 1999.
- [28] L.R. Hunt, V. Ramakrishna and G. Meyer, "Stable Inversion and Parameter Variations," *Systems & Control Letters*, 1997.
- [29] V. Ramakrisjna, L.R. Hunt and G. Meyer, "Parameter Variations, Relative Degree, and Stable Inversion," *Automatica*, Vol. 37, pp. 871-880.

- [30] L.R. Hunt and G. Meter, "Stable Inversion for Nonlinear Systems," *Automatica*, Vol. 23, pp. 1549-1554.
- [31] S. Devasia, D. Chen and B. Paden, "Nonlinear Inversion-Based Output Tracking," *IEEE Transactions on Automatic Control*, Vol. 41, No. 7, pp. 930-942, 1996.
- [32] R.M. Hirschorn, "Invertibility of Nonlinear Control Systems," *Siam J. Control and Optimization*, Vol. 17, No. 2, pp. 289-297, March 1979.
- [33] L.R. Hunt, G. Meyer and V. Ramakrishna, "Output Tracking and Steady State for Nonlinear Systems," *Proceedings of the 35th Conference on Decision of Control*, Japan, pp. 2064-2068, December 1996.
- [34] R. Su, "On the Linear Equivalent of Nonlinear Systems," *Systems and Control Letters*, Vol. 2, No. 1, pp. 48-52, July 1982.
- [35] L.R. Hunt, R. Su and G. Meyer, "Global Transformations of Nonlinear Systems," *IEEE Transactions on Automatic Control*, Vol. AC-28, No. 1, pp. 24-31, January 1983.
- [36] L.R. Hunt, R. Su and G. Meyer, "Design for Multi-Input Nonlinear Systems," *Differential Geometric Control Systems*, Boston: Birkhäuser, 1983.
- [37] K.S. Yeung, EE 5308 Linear System Theory Class Notes, 2003
- [38] J.L. Crassidis and J.L. Junkins, *Optimal Estimation of Dynamic Systems*, NY: Chapman & Hall/CRC Applied Mathematics and Nonlinear Science Series, 2004.
- [39] R.F. Stengel, *Optimal Control and Estimation*, NY: Dover Publications, Inc., 1994.
- [40] D.G. Luenberger, "Determining the State of a Linear System with Observers of Low Dynamic Order," *Dissertation*, Electrical Engineering, Stanford University, 1963.
- [41] A.J. Krener and W. Respondek, "Nonlinear Observers with Linearizable Error Dynamics," *Siam J. Control and Optimization*, Vol. 23, No. 2, pp. 197-216, March 1985.
- [42] J.L. Crassidis and J.L. Junkins, *Optimal Estimation of Dynamic Systems*, http://www.acsu.buffalo.edu/~johnc/estim_book.htm, 2004.
- [43] *Real Time Workshop User's Guide*, The MathWorks Inc., MA, 1999.
- [44] *Using Simulink*, Math Works Inc, MA, 1999.
- [45] B.A. McCreight, "A Magnetic Levitation Device: an Engineering Education Testbed," *Senior Project*, Mechanical and Aerospace Engineering, UT-Arlington, 1999.
- [46] J.L. Devore, *Probability and Statistics*, Pacific Grove, CA: Duxbury, 2000.

BIOGRAPHICAL INFORMATION

John Henley was born in Arlington, Texas in 1976. He received the Bachelor of Science in Mechanical Engineering from Texas A&M University, College Station, Texas in 2001. Since the completion of his Bachelors degree, he has been employed by Halliburton Energy Services in Carrollton, Texas as a development engineer designing downhole tools. His current development role at Halliburton is as a Senior Technical Professional – Mechanical in the Expandable Liner Hanger Product Service Line. In 2002, he began work on his Master of Science in Mechanical Engineering at the University of Texas at Arlington. While a student, he worked as a Graduate Research Assistant in the Manufacturing, Automation and Robotics Systems Laboratory during the course of his Masters. His current research interests include Control Systems, State Estimation, Sensor Fusion, Dynamics and Kinematics, Unmanned Autonomous Vehicles, Neural Nets, Intelligent Systems and Evolutionary Computation. He received his Masters of Science in Mechanical Engineering from the University of Texas at Arlington in May 2007.